TABLE OF CONTENTS

LIST OF FIGURES

LIST OF TABLES

CHAPTER 1

INTRODUCTION

1.1 Background

Semisolid forming of metals is an attractive technology that offers a great chance to manufacture net-shaped metal components in only one forming operation. In addition, elevated mechanical properties can be achieved because of the unique globular microstructure and flow behaviour within the die. In order to successfully perform semisolid forming process, it is required to establish a critical control on all process parameters, particularly feedstock preparation and forming process. The interrelation between parameters of each process step and the material microstructure and flow behaviour is highly nonlinear. This causes a major challenge for scientific understanding and economic mass production.

Semisolid metal (SSM) processing is based on the thixotropic behavior of alloys with a non-dendritic microstructure in the semisolid state. If the microstructure consists of spheroids of solid (globular grains) in a liquid matrix, its viscosity is time and shear rate dependent; if it is sheared it flows and if it is allowed to stand it thickens again. This behavior leads to laminar rather than turbulent die fill and avoid defects such as porosity and improves mechanical properties. The improved mechanical integrity allows components to have smaller cross-sections and the replacement of steel with aluminum for safety critical components such as suspension components for cars.

In comparison with cast aluminum alloys, wrought aluminum alloys have superior mechanical properties, thereby offering a wider application. There has been a strong demand to produce to near-net-shape components with aluminum 7xxx series alloys, which are mainly machined from the wrought state involving considerable waste. Semisolid forming can be a potential alternative near-net-shaping technology. The approach in this project is to first produce a starting material of 7075 alloy which is treated such that the microstructure consists of globular grains in a matrix of liquid phase. The *Swirled Equilibrium Enthalpy Device* (SEED) is a novel SSM process that will be undertaken for preparing the feedstock material. The SEED processing is a cost-effective feedstock preparation method due to its capability of using all the possible material sources (primary, secondary and particular process scrap).

A major problem for semisolid forming has been the lack of fundamental understanding of the rheological behavior and the flow of alloys in the semisolid state that impairs our ability to simulate, optimize the processing and improve the repeatability. In order to achieve a deep understanding of rheological behavior of wrought aluminum alloys, a fundamental study would be performed to develop a share rate-viscosity relationship in the semisolid state of the wrought aluminum 7xxx alloys by parallel plate rapid compression viscometer.

1.2 Objectives

The general objective of the present project is to study the microstructure evolution and rheoformability of 7075 wrought aluminum alloy produced by SEED processing. In reality, in semisolid forming, the semisolid billets will undergo a sudden increase in shear rate as it enters the die. This process takes place in less than one second. This transient process is the key point that researchers concern. The present project aims to characterize the microstructure evolution in

semisolid state and find out how shear rate and viscosity change with time and their mathematical relation during the rheology test process. More specifically, the objectives of the present research can be categorized into three parts.

Part I – SEED processing

1) The effect of the SEED processing parameters on the microstructures of the 7075 wrought aluminum alloy will be investigated.

2) The optimum processing temperature and stirring frequency (processing conditions) will be obtained and high quality 7075 wrought aluminum alloy semisolid billets will be prepared through SEED processing.

Part II – Grain refinement

1) The influence of TiB_2 addition on the microstructures of semisolid AA7075 alloy produced by SEED process will be studied.

2) The influence of Zr addition and the combined addition of Zr and Ti on the microstructure of the studied base alloy will be compared.

Part III – Rheology analysis

1) The rheological behavior of SEED processed 7075 wrought aluminum alloy will be thoroughly investigated by rapid parallel-plate compression test.

2) A share rate-viscosity relationship (an equation) will be developed mathematically to describe the rheological behaviour of the AA7075 semisolid alloys for modeling of die filling in the semisolid forming.

CHAPTER 2

LITERATURE REVIEW

2.1 Semisolid Metal Processing

Semisolid metal (SSM) processing is one of the most important and promising processing in current industry. SSM processing is first proposed by Flemings and his co-workers at MIT in the early 1970s[1].

2.1.1 Characteristic of semisolid processing

This processing is mainly based on the unique intermediate state between solid and liquid state, which is termed semisolid state. This state contains both solid phase and liquid phase, in which non-dendritic (or spheroidal) solid particles are dispersed in the liquid matrix. The unique microstructures gives semisolid billets distinctive rheological properties : in the steady state, the semisolid billet exhibits pseudoplastic behaviour, while in the transient state it shows thixotropic behaviour[2, 3]. The semisolid billets produced by rheocasting process can stand as a solid on its own weight; while under the application of shear force, it can be easily sliced and will flow like a liquid due to the instant viscosity drop. **Fig. 2.1** shows the rheological behaviors[4].

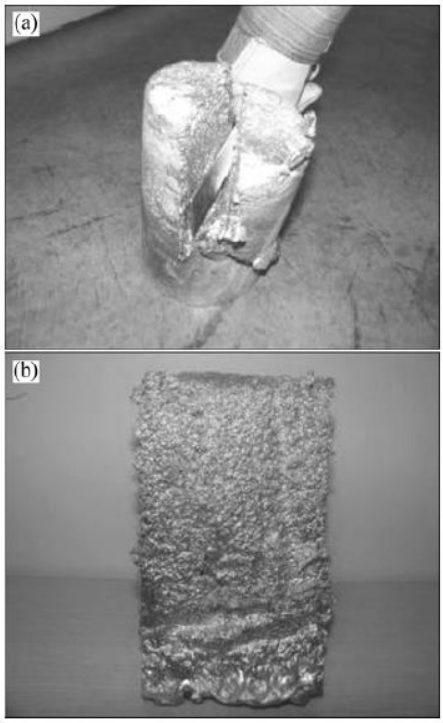

Fig. 2.1 Semi-solid self-supported (a) and easy to cut (b)

Semisolid casting involved in SSM processing is quite different from the conventional die casting. For semisolid formed components, the microstructures consist of fine globular grains in a matrix of solidified liquid phase. This is distinct from a dendritic microstructure, which is typical for conventional casting. In semisolid forming process, by controlling the injection process gas entrapment can be avoid during die filling process. In other words, flow of semisolid slurries is laminar flow rather than turbulent flow. While in conventional die casting gas entrapment can occur due to turbulent flow of liquid alloys. **Fig. 2.2** shows the difference between semisolid casting and conventional die casting[1]. Compared to the conventional die casting, the advantages of semisolid casting can be summarized as the following:

- More energy efficient due to less heat content of the billets than that of the superheated liquid melt in conventional die casting

- Finer and much uniform microstructures, leading to enhanced mechanical properties
- Smooth filling of the die, avoiding gas entrapment and shrinkage porosity
- Less thermal shock to the die, resulting in longer die life[5]

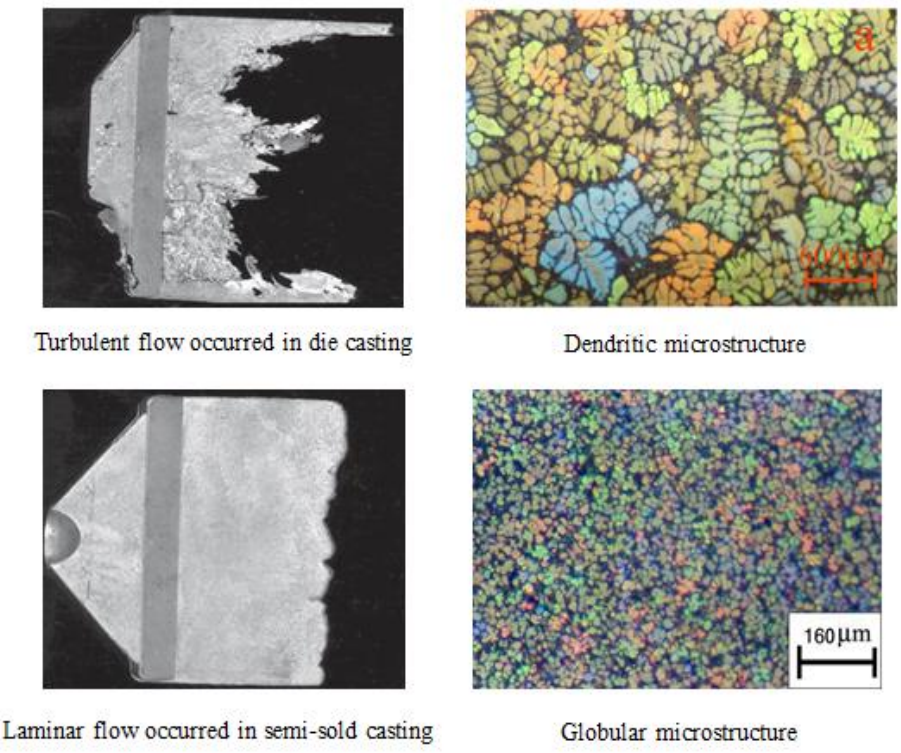

Fig. 2.2 Difference between semisolid casting and conventional die casting

2.1.2 Mechanism of microstructure evolution in semisolid processing

Dendritic microstructure is a typical microstructure in conventional casting processing, while finer globular grains in liquid matrix is a dominant microstructure in SSM processing. Therefore, since the SSM processing occurred, a number of researchers were dedicated to find out the conversion mechanisms from dendritic to globular morphology. Mechanisms for the transformation of dendrites to non-dendritic spherical morphology is vital important in semi-solid processing, leading to comprehensive understanding of SSM processing.

The dominant mechanisms include dendrite arm fragmentation, dendrite arm root remelting and growth control mechanisms. However, the most accurate mechanism for the transformation of dendrites to the spherical morphology is still not identified[6].

All the mechanisms mentioned above involve the disintegration of dendritic structure during solidification to form the globular structure. With more research in the SSM processing field, it is believed that globularization can be achieved either by mechanical fragmentation of dendritic structure or by creating multiple nucleations to obtain spherical primary phase particles directly. Compared to the mechanical fragmentation mechanism, generating multiple nucleations shortens the processing time and obtains better globular morphology, making it much preferred.

2.1.3 Technologies for semisolid metal processing

It is generally believed that the SSM processing refers to the whole forming process of commercial components production from the preparation of the semisolid billets to the final forming processing (e.g. forging). Technologies for SSM processing, which specially refers to the processing of the preparation of semisolid billets used for the subsequent forming process, can be generally classified into two basic routes based on the starting material status (**Fig. 2.3**)[7]:

- Rheo-routes

- Thixo-routes

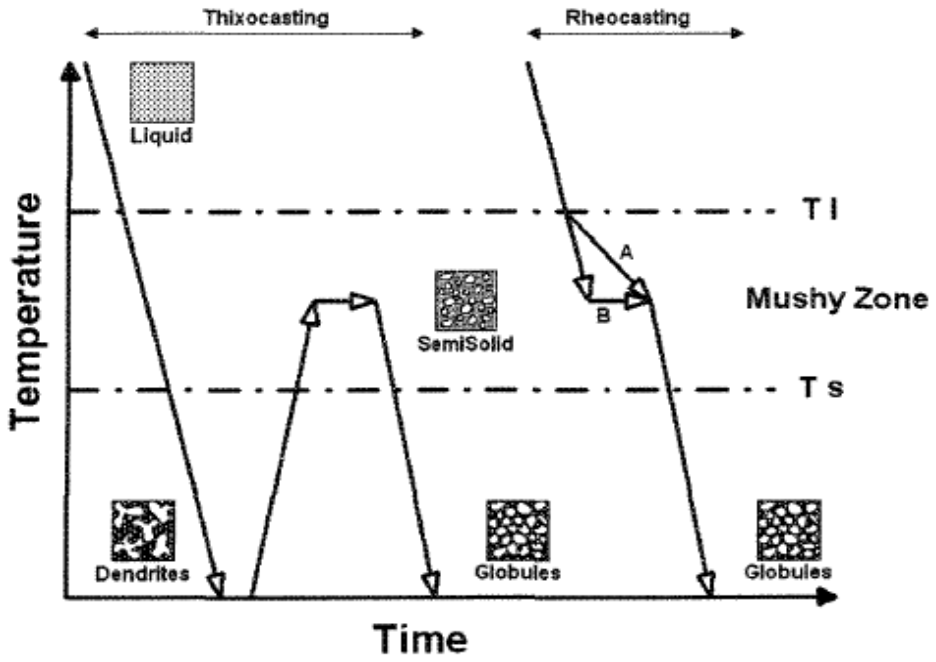

Fig. 2.3 Schematic of two kinds of semi-solid technologies (In rheocasting, A refers to continuous cooling and stirring and B illustrates isothermal stirring)

In rheo-routes technology, the semisolid billet is prepared from the liquid phase and then directly transfers into a die or mold for subsequent shaping. The process of preparing the non-dendritic semisolid billet is achieved by controlled solidification under specific conditions, which is termed rheocasting.

In the rheo-routes, or rather rheocasting process, the target is to get non-dendritic microstructure during the solidification process. To produce this kind of non-dendritic billets, several techniques are available, including *Mechanical stirring*[8], *Electromagnetic stirring*[9], [10, 11], *SEED process*[12], *semisolid rheocasting (SSR)*[13, 14], *twin screw rheomolding*

process[15], *new rheocasting process (NRC)*[16], *ultrasonic treatment*[17], *forced convection rheoforming (FCR)*[18], *recrystallization and partial remelting (RAP)*[19] and so on.

Thixo-route is another technique of SSM processing which classically involves three stages. The first stage is to prepare the billet with non-dendritic or equiaxed structure or having the potential to transform to the spherical morphology in the subsequence processing. The second step is to reheat the billet to the temperature between the solidus and liquidus to get the semisolid structure. The final stage is to transfer the semisolid billet to the shaping die. If the component shaping is performed in a closed die, it is referred to as thixocasting; while if the shaping is achieved in an open die, it is called thixoforming[2].

Among the three stages in thixo-routes process, the second step is the most important process because the semi-solid microstructure is controlled during the reheating process. The required semisolid microstructure is fine and spherical solid particles uniformly dispersed in a liquid matrix of low melting point. To achieve this microstructure, several important parameters during the reheating process should be controlled accurately. The reheating temperature controls the solid fraction, which has a great impact on the viscosity of the billet. A uniform temperature distribution throughout the billet is important to obtain homogeneous solid particles distribution and good rheological characteristic. Furthermore, the reheating time should be properly performed. Now days, with continually study on thixoforming technology, some other processes applied in thixo-routes were developed, like innovative two-stage reheating process which has been developed to improve the thixotropic behavior of semisolid aluminum alloys[20, 21].

The main advantage of the thixo-routes process is that the forming is free from handling the superheated liquid metal and this process can be highly automated like forging. The

disadvantage of thixo-routes is that it is hard to obtain fully homogeneous billets and there may be metal loss during the reheating process. Compared to the rheo-routes techniques, thixo-routes contains three steps, which is less economical than the rheo-routes which only consists of a simple step from liquid to the feedstock directly.

2.2 SEED Processing of Aluminum Alloys

The SEED process is a recently developed rheocasting technology for semisolid metal processing by Doutre et al[12]. The SEED process is an economical and reliable process with simple operation for the preparation of feedstock for semisolid metal processing, which is suitable for a wide range of aluminum alloys.

2.2.1 Process description

2.2.1.1 Initial designed SEED process

The SEED process is schematically shown in **Fig. 2.4**[22]. The initial designed SEED process can be divided into three stages[23].

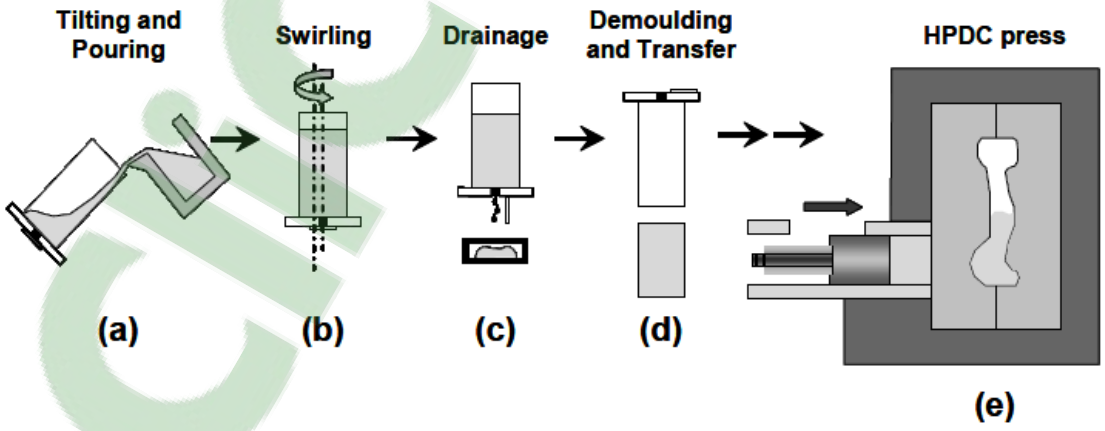

Fig. 2.4 Schematic of the SEED process and HPDC press

First, the master aluminum alloys are melted in a crucible heated by the electricity furnace to obtain the designed composition. The melt aluminum of the designed composition is transferred to the preheated mold which is fixed on the SEED machine before each experiment at a certain pouring temperature. During each pouring operation, the mold should be tilted to make sure that there is no turbulence in the melt aluminum. Then the mold with the platform is swirled at a chosen frequency ranging from 100~200rpm with an eccentricity of the order of 12mm[23]. During the swirling process, a thermocouple is plug into the melt aluminum at the center and the edge of the mold to monitor the instant temperature. When the temperature reaches the target temperature, a semisolid billets with a certain fraction solid is produced. The first stage ends. The swirling motion during this stage, similar to the stirring motion in the Mechanical or the Electromagnetic stirring technique, helps to ensure that the primary solid phases are distributed uniformly throughout the whole semisolid billet.

In the second stage, the swirling motion is stopped. The valve at the bottom of the mold is opened after a few seconds pause, and the excess eutectic liquid will be drained out from the mold. The drainage is allowed to continue until the solid particles aggregate at the bottom of the mold stopping the liquid running out. This process usually takes 30~45 seconds from the original experience.

The third stage involves in the demolding process. After the drainage of the excess eutectic liquid, the semisolid billet is ready to demold either to the subsequence forming process directly or to quench as thixocasting billet. In this stage the semisolid billet behaves thixotropic or pseudoplastic property similar to a room temperature butter, which can be self-supporting and can be easily cut.

2.2.1.2 Development of SEED process

With further investigation and research in the SEED process, Pascal Cote al et al[24] optimized the process parameters and the comprehensive techniques involved in the SEED process, proposing the non-drained SEED version. This simplified SEED process has been proved adaptable with works on AA6061 wrought alloys and high strength 206 cast alloys [22, 25, 26]. The bypass of the drainage step leads to a significant simplification of the process and eliminates the work of sweeping the drain cakes. Pascal Cote and his teammates' work shows that there is no distinct difference in the microstructure, mechanical properties of the semisolid billets produced by drain or non-drain mode[24].

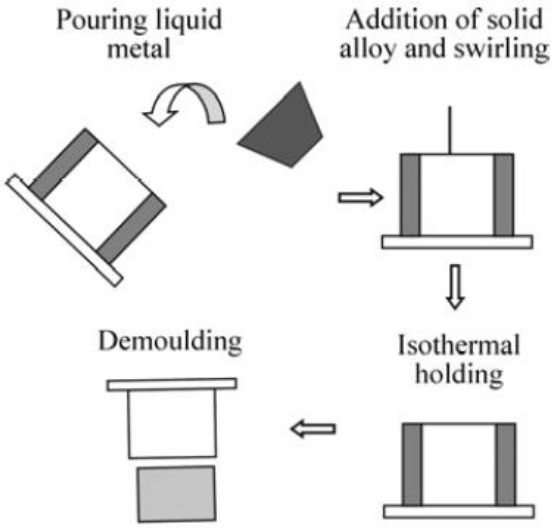

Fig. 2.5 Schematic of the developed SEED process

In the work of the semisolid processing of hypereutectic A390 alloys using SEED process, M. Tebib et al[4] introduced further improvement for the SEED process(**Fig. 2.5**[4]). In their works, they made two significant modification of the SEED process. Firstly, during the

swirling process, isothermal holding using insulation is introduced, reducing the heat lose at the wall of the mold. Secondly, solid alloy is added during swirling process. The addition of solid alloy during swirling allows high extraction of latent heat at the center of the billet, leading to a decrease of the temperature gradient within the whole billet.

2.2.2 Process parameters

In the SEED process, there are several crucial process parameters that have significant influence on the productivity of the billets and the microstructure and physical properties of the final products. These process parameters include the pouring temperature, the processing time, the temperature of the semisolid metal, the cooling rate of the melt and the swirling intensity.

2.2.2.1 The influence of pouring temperature on microstructure

The pouring temperature in the solidification process indicates the extent of the superheat of the melt. It directly affects the nucleation and the growth of the primary phase, leading to great influence on the final morphology of the primary phase. In the rheo-routes semisolid process, the morphology of the primary phase must be strictly controlled since the semisolid billet will be used to rheoforming directly. While in the thixo-routes, the primary phase morphology of the semisolid billet can be improved by the subsequent reheating process. Therefore, the controlled pouring temperature turns to be much more important in this kind of rheo-route technique, the SEED processing.

Typically, amongst all kinds of SSM processing, lower pouring temperature is regarded as the most economic alternative to produce semisolid billets. Because it not only promotes the formation of globular grains but also reduces casting defects and decreases the heat consumption.

During the SEED process, the temperature of the center and the edge of the liquid would be monitored through the thermocouple. It is noticeable that the temperature between the center

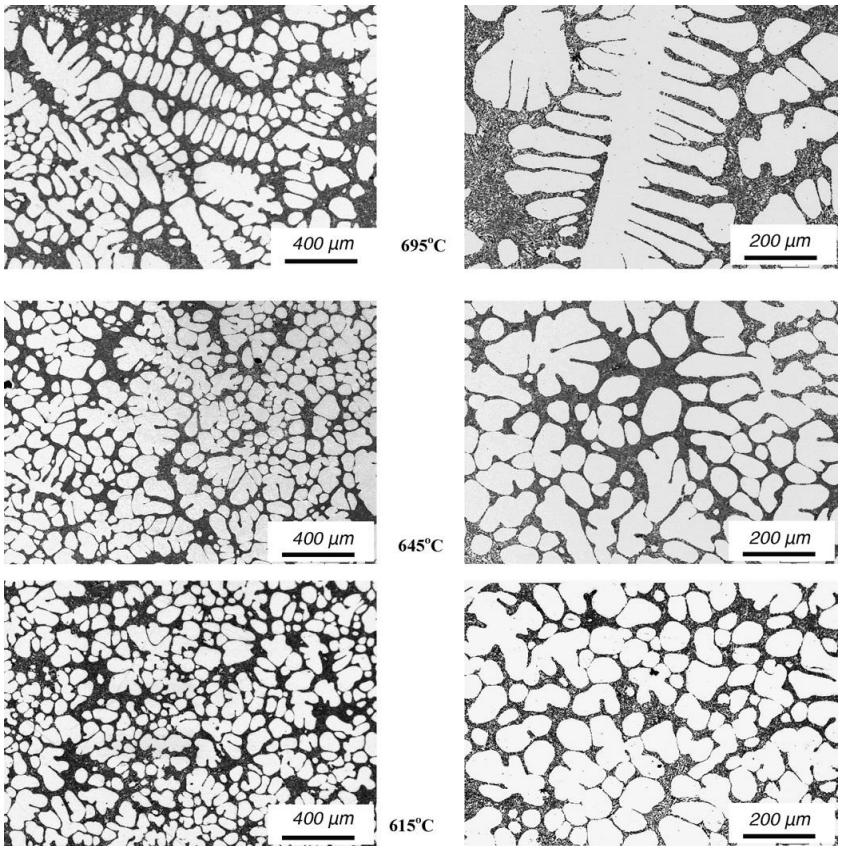

Fig. 2.6 Various morphologies of primary α-Al particles at different pouring temperatures for semisolid Al-Si 356 alloy in SEED process

and the edge is different, which indicate that there are two different cooling regimes for them. According to the work of Omid Lashkari et al[27], different pouring temperatures result in various cooling regimes of the melt, leading to various morphologies of primary α-Al particles(**Fig. 2.6**[27]).

At the low pouring temperature, the edge area of the melt is highly undercooled, pronouncing a much larger number of nuclei than that at high pouring temperature. The temperature near the mold wall is much lower and is not sufficient enough to remelt the existing nuclei even with the heat flow from the center of the melt. Furthermore, lower pouring temperature establishing larger temperature gap between the center and the edge at the beginning of the solidification, encourages faster heat flow from the center towards the mold. Therefore, a uniform temperature distribution throughout the bulk liquid is occurred in a much shorter time at a lower pouring temperature. The rate of heat flow reduces rapidly and the growth rate of the nucleation is also reduced. To summarize, large number of nuclei and low growth rate at the low pouring temperature promote the globular primary α-Al morphology corporately.

2.2.2.2 The temperature of the semisolid metal

During the whole SEED process, the temperature of the melt will be monitored, both at the center and the edge of the mold. **Fig. 2.7** shows the temperature profiles during the production of semisolid billets of 7075 wrought aluminum through SEED processing in two modes: with and without insulation. In this test, the mold was preheated to about 200℃ and the pouring temperature was fixed at 750℃. In the SEED processing without insulation (**Fig. 2.7 (b)**), the temperature gradient between center and wall during the initial stage of cooling is very large because of the temperature difference between the mold and the melt liquid. As cooling down the temperature of the wall increases a bit, then decreases slowly with the center part, resulting in a temperature gradient of 6℃~10℃ in the final stage.

Fig. 2.7 (b) shows the temperature profile using the SEED processing with insulation recorded in present project. In the initial cooling stage the temperature gradient between center

and wall is much smaller than that without insulation. It is noticeable that the temperature gradient almost disappeared as the temperature went down, resulting in less than 2℃ difference in the final stage. Consequently, the temperature of the whole semisolid billet becomes much more uniform which is benefit for the formation of globular structure.

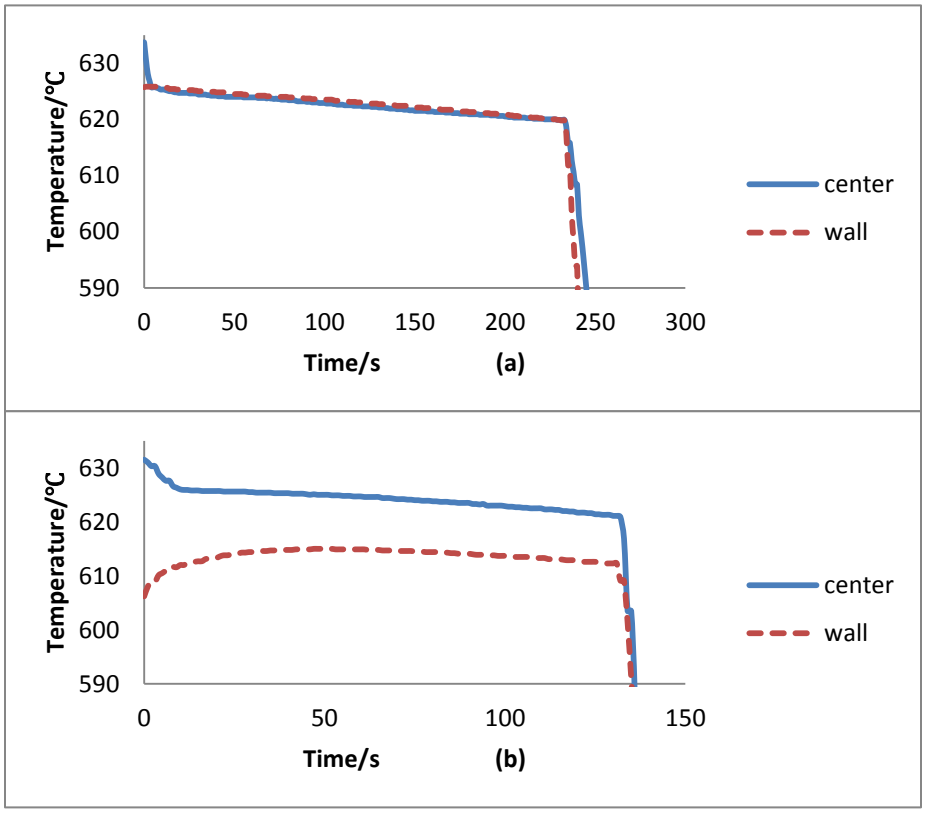

Fig. 2.7 Temperatures measured at the center and the wall during SEED processing with (a) and without insulation (b)

Temperature is an important process parameter in SEED processing as well as other semisolid processes. Typically, it is believed that higher temperature results in lower solid fraction, better deformability and more easily filling the die. Semisolid billets perform better deformation behavior, which attributes to both the high liquid fraction and primary Al particles. In the semisolid casting field, the viscosity is the most important parameter to characterize the

rheological behavior of the semisolid billet. It is believed that the temperature with the solid fraction has a strong influence on the viscosity. An inverse relationship for viscosity and temperature was carried out to qualify this influence[28], shown in Eq. (2-1). This equation is only valid for the system that there is no phase change due to the temperature variation, for example, in polymeric materials.

$$\eta = \eta_0 \exp(\frac{\Delta E}{RT}) \tag{2-1}$$

2.2.2.3 The swirling intensity

In the production of semisolid billets, shear force is applied at different shear rate to promote the formation of semisolid microstructure. Application of shear force is the crucial operation to semisolid techniques, for instance, mechanical stirring, magneto hydrodynamic (MHD) stirring, ultrasonic vibration or swirling of the melt in SEED process.

Shear force is another important factor that has great effect on the viscosity of the semisolid billets. It causes laminar or turbulent flow within the melt during the solidification. The driving force for the mechanical fraction of dendrite arms comes from the applied shear force. And it is also the main dynamic for fine distribution of globular particles in liquid matrix. To figure out the relationship between shear force and viscosity, the term of “apparent viscosity” is proposed. In the steady state, the apparent viscosity decreases with the increasing of the shear force at the same solid fraction.

Shear rate is a correlative parameter that varies with shear force. In Newtonian fluids, the shear rate varies linearly with shear force while in non-Newtonian fluids it varies non-linearly

with shear force. Shear rate also affects the viscosity where the increasing of shear rate decreases the viscosity.

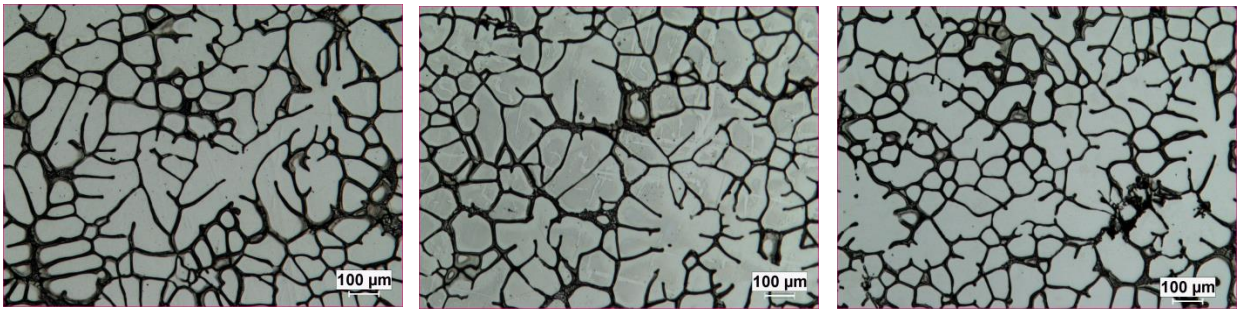

Fig. 2.8 Microstructure of semisolid AA7075 wrought alloy at different swirling frequency: (a) dendrite, low rpm; (b) rosette, medium rpm; (c) globular, high rpm.

In SEED process, swirling is the agitation mean to offer shear force. Swirling operation can alleviate the temperature gradient between the semisolid billets, leading to thermal homogeneity. Swirling also provides assistance in the fraction of dendrite arms, resulting in the globular microstructure. The SEED equipment in the lab can offer different swirling frequency (ranging 100rpm ~ 250rpm) to apply variation shear force. **Fig. 2.8** shows the microstructure difference at different swirling intensity of semisolid 7075 alloy used in present experiment.

2.2.3 Application on casting and wrought aluminum alloys

In recent years, the SEED process has attracted many attentions in semisolid field. A team of scientists, engineers, technicians and research students are still working on the optimizing and fully development of this promising semisolid process to popularize its application. Till now, a large number of experiments have been conducted on common foundry alloys as A356, A390 and A206, as well as on wrought alloys as AA6061. And relevant literatures have been published.

In 2006, the SEED process was first applied on semisolid A356 alloy by S. Nafisi et al[27, 29, 30]. Grain refiner effect on the microstructure evolution and rheological properties of A356 alloy in semisolid state were investigated by them. In their study, A356 semisolid billets of 75mm in diameter and ~140mm in height were produced by SEED process. After that, compression test was conducted to characterize the flow behavior of the semisolid billets. Strain-time graphs were drawn to analyze the rheological behavior and quantitative metallography was carried out to characterize the effect of pouring temperature on the microstructure of semisolid A356 alloy.

In the year of 2008, the SEED process was first applied in the wrought aluminum alloys to produce the semisolid AA6061 feedstock by J. Langlais et al[22]. They offered the possibility of SEED processed wrought aluminum, proving the wide feasibility of SEED process. They overcame the hot tearing problem, one of the most common defects in wrought aluminum, with optimal SEED process and die casting parameters. The overview of the industrial SEED process used to produce AA6061 was presented. Furthermore, the fatigue behavior of the SEED processed semisolid AA6061 die cast parts was investigated.

In later years, M. Tebib et al[4, 31] used the SEED process to produce semisolid billets of hypereutectic Al-17Si-4.5Cu (A390). In their study, the isothermal holding using the insulation and addition of solid alloy during swirling was introduced, and their influence on the temperature gradient between the center and the wall and on the formation of α-Al particles was investigated. Moreover, phosphorus and strontium was added to the A390 melt to refine the primary and eutectic microstructure to optimize the SEED process. Similarly, the rheological behavior of semisolid A390 alloy was studied at different deformation rate and different solid fraction. Furthermore, the influence of Mg amount in A390 on viscosity was investigated.

2.3 Characteristics of Semisolid Microstructures

In industry production, the common goal in SSM processing is to obtain an ideal microstructure of the semisolid slurry to facilitate the subsequent component shaping process. It is generally believed that the ideal microstructure for a semisolid billet should be a specified solid fraction of fine and globular solid particles uniformly dispersed in the liquid matrix. Such a structure can ensure the required rheological behavior for shaping.

For a given composition of a semisolid alloy, the characterization of its microstructure involves quantifying the solid fraction, the grain size and shape, and the distribution of the solid particles[30]. The typical method to quantify these characteristics is metallography of the immediately quenched samples from the semisolid temperature. Those microstructure parameters above have strong influence on the viscosity of the semisolid alloy, which would further affect the flow behavior and rheological behavior of the semisolid alloy.

2.3.1 Solid fraction

Among all the parameters that have effect on the rheological behavior of semisolid billet, the solid fraction is the most important one. For a given alloy, the solid fraction is only determined by the semisolid temperature. Generally, the lower temperature gives the greater amount of solid fraction, resulting in higher viscosity. Then the mold filling would be difficult.

To measure the solid fraction, several methods are proposed in the open literatures. Among them, the quantitative metallography, thermal analysis and the application of thermodynamic data are the most common used[32]. All these three methods give the approximate measurement and each of them has unique advantages.

Quantitative metallography is the most common used method in solid fraction measurement. In this method, the sample is quenched rapidly at the semisolid temperature to preserve the semisolid structure. After quenching, a two-dimensional image from the polished surface is analysed to determine the solid fraction or the liquid fraction. The cooling rate of the quench medium (usually cold water) has a great effect on the accuracy of the results.

The other method is the thermal analysis method. This technique can be divided into two routes: differential scanning calorimetry (DSC) and cooling curve analysis (CCA). In comparison of these two routes, the DSC route is more accurate than the CCA for many materials, especially for alloys. DSC measures the heat absorbed or released in the phase transition process. The difference in the amount of heat required to maintain the temperature of the test sample and the reference is measured as a function of temperature. This amount of heat is proportional to the solid fraction.

In the third technique, the Gibbs free energy of individual phases is molded as a function of composition, temperature or pressure, and the results are collected in a thermodynamic database. Therefore the solid fraction is calculated by the lever rule and models.

2.3.2 Grain size

Grain size has a strongly influence on the physical properties of the materials. In natural solidification process, the grains tend to form dendritic structures. In industry production, the casting conditions must be controlled to promote the formation of equiaxed structure, which is more favorable to satisfy the property requirement. For semisolid alloys, the much finer, globular dispersed solid particles are preferred.

According to the solidification principles, there are two mechanisms to control the grain size and its distribution: nucleation and growth mechanisms. Nucleation controls the size of the grains and the growth determines the grain distribution. The degree of undercooling controls the nucleation process and the growth of the grain is affected by the temperature gradient in the liquid.

Based on the two mechanisms above, there are several methods to control the grain size, achieving finer grains.

- Rapid cooling during solidification
- Agitation of the melt in SSM processing
- Addition of a grain refiner

2.3.3 The shape factor

The ideal microstructure in semisolid alloys should be finer and globular solid particles. So it is necessary to describe the sphericity of the solid particles quantitatively. The shape factor F is introduced. The most common used method is to analysis the two dimensional sections obtain from the complex three dimensional structure (**Fig. 2.9**[1]). The perimeter P and the area A of the object present on the section are measured, and the shape factor is calculated through the following expression:

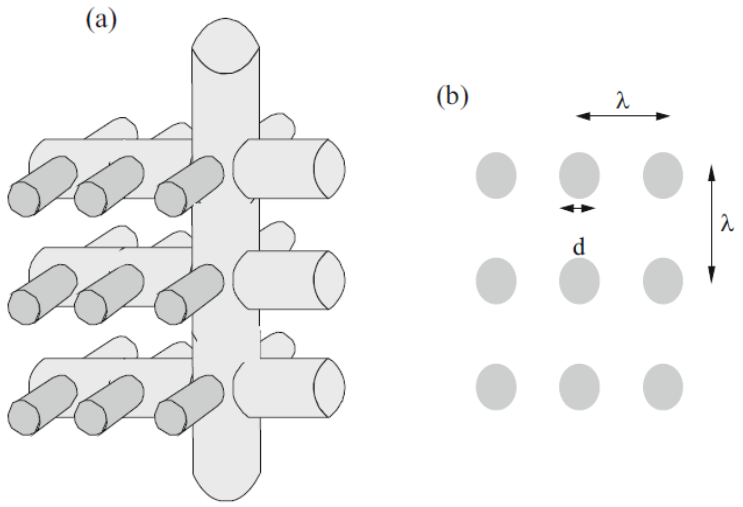

Fig. 2.9 Schematic of complex structure and cross section, (a) 3D structure (b) 2D section

$$F = \frac{4\pi A}{P^2} \tag{2-2}$$

In this expression, F=1 refers to a perfectly spherical morphology; $F \rightarrow 0$ means a complex shape. This equation only adequate for well dispersed non-dendrite particles. d_{min} d_{max} $A_R P^2$

2.4 Rheology of Semisolid Alloys

2.4.1 Introduction

Semisolid alloy contains both solid phase and liquid phase, in which non-dendritic (or spheroidal) solid particles are dispersed in the liquid matrix. This unique microstructure gives semisolid billets distinctive properties depending on the applied force. In the absence of the external force, the semisolid material can stand by itself like room temperature butter; when the external force is applied, the semisolid material flows like a liquid that can fill the die. To better

study this flow behavior, the term of “rheology” is subjected. Rheology is a physic science that deals with deformation and flow of material simultaneously. The relationship between rheology and mechanical properties of the materials is closely related to the materials' viscosity within semisolid state (or mushy state).

To understand rheology, Newtonian fluid and non-Newtonian fluid must be introduced. The Newtonian fluid is defined as that the shear stress of the fluid arising from its flow is linearly proportional to its shear rate. The ratio of shear stress and shear rate is termed as its viscosity. That means, for the Newtonian fluid, the viscosity is constant at a given temperature, independent of shear stress and shear rate. Any other fluid that doesn’t obey the Newtonian relationship is clarified as non-Newtonian fluid. Newtonian fluid is regarded as an ideal model that account for viscosity, while non-Newtonian fluid is much more common in real life. Rheology generally accounts for the behavior of non-Newtonian fluids, termed as “thixotropic behavior”.

In non-Newtonian fluids, they can be clarified into two catalogues: shear thinning and shear thickening fluid. When the viscosity decrease with the increasing of shear rate, the fluid is called shear thinning fluid. For instant, ketchup is a common shear thinning fluid since its viscosity reduces by shaking, like mechanical agitation in industry. Compared to shear thinning fluid, shear thickening fluid is that the viscosity increases with the increasing of shear rate (**Fig. 2.10**[1]). Semisolid metal processing involves the shaping of the metal components in the semisolid state by injection of the billets into a die[33]. For this to be possible, the semisolid state must have shear thinning thixotropic behavior, because a lower viscosity causes better movement of material through the die.

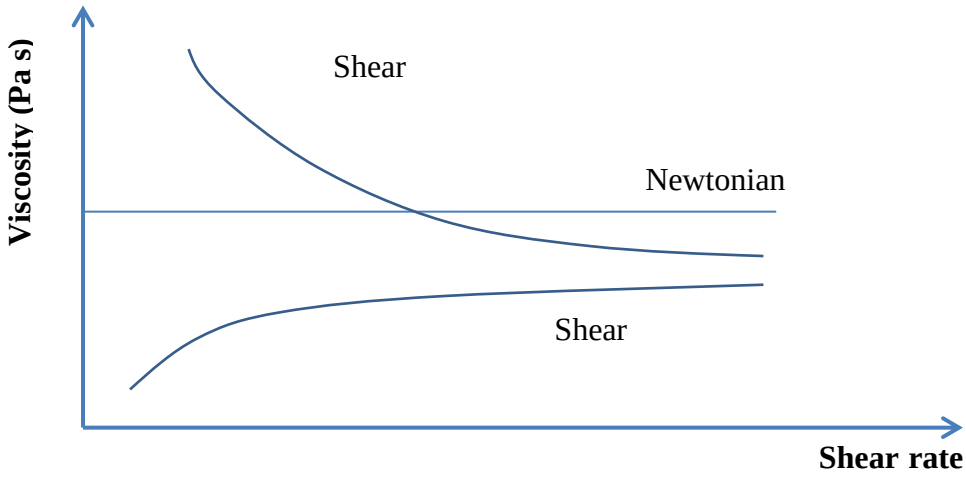

Fig. 2.10 Viscosity versus shear rate curves for a variety of types of rheological behavior

Viscosity is the most important parameter to characterize the rheological behavior of the semisolid alloy. It is dependent on the process parameters and metallurgical characteristic of the alloy including pouring temperature, applied shear rate, the fraction solid, solid particle size and its distribution respectively[34]. The experimental characterization of a material's rheological behavior or experimental determination for a material's viscosity is known as rheometry or viscometry. Understanding the effect of thixotropy property on the flow behavior and the structural evolution of these semisolid materials during flow is significant to the industry[35]. Therefore many techniques for measuring the viscosity were proposed by researchers: rotational viscometry[36, 37], drop-forge viscometry[38], parallel plate compression viscometry[39, 40],extrusion methods[41-43] and indentation tests[44].

2.4.2 Measurement of the steady-state rheological behavior

For non-Newtonian fluid, apparent viscosity is usually measured to characterize the rheological behavior. In real test, the requirements for absolute viscometry are rather difficult to

achieve, because the test condition must be assumed that there must be laminar flow, the material must be uniform and there is no physical or chemical changes during testing. In fact, it is impossible to achieve this condition for thixotropic materials. Therefore, to investigate semisolid alloys' rheological behavior, apparent viscosity is applied. Among all types of viscometers, rotational viscometer is regarded as the most common method to measure the apparent viscosity.

The rotational viscometer consists of two concentric cylinders (the inner rotor and the outer crucible) with the test material in the annular space between them, termed as coaxial cylinder rotational viscometer. Either the inner rotor or the outer crucible is rotated, leading to the material being sheared. The torque date on the cylinders can be carried out to calculate the viscosity. The sample can be sheared with a given shear stress and the shear rate is measured, or it can be sheared at a selected shear rate and the shear stress is measured.

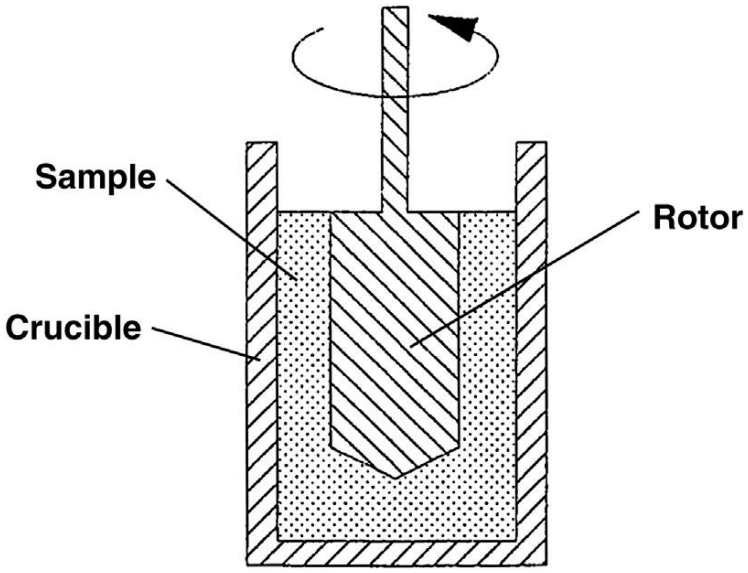

Fig. 2.11 Schematic of Searle-type rotational viscometer

There are two types of coaxial cylinder rotational viscometers: Searle-type and Couette-type. With the Searle-type rheometer, the inner rotor is rotated, shearing the material and the outer cylinder is static. During the rotation, a torque is produced because of the resistance of the material to the rotation movement, which can be monitored by torque sensors (**Fig. 2.11**[45]). Then the output of the torque sensor can be used to calculate the viscosity of the test material. This type of rotational viscometer cannot be applied on the low-viscosity material, because high shear rate can cause turbulent flow within the fluid.

To the contrary, in the Couette-type, the inner rotor is kept static and the outer cylinder rotates at a certain speed. The torque produced in the material is determined by the exact counteracting torque required to keep the inner rotor motionless. Compared to the Searle-type, turbulent flow is less common in Couette-type viscometer. However, the rotated outer cylinder makes accurate temperature control much difficult. Hence, Searle-type viscometer is much more welcome in practical measurement.

From the previous research, it is generally believed that the apparent viscosity at the steady state is influenced by solid fraction and the shearing rate. The viscosity increases with an increasing solid fraction. The increasing is slight at the early stage, while it becomes dramatic at high solid fraction. The viscosity decreases with an increase in shear rate. With the increasing shear rate, the morphology becomes more globular and the liquid trapped in the solid particles is reducing, leading to a smaller solid fraction, resulting in decreasing viscosity.

2.4.3 Measurement of the transient rheological behavior

In steady state, the semisolid material experiences a certain shear rate for a period time. But in the real industry, the die filling process finishes quickly, actually less than one second.

The slurry for die filling undergoes a sudden increase in shear rate as it enters the die. In that second, the shear rate of the slurry increases dramatically, from rest to 100 s^{-1} or more. This process is regarded as unsteady state or transient state. Rheological behavior in transient state is totally different to that in steady state. Therefore, it is much more meaningful to measure the rheological behavior in transient state for the modeling of die filling and die design in real industry.

Rheological behavior in transient state can be measured by rotational viscometer only for lower solid fraction (less than 0.45). For higher solid fraction, rapid compression viscometer or drop-forge viscometer is more suitable.

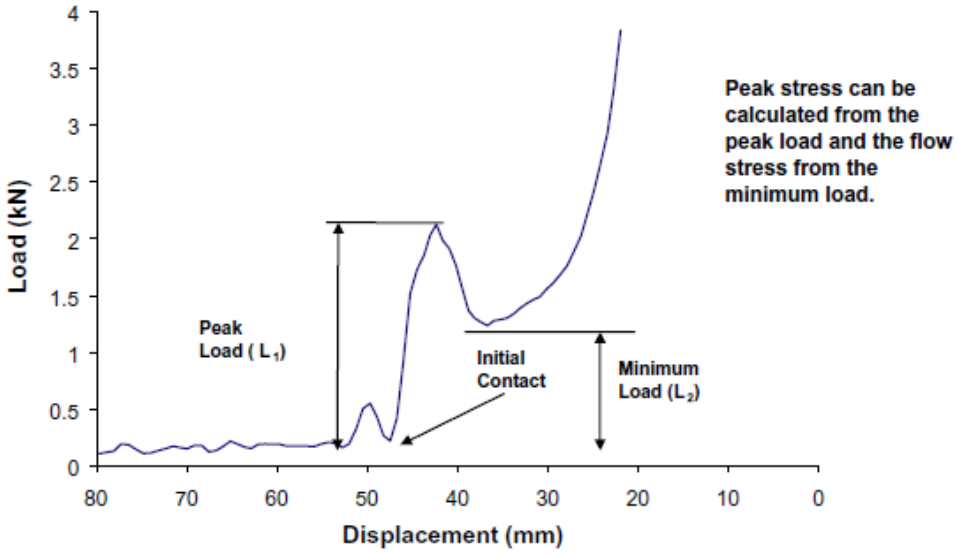

Fig. 2.12 Typical signal response to rapid compression of a semisolid alloy slug

Some experiments of rapid compression viscometry have been carried out for Sn-15%Pb semisolid alloy by Laxmanan and Flemings[39]. In their work, the billet was compressed between two parallel plates under a selected load, and the load and the displacement was

measured as the raw date to calculate the viscosity. An analytical formula was used to derive the relationship between viscosity and shear rate through the load and displacement measured under appropriate assumptions. **Fig. 2.12** shows a typical example of the load signal obtained during the rapid compression test from P. Kapranos et al[33]. There is a peak load in the load-displacement curve because of the breaking down of the skeletal structure in semisolid slurry. The height of the minimum load is associated with the temperature of the slurry.

Another viscometer to measure the rheological behavior at transient state is drop-forge viscometer, produced by Yurko and Flemings[38].

1. David H. Kirkwood, M.S., Plato Kapranos, Helen V. Atkinson and Kenneth P. Young, *Semi-solid Processing of Alloys*, ed. J.P. Robert Hull, R. M. Osgood and Hans Warlimont Vol. 124. 2010: Springer Series in Materials Science.
2. Fan, Z., *Semisolid metal processing.* International Materials Reviews, 2002. **47**(2): p. 49-85.
3. Zoqui, E.J., *Alloys for Semisolid Processing.* Comprehensive Materials Processing, 2014. **5**: p. 163-190.
4. Tebib, M., et al., *Semi-solid processing of hypereutectic A390 alloys using novel rheoforming process.* Transactions of Nonferrous Metals Society of China, 2010. **20**(9): p. 1743-1748.
5. Salleh, M.S., et al., *An Overview of Semisolid Processing of Aluminium Alloys.* Isrn Materials Science, 2013. **2013**(5).
6. Atkinson, H.V., *Semisolid processing of metallic meterials* Materials Science and Technology 2010. **26**(12): p. 1401-1413.
7. Ghomashchi, S.N.a.R., *Semi-solid Metal Processing Routes: An Overview* Canadian Metallurgical Quarterly 2005. **44**(3): p. 289-304.
8. M.C.Flemings, R.M.a., *Die Casting of Partially Solidified Alloys.* AFS Transactions 1972. **80**: p. 173-182.
9. Chung, I.-G., A. Bolouri, and C.-g. Kang, *A study on semisolid processing of A356 aluminum alloy through vacuum-assisted electromagnetic stirring.* The International Journal of Advanced Manufacturing Technology, 2011. **58**(1-4): p. 237-245.
10. K.P.Young, C.P.K.a.F.C., *Fine Grained Metal Composition* U.S. Patent, Editor. November 15, 1983.
11. K.P.Young, D.E.T., H.P.Cheskis and W.G.Watson *Process and Apparatus for Continuous Slurry Casting* U.S. Patent, Editor. November 13,1984.
12. D. Doutre, G.H., and P. Wales, *Semi-solid Concentration Processing of Metallic Alloys.* U.S. Patent August 2002. **6**(428): p. 636 B2.
13. R. Martinez, A.F., J.A. Yurko and M.C. Flemings *Efficient Formation of Structures Suitable for Semi-Solid Forming* Transactions of the 21th International Die Casting Congress, 2001: p. 47-54.
14. J.A. Yurko, R.A.M.a.M.C.F., *Commercial Development of the Semi-Solid Rheocasting (SSR)* Transactions of the International Die Casting Congress 2003: p. 379-384.
15. Ji, S., Z. Fan, and M.J. Bevis, *Semi-solid processing of engineering alloys by a twin-screw rheomoulding process.* Materials Science and Engineering: A, 2001. **299**(1–2): p. 210-217.
16. Adachi, M., Sasaki, H., Harada, Y., *Methods and Apprratus for Shaping SemiSolidMetlas*, in *European Patent EP 0 745 684 Al*, U. Industries, Editor. Dec. 4, 1996.
17. Abramov, V., et al., *Solidification of aluminium alloys under ultrasonic irradiation using water-cooled resonator.* Materials Letters, 1998. **37**(1–2): p. 27-34.
18. Zhou, B., et al., *Preparation of semisolid aluminum alloy slurry by forced convection mixing and its microstructure evolution.* Zhongguo Youse Jinshu Xuebao/chinese Journal of Nonferrous Metals, 2014. **24**(1): p. 61-68.
19. Jiang, J., H.V. Atkinson, and Y. Wang, *Microstructure and Mechanical Properties of 7005 Aluminum Alloy Components Formed by Thixoforming.* Journal of Materials Science & Technology, 2016.

20. Wang, J.J., et al., *An Innovative Two-Stage Reheating Process for Wrought Aluminum Alloy During Thixoforming.* Metallurgical & Materials Transactions A, 2015. **46**(9): p. 4191-4201.
21. J. J. Wang, Z.M.Z., A.B. Phillion *Alloy development and reheating process exploration of Al-Si casting alloys with globular grains for thixoforming* Journal of Materials Research 2016. **31**(16): p. 2482-2492.
22. Joseph Langlais, N.A., Alain Lemieux, X.G.Chen and Laurent Bucher, *The Semi-Solid Forming of an Improved AA6061 Wrought Aluminum Alloy Composition* Solid State Phenomena, 2008. **141-143**: p. 511-516.
23. D. Doutre, J.L., S. Roy, *The SEED Process for Semi-Solid Forming* in *The 8th International Conference on Solid Processing of Alloys and Composites*. 2004: Limassol Cyprus p. 397-408.
24. Pascal Coté, M.-È.L., X. Grant Chen, *New Developments with the SEED Technology.* Solid State Phenomena, 2013. **193-193**: p. 373-378.
25. Lemieux, A., et al., *Effect of Si, Cu and Fe on mechanical properties of cast semi-solid 206 alloys.* Transactions of Nonferrous Metals Society of China, 2010. **20**(9): p. 1555-1560.
26. A. Lemieux, J.L.a.X.G.C., *Reduction of Hot Tearing of Cast Semi-Solid 206 Alloys* in *The 12th International Conference on Semi-Solid Processing of Alloys and Composites* October 2012: Cape Town, South Africa.
27. Lashkari, O., S. Nafisi, and R. Ghomashchi, *Microstructural characterization of rheo-cast billets prepared by variant pouring temperatures.* Materials Science and Engineering: A, 2006. **441**(1-2): p. 49-59.
28. Lashkari, O. and R. Ghomashchi, *The implication of rheology in semi-solid metal processes: An overview.* Journal of Materials Processing Technology, 2007. **182**(1-3): p. 229-240.
29. Nafisi, S., et al., *Microstructure and rheological behavior of grain refined and modified semi-solid A356 Al–Si slurries.* Acta Materialia, 2006. **54**(13): p. 3503-3511.
30. Lashkari, O. and R. Ghomashchi, *Deformation behavior of semi-solid A356 Al–Si alloy at low shear rates: Effect of fraction solid.* Materials Science and Engineering: A, 2008. **486**(1-2): p. 333-340.
31. Tebib, M., F. Ajersch, and X.G. Chen, *Rheological Properties and Microstructure of Hypereutectic Semi-Solid Al-Si-Mg Alloys Using Rheocasting Route.* Solid State Phenomena, 2012. **192-193**: p. 323-328.
32. Nafisi, S., D. Emadi, and R. Ghomashchi, *Semi solid metal processing: The fraction solid dilemma.* Materials Science and Engineering: A, 2009. **507**(1–2): p. 87-92.
33. Kapranos, P., et al., *Investigation into the rapid compression of semi-solid alloy slugs.* Journal of Materials Processing Technology, 2001. **111**(1–3): p. 31-36.
34. Lashkari, O. and R. Ghomashchi, *Deformation behavior of semi-solid A356 Al–Si alloy at low shear rates: Effect of fraction solid.* Materials Science and Engineering: A, 2008. **486**(1–2): p. 333-340.
35. Andreas N. Alexandrou, G.C.F., Georgios C. Georgiou *Squeeze flow of semi-solid slurries* Joural of Non-Newtonian Fluid Mechanics 2013. **193**: p. 103-115.
36. Ichikawa, K., Kinoshita, Y., *Rheocasting Techniques Applied to Intermetallic TiAl Alloys and Composites.* Material Science and Engineering, 1997. **A239**: p. 493-502.

37. Martin, L.M., Brown,S.B., FavierJD., Suery,M., *Shear Deformation of High Solid Fraction (>0.60) Semi-Solid Sn-Pb under Various Structures.* Material Science and Engineering, 1995. **A202**: p. 112-122.
38. J.A. Yurko, a.M.C.F., *Rheology and Microstructure of Semi-Solid Aluminum Alloys Compressed in the Drop-Forge Viscometry* Metallurgical and Materials Transactions A, 2002. **33A**: p. 2737-2746.
39. Laxmanan V, F.M., *Deformation of semi-solid Sn–15%Pb alloy.* Metal Trans A, 1980. **11A**: p. 1927-37.
40. Lashkari, O. and R. Ghomashchi, *A new machine to characterize microstructural evolution of semi-solid metal billets through viscometery.* Materials & Design, 2007. **28**(4): p. 1321-1325.
41. Draper O, B.S., Dolman G, Smalley K, Griffiths A, *A comparison of paste rheology and extrudate strength with respect to binder formulation and forming technique.* J Mater Proc Tech 1999. **141-6**: p. 92-93.
42. Turenne S, L.N., Laplante S, Ajersch F, *Mechanical behavior of Aluminum matrix composite during extrusion in the semisolid state.* Metal Mater Trans A, 1993. **30A**: p. 1137-46.
43. Ferrante M, d.F.E., *Rheology and microstructural development of Al-4wt% Cu alloy in semi-solid state.* Mater Sci Eng A, 1999. **A271**: p. 172-80.
44. Ferrante M, d.F.E., Bonilha M, Sinka V, *Rheological properties and microstructural evolution of semi-solid aluminum alloys inoculated with mischmetal and with titanium*, in *5th International conference on semisolid processing of alloys and composites*. 1998. p. 35-42.
45. Atkinson, H.V., *5.08 – Rheology of Semisolid Metallic Alloys.* Comprehensive Materials Processing, 2014: p. 149-162.

CHAPTER 3

EXPERIMENTAL PROCEDURES

3.1 Alloys Preparation and Composition

The main alloys used in this project are 7075 wrought aluminum base alloy and its grain refiner modified alloy. The AA7075 base alloy was prepared using 99.99% pure aluminum ingots mixed with various master alloys such as 100%Zr, 100%Mg, 50%Cu-Al, 50%Si-Al, 25%Mn-Al and 25%Fe-Al. All the master alloys were carefully weight measured and heated to the liquid state at around 750℃ in a 30kg capacity crucible using an electrical resistance furnace. Degassing was conducted 30mins before pouring. Degassing process was carried out inside the melt using a graphite lance of 1 inch diameter by the Argon gas following the rate of 0.14m^3/h for 10 minutes. For the grain refiner modified AA7075 alloy, the grain refiners were added to the melt in the form of their master alloys of 5%Ti1%B-Al and 10%Zr-Al in rod shape.

The chemical composition was determined by Alcan using optical emission spectrographic analysis on the casted disks of 56mm in diameter and 10mm in thick. Based on the standard procedure, 6-8 ablations were performed on the machined surface of the disk samples and the average results were presented, shown in Table 3.1.

Table 3.1 Chemical composition of AA7075 used in the experiment (wt. %)

Alloy #	Zn	Mg	Cu	Fe	Si	Mn	**Ti**	**Zr**	Al
1	5.77	3.14	1.62	0.38	0.38	0.28	**0**	**0**	Bal.
2	5.70	2.88	1.58	0.41	0.44	0.30	**0.04**	**0**	Bal.
3	5.75	2.76	1.75	0.43	0.58	0.30	**0.06**	**0**	Bal.
4	5.50	3.07	1.67	0.35	0.45	0.32	**0**	**0.06**	Bal.
5	5.61	2.80	1.63	0.36	0.48	0.31	**0.06**	**0.06**	Bal.

3.2 Semisolid Billets Fabrication by SEED Processing

For the fabrication of the semisolid billets, a standard SEED processing will be employed. **Fig. 3.1** shows a schematic of SEED processing and **Fig. 3.2** presents the SEED machine in the lab， patented by Alcan[2]. Generally, after degassing of the superheated molten metal with Argon gas for 20-30 min, about 1.0kg melt is poured into a preheated coated steel mold of 90 mm diameter and 250 mm high. The mold is held on the SEED machine. As per requirement of each test, the mold should be tilted to a certain angle to reduce turbulence flow during pouring. Two K-type thermocouples are installed at the mold center and near the wall to monitor the temperatures distribution within the bulk liquid during solidification. After that, the mold was rotated by SEED machine at different frequencies. Stirring and air cooling of molten metal are simultaneously preformed. In order to study the effect of rotating (stirring) frequency on the microstructures of semisolid billets, stirring frequencies of 120, 180 and 210 rpm will be applied according to the experiments requirements and machine capacity. The SEED processing and solidification continue until the bulk temperature at the center of the billets reaches the

predetermined temperatures. Subsequently, the prepared semisolid billet will be demolded and immediately water quenched or transferred to the viscometer for rapid compression test. The target temperatures will be defined according to the solid fraction-temperature curve obtained by DSC analysis of 7075 wrought aluminum alloy. For semisolid forming, a solid fraction range of 30-70% is suggested according to literature[3].

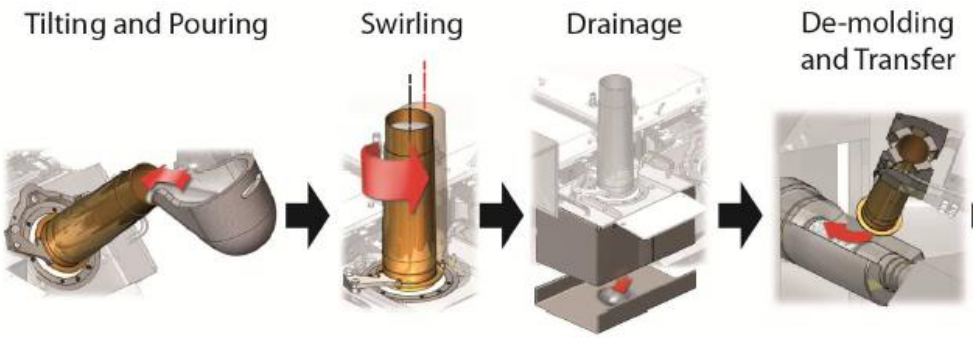

Fig. 3.1 The schematic procedure of SEED processing (by Pascal Côté etc[1].)

Fig. 3.2 The SEED machine designed by Alcan applied in this project.

3.3 Characterization of Microstructures

3.3.1 OM observation and image analysis

For as-cast billets fabricated by SEED process, the billet was cold water quenched once the process ends and was properly cut for microstructure study. The middle area of each billet was examined to represent the microstructure of as-cast billet, as shown in **Fig. 3.3 (a)**. **Fig. 3.3 (b)** illustrates the typical areas of deformed billets studied during metallographic procedure. The cut specimens were carbon powder mounted, sandpaper grounded and polished down to 0.5 micron diamond suspension. If necessary, some of the polished samples were chemically etched by Keller etchant for 20 seconds.

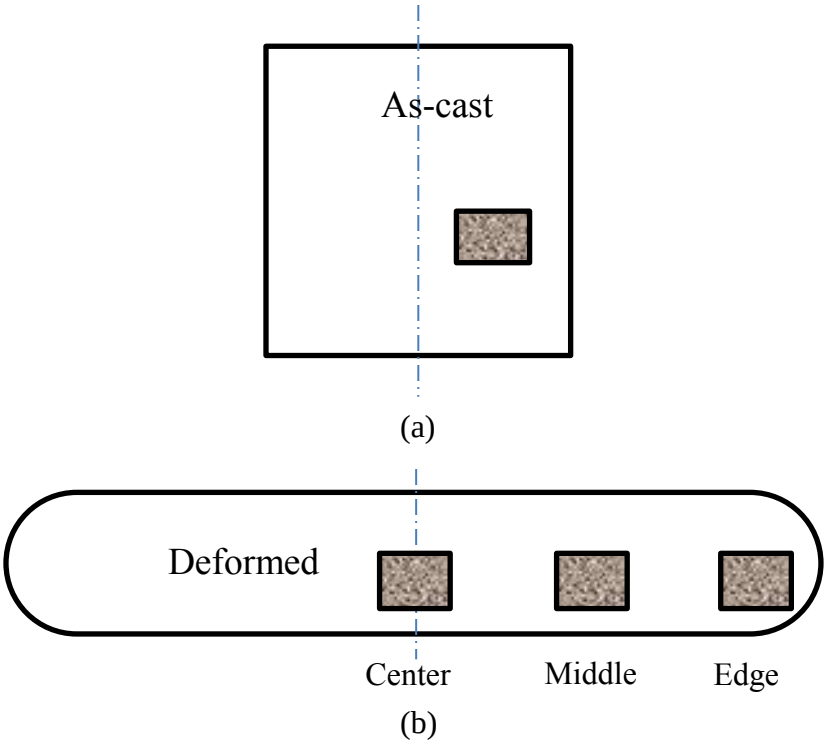

Fig. 3.3 Area of samples sectioned for observations for (a) as-cast and (b) deformed billets

Nikon Eclipse SE600 optical microscopy (**Fig. 3.5**) was used to observe the microstructures of the prepared samples. Magnifications from 50X to 200X were used accordingly. The Clemex image analyzer coupled with the OM was applied to carry out the quantitative characterization through different parameters as following;

- Aspect ratio: ratio of length over width of the measured particle.
- Mean grain size: average spherical diameter of primary α-Al particles based on the estimated size of an object as if it was a sphere.
- String length: length of a thin curved object, measured along its medial axis. String length is approximated by:

$$\text{String length} = \frac{Perimeter + \sqrt{Perimeter^2 - (16 \times Area)}}{4}$$

- String width: width of a thin curved object, measured across its medial axis. The object is assumed to have a constant width. String width is approximated by:

$$\text{String width} = \frac{Perimeter - \sqrt{Perimeter^2 - (16 \times Area)}}{4}$$

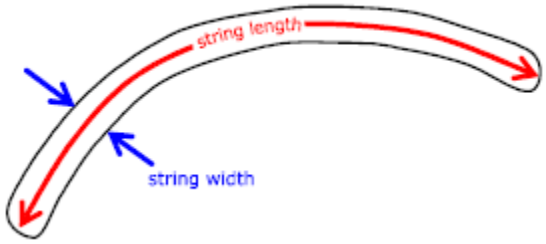

Fig. 3.4 Schematic of string length and string width.

- Area percentage: percent of area occupied by object particles relative to the whole area.

- Particle density: number of object particles per unit area.

For quantitative image analysis of the microstructure of as-cast or deformed billets, a sufficient number of randomly selected fields were automatically analyzed. For characterization of α-Al particles in the SEED specimens, 45 fields with the total area of 50mm^2 were examined per specimen (Mag. x50); and for intermetallic particles, 100 fields with the total area of 10mm^2 were measured (Mag. x200).

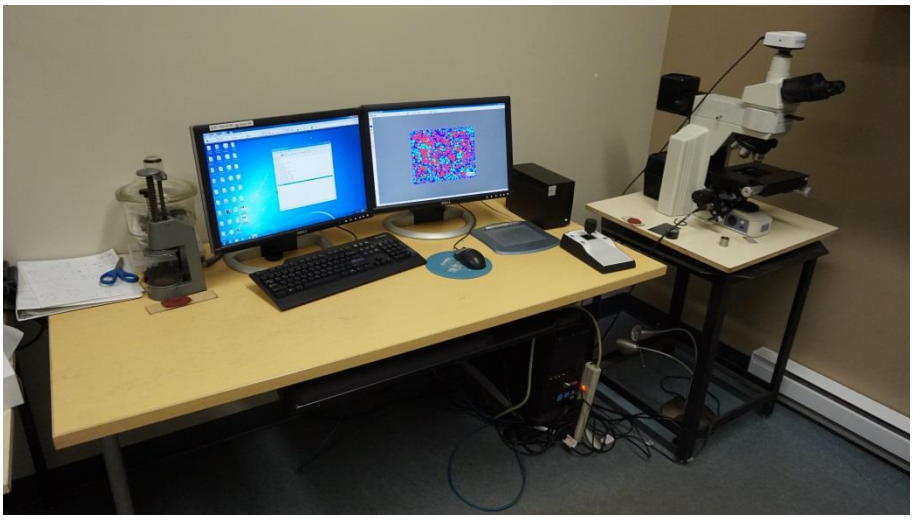

Fig. 3.5 Nikon Eclipse SE600 optical microscopy coupled with Clemex image analyzer used in present project.

3.3.2 SEM observation and elemental analysis

A scanning electron microscope (SEM, JSM-6480LV) equipped with energy-dispersive X-ray spectroscopic (EDS) facility was also used to examine the morphological features and elemental analysis of the intermetallic phases appeared in AA7075 alloys.

3.4 Rheology Test

3.4.1 Parallel-plate compression viscometer

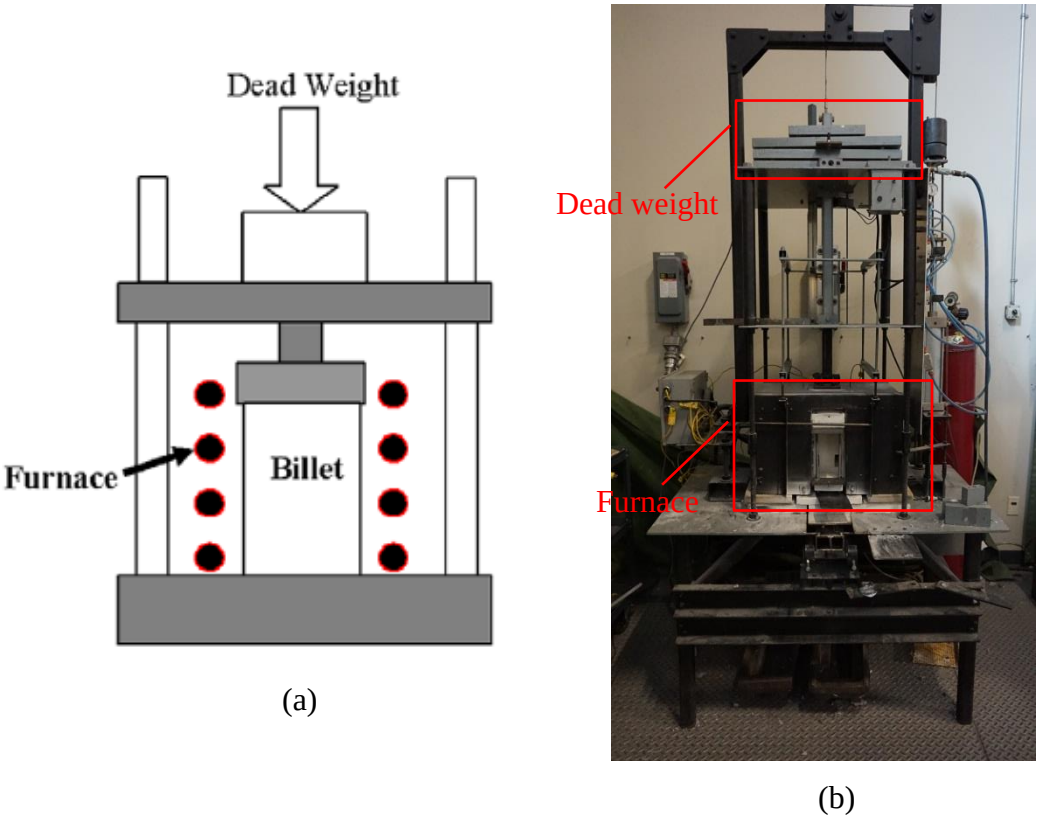

(a) (b)

Fig. 3.6 (a) Schematic and (b) actual view of parallel plate compression viscometer

For these series of tests, the semisolid feedstock will be prepared as described in section 3.2. The optimum processing conditions will be used. When the temperature of the center of the billets reaches the predetermined value, the billet will be demolded and quickly transferred to a parallel plate compression viscometer. Subsequently, the semisolid billets will be rapidly compressed under an isothermal condition.

Fig. 3.6 shows the schematic and the real view of the parallel plate compression viscometer[4]. The parallel-plate compression viscometer consists of a lower and upper plate, with frame rod between them tracking the motion of upper plate. A furnace with heat resistant windows is installed on the press bed to ensure the billet isothermal during the compression test. Both of the plates are made of refractory material with graphite and boron nitride coating to prevent it from sticking to the billet. The lower plate rests on the floor of the furnace and the 20cm length square upper plate is connected with the track rod which is suspended outside of the furnace. Dead weight is added to the upper plate to offer the force on the fluid during compression. During the test, the upper plate drops down to the lower plate driven by gravity of the dead weight.

The rapid compression will be conducted under a constant force condition (desired dead weight). The motion of dead weight-rod-upper plate is controlled by a pneumatical system. This system enables that the upper plate can either be moved manually at low speed to determine the height of test billet or be dropped from a known height to compress the sample. The resulting displacement is monitored by a displacement transducer (0-255mm) of ±0.1-0.2% precision at full stroke. 1000 data points per second will be captured during the test. The maximum height of the upper plate is 25.0cm and the maximum velocity of the plate when it firstly contacts the billet can be 0.30m/s approximately. Therefore, this test machine can produce rheological data over a range of shear rate between 0 and $6.5s^{-1}$.

During a typical test, the furnace is first set at a desired temperature. Then, the billet is rheocasted by SEED processing under desired processing parameters. Once the billet reaches the desired semisolid temperature, it is demolded to the center position of the lower plate in the viscometer furnace. Firstly, manually move down the upper plate to find out the estimated height

of the sample; then, move up the upper plate to the initial position (highest position, 25.0 cm). After that, release the upper plate and let it drop freely to compress the billet. After compression, the billet is removed to the cold water quenching. The process is repeatable. The semisolid billet containing different levels of solid fractions will be rapidly compressed under certain dead weight.

3.4.2 Calculation of viscosity and shear rate

In this parallel plate compression viscometer, the semisolid alloy is compressed under a constant load between two plates and the viscosity was calculated from the displacement-time curve obtained during the compression test. To analyze the rheological behavior of the semisolid alloy, Stephan equation model was applied.

In this model, some assumptions are considered. It is assumed that the flow is only happened in radial direction, the liquid phase in the semisolid billet is incompressible, and the entire billet is compressed between the two plates. Then, the viscosity of the billets under compression test can be calculated from the final Stefan equation [5-7]:

$$F = -\frac{3\mu V^2}{2\pi h^5}\left(\frac{dh}{dt}\right) \qquad [3-1]$$

Where F = the applied force on the billet,

μ = the calculated viscosity,

V = the volume of the billet,

h = the instantaneous height of the billet,

t = time.

In conventional viscometers, the compress velocity is usually manually controlled. It is usually kept a low and constant speed resulting in a low and near constant shear rate (less than $1s^{-1}$) to study the rheological behavior in the steady state. In this kind of test, the operation normally takes a long duration and the produced rheological data has limited guidance to the real industry commercial forming operations. Because in traditional die forming, the slurry would undergo a sudden increase in shear rate from rest and this shear rate change takes place in less than one second. This short state is termed of transient state relative to steady state. And till now, the rheological analysis on the transient state is limited. In present project, the rheological date is mainly focus on the transient state.

In the parallel-plate compression viscometer, the dead weight is considered as the applied force on the slurry and it is constant. However, the compression velocity varies with time and it can be calculated from the displacement date by derivatives to time, which is termed as dh/dt (**Fig. 3.7 (b)**).

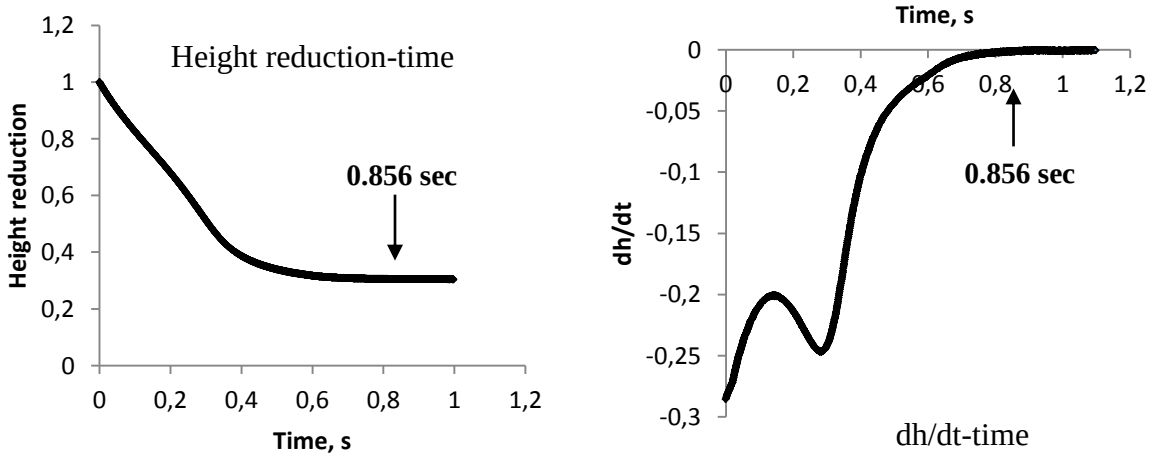

Fig. 3.7 (a) The height reduction-time and (b) instantaneous compression velocity-time calculated from the displacement date

After a series of calculation, the viscosity as a function of time can be obtained from Eq. [3-1], where the viscosity is an average and instantaneous value.

Assuming that the volume of the billet does not change during compression test, the average shear rate can be obtained by integrating throughout the volume[5]:

$$\gamma = -\frac{R}{2h^2}\frac{dh}{dt} \qquad [3-2]$$

Where R = the instantaneous radius of the billet,

γ = the average shear rate.

Therefore, a relationship between viscosity and shear rate would be established fundamentally and the rheoformability of the semisolid AA7075 alloy would be assessed and characterized.

1. Pascal Coté, M.-È.L., X. Grant Chen, *New Developments with the SEED Technology.* Solid State Phenomena, 2013. **193-193**: p. 373-378.
2. D. Doutre, G.H., and P. Wales, *Semi-Solid Concentration Processing of Metallic Alloys* U.S. Patent, Editor. August 6, 2002.
3. David H. Kirkwood, M.S., Plato Kapranos, Helen V. Atkinson and Kenneth P. Young, *Semi-solid Processing of Alloys*, ed. J.P. Robert Hull, R. M. Osgood and Hans Warlimont Vol. 124. 2010: Springer Series in Materials Science.
4. Lashkari, O. and R. Ghomashchi, *Deformation behavior of semi-solid A356 Al–Si alloy at low shear rates: Effect of fraction solid.* Materials Science and Engineering: A, 2008. **486**(1-2): p. 333-340.
5. J.A. Yurko, a.M.C.F., *Rheology and Microstructure of Semi-Solid Aluminum Alloys Compressed in the Drop-Forge Viscometry* Metallurgical and Materials Transactions A, 2002. **33A**: p. 2737-2746.
6. Laxmanan, V. and M.C. Flemings, *Deformation of semi-solid Sn-15 Pct Pb alloy.* Metallurgical Transactions A, 1980. **11**(12): p. 1927-1937.
7. Liu, T.Y., et al., *Rapid compression of aluminum alloys and its relationship to thixoformability.* Metallurgical and Materials Transactions A, 2003. **34**(7): p. 1545-1554.

CHAPTER 4

RESULTS AND DISCUSSION

4.1 DSC Analysis and Liquid Fraction

To a large extent, liquid fraction controls the rheoformability and the evolution of microstructure of semisolid billets. Thus, this parameter is significant important and priori for the whole semisolid metal processing. Therefore, it is critical to firstly investigate the evolution of liquid fraction to temperature to determine the working temperatures (semisolid temperature window) to be employed in this study. For this to be possible, a Differential Scanning Calorimetry (DSC) was used.

During the DSC test, the critical prepared sample was heated to 700℃ at the rate of 10 ℃ per minite and cooled to room temperature at the same rate. The heat flow and the temperature were both monitered to obtain heating or cooling curves. Then, the liquid fraction to temperature was intergrated from the heat flow vs temperature data recorded from the solidification curve of semisolid AA7075 alloy with the guidance of *Birol's* study[1].

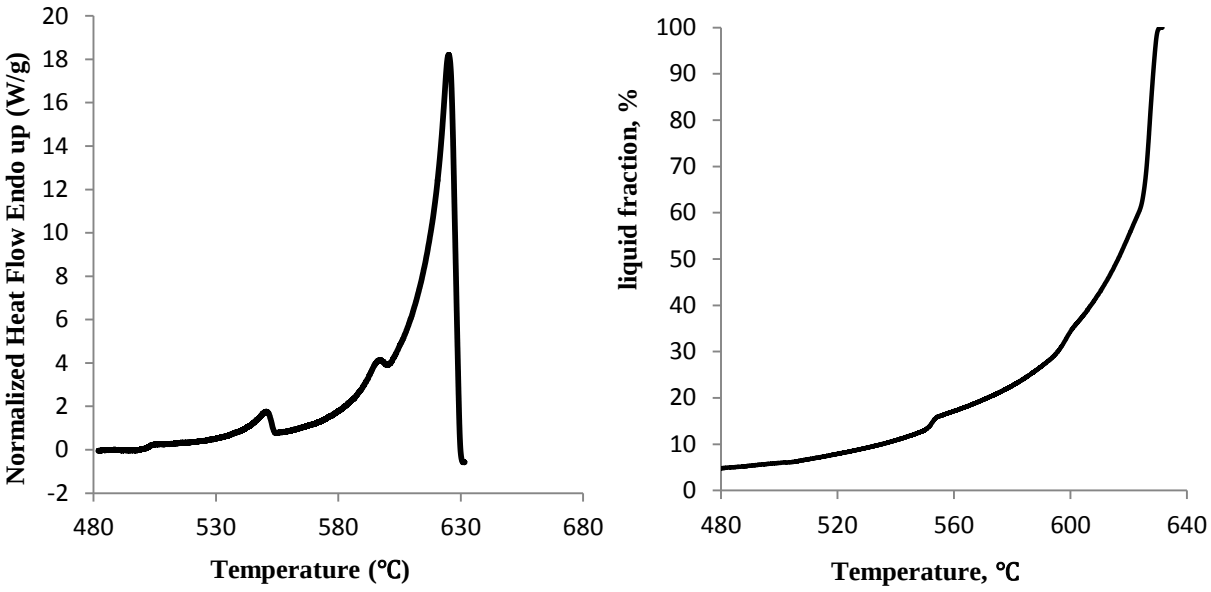

(a) (b)

Fig. 4.1 (a) DSC and (b) liquid fraction versus temperature of AA7075 alloy obtained from heat flow vs temperature data recorded during cooling from the molten state.

Fig. 4.1 shows the DSC curve and the curve of liquid fraction vs. temperature obtained from DSC solidification curve of AA7075 base alloy. It is found that the liquidus and solidus temperature of the alloy are 631℃ and 490℃ respectively. Thus, the solidification temperature range, which is difined as the temperature range between the solidus and liquidus of an alloy, is about 141℃, which is in the range of 10 to 150℃ suggested by Patel et al[2] for good processability of semisolid forming. From **Fig. 4.1 (b)**, it is discovered that the temperature sensitivity, which can be defined as the slope of liquid fraction versus temperature curve, increases with the increasing temperature. Hence, when the temperature is relative high, a slight fluctuation in temperature would induce a large difference in the liquid fraction, which requies careful control of the temperature during semisolid metal processing of AA7075 alloy.

It is suggested that the liquid fraction should be in the range of 35% and 65% ideally. Then, from the obtained curve of liquid fraction to temperature, the semisolid temperature of AA7075 alloy should be set between 610 and 625℃, which has been the guidence temperature in the following experiments.

4.2 Effect of SEED Processing Parameters on the Microstructure of Semisolid 7075 Alloys

The SEED processing is regarded as a novel and simplified rheocasting technique for the preparation of billets for the semisolid forming processing, which is patented by Alcan[3]. In the SEED process, there are several crucial process parameters that have significant influence on the microstructure of the final products. These process parameters include the pouring temperature, the processing time, the demolding temperature of the semisolid billets, the cooling rate of the melt and the swirling frequency. The effect of the SEED processing parameters, mainly demolding temperature and swirling frequency, on the microstructure of unrefined 7075 base alloy and its TiB_2 refined alloy were both investigated in order to identify the optimal processing conditions for high quality 7075 semisolid billets.

During the SEED processing, the crucible was preheated at 200℃ approximately, and the pouring temperature was fixed at 750℃ constantly. All the billets were immediately cold water quenched to the room temperature after the SEED processing. All the samples were mounted and polished down to 0.5 micron diamond suspension, then etched by the common used Keller etchant. Microstructures were examined by the optical microscope (Nikon Eclipse ME600). Quantitative analysis was carried out by a Clemex image analyser.

4.2.1 SEED processed unrefined AA7075 base alloy

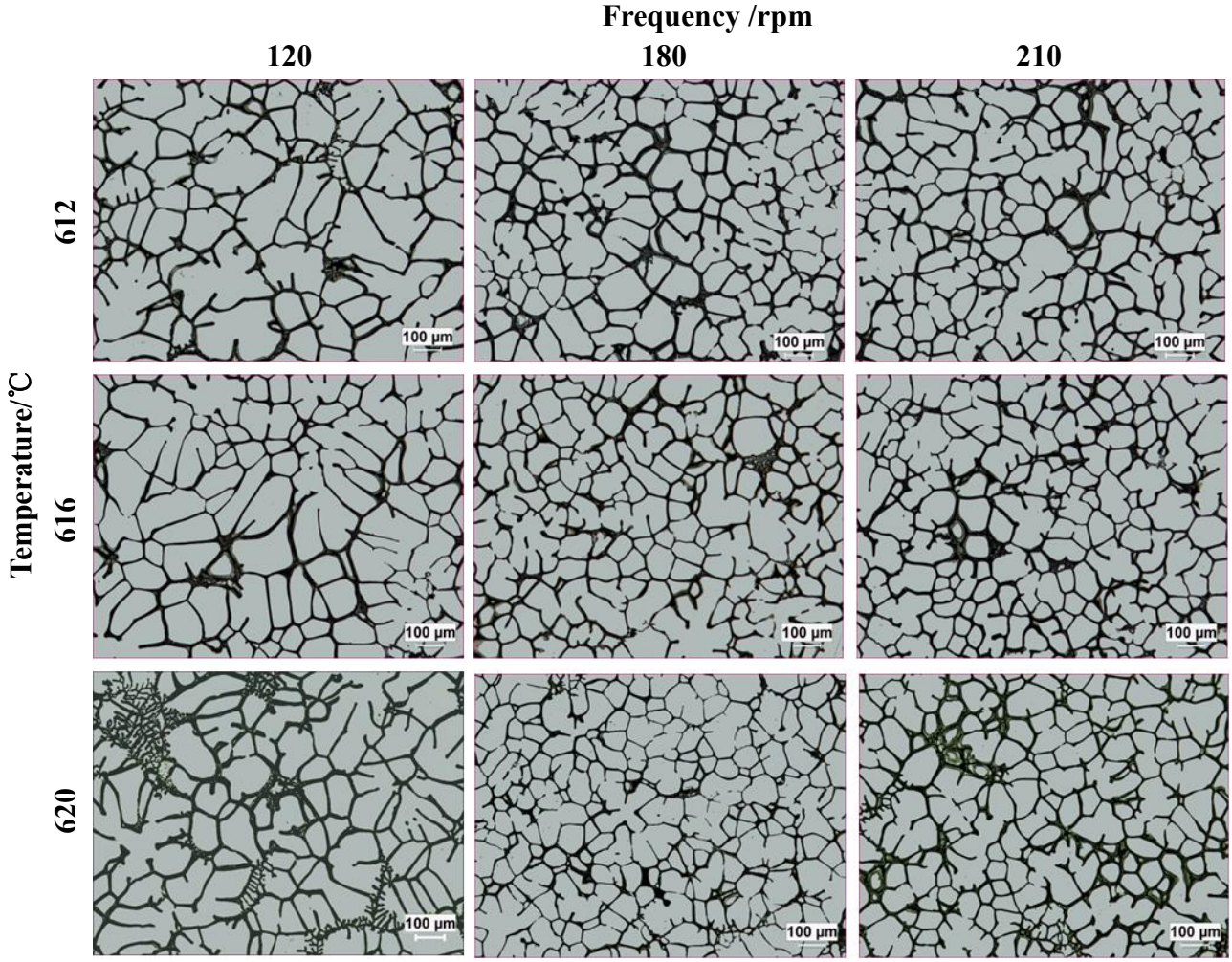

Fig. 4.2 Optical micrographs of SEED processed semisolid billets AA7075 base alloy under different processing conditions

The optical micrographs in **Figure 4.2** show the microstructure variations for the 7075 base alloy under different SEED processing conditions. From the optical micrographs, it is clear to identify that microstructures of the billets fabricated by the SEED processing mainly consist of

primary α-Al particles, surrounded by a small amount of eutectic liquid. The bright particles are primary α-Al and the dark phase is the eutectic phase. From the micrographs, it is clear shown that the string frequency has a strong influence on the morphology of the grains. With the increasing of the string frequency from 120 rpm to 210 rpm for each demolding temperature, the amount of dendrite grains becomes smaller and the number of grains in rosette-like or globular shape becomes larger. Besides, with the increasing string motion the grain size tend to become smaller. This is mainly because that the string movement causes the fragment of the dendrite arms and those broken arms grow up as new grains. This indicates that from the lower swirling frequency to the higher, it is shown great tendency to the transformation of the α-Al grains from large dendrite structure to the finer rosette-like or fairly globular gains. This grain transformation significantly reduces the resistance of melt flow during the die filling processing. **Fig. 4.2** also shows that with the increasing of the demolding temperatures, the grain size tend to be smaller because to reach a lower demolding temperature longer processing time is needed and grains grow up larger.

In order to further highlight the inter-relationship between microstructures and SEED processing parameters, quantitative metallography was carried out by Clemex image analysis system. Mean grain size and grain's aspect ratio of SEED processed 7075 base alloy were measured. To guarantee the accuracy of the data, at least 800 grains were measured.

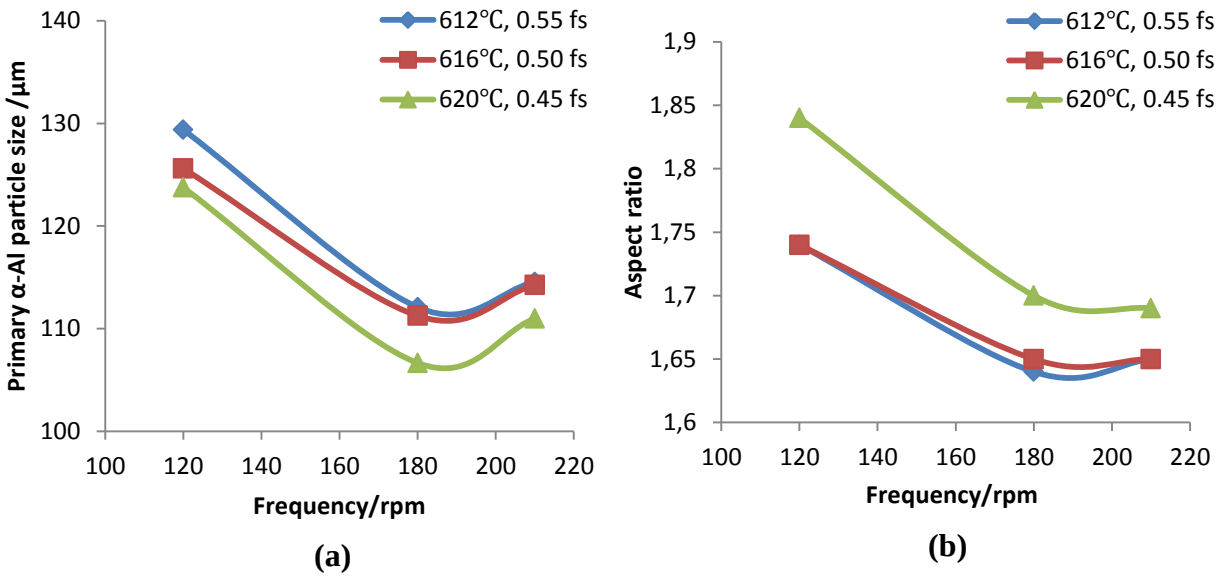

Note: an error of ±10% must be considered for graphs.

Fig. 4.3 Effect of SEED processing parameters on (a) Mean grain size and (b) Grain aspect ratio of AA7075 base alloy

Fig. 4.3 (a) shows the mean grain size of the primary α-Al particles. It was found that the average primary α-Al particle size decreased from 125.61μm at 120 rpm frequency to 111.25μm at 180 rpm for the semisolid billet demolded at 616 ℃, which the stirring movement gave rise to the fragmentation of large dendrite arms, resulting in smaller grain size. However, by further increase to the maximum frequency that the SEED equipment could offer, 210 rpm, the mean grain size stayed constant or increased slightly. It might be explained from that with further increase of swirling, the grains' fragmentation no longer occurred, and individual grains even tend to attach each other, resulting in slightly larger grain size. Comparing the mean grain size at various demolding temperatures at certain frequency, it can be seen that the average α-Al particles size marginally increased with lower demolding temperature. To reach lower demolding

temperature, longer processing time was required, which gave grains longer growing time, leading to slightly larger grain size.

Fig. 4.3 (b) shows the aspect ratio of primary α-Al particles. For the billet demolded at 620℃, by increasing the frequency from 120 to 180 rpm the aspect ratio significantly decreased from 1.84 to 1.7, respectively, indicating improved globularity. However, with additional increase to 210 rpm, it kept constant or slightly increased. On the contrary, lower demolding temperature produced higher aspect ratio, which can also be related to long processing time or long grown time.

4.2.2 SEED processed TiB_2 refined AA7075 alloy

According to the results above, the minimum grain size of the SEED processed AA7075 base alloy proofed to be 107μm at 180 rpm swirling frequency and 620℃ demolding temperature. Meanwhile, the minimum aspect ratio is 1.64 at 180 rpm swirling frequency and 612℃ demolding temperature. In order to obtain much more finer and globular grains for semisolid AA7075 alloy, typical grain refiner TiB_2 was applied. And the effect of SEED processing parameters on microstructure of this refined alloy was also investigated.

Fig. 4.4 shows the optical micrographs of SEED processed semisolid billets of AA7075 alloy modified with 0.03% TiB_2 under different processing conditions. From the optical micrographs, it is clear to recognize that the grains are considerably finer than AA7075 base alloy. Dendrite structures disappeared even at very low swirling frequency. Instead, the primary α-Al particles show a small amount of rosette-like and a large proportion of fine globular grains.

Generally, with the increasing of string frequency the grain size has a slight decreasing and the morphology of grains tends to be more globular.

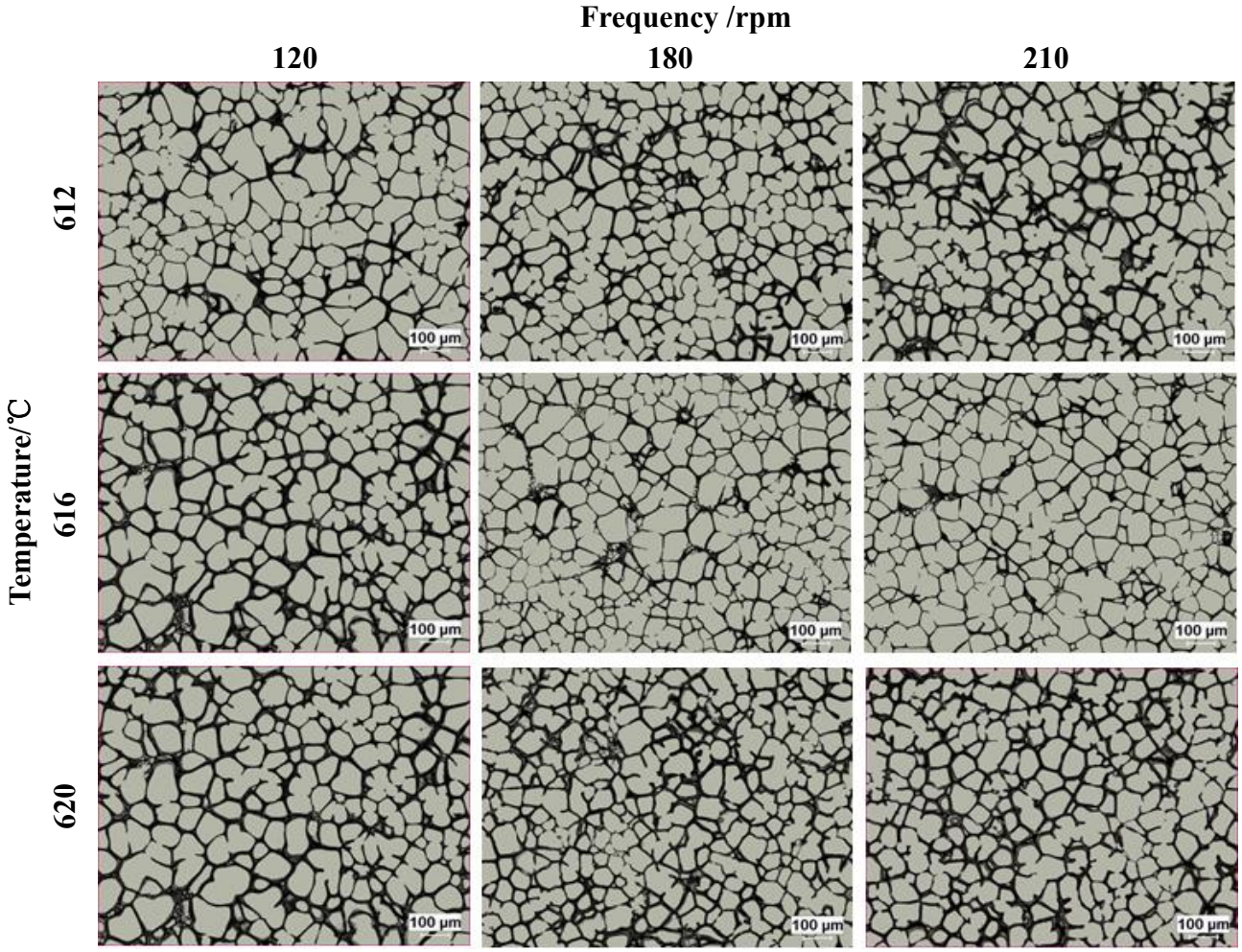

Fig. 4.4 Optical micrographs of SEED processed semisolid billets of AA7075 alloy modified with 0.03% TiB_2 under different processing conditions

In the same way, the mean grain size and the aspect ratio of this SEED processed alloy was quantitively characterized by Clemex analyzer same as for AA7075 base alloy as shown in **Fig. 4.5**. From **Fig. 4.5 (a)**, it is found that for a given temperature, the change of the mean α-Al particle size for this refined alloy with the increasing frequency follows almost similar trend as

unrefined base alloy. At the 180 rpm frequency and 620℃ temperature, the mean grain size reaches the minimum value of 94μm. In the meantime, higher demolding temperature results in smaller grain size at a fixed frequency, which due to shorter grown up time for grains.

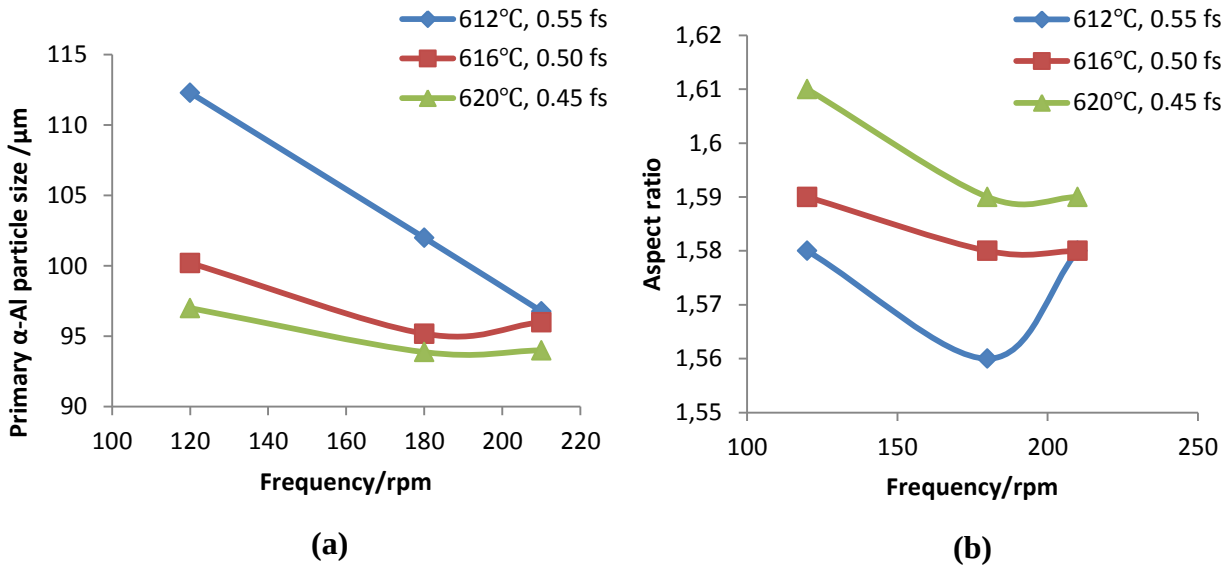

Note: an error of ±10% must be considered for graphs.

Fig. 4.5 Effect of SEED processing parameters on (a) Mean grain size and (b) Grain aspect ratio of 0.03wt%TiB_2 modified AA7075 alloy

However, considering the billets SEED processed at 616℃ and various swirling frequencies, the maximum and minimum grain size of the modified AA7075 alloy are 100μm and 95μm respectively. It can be recognized that the SEED processing frequency triggers 6.0% reduction in mean grain size, which is more than two times smaller than that of AA7075 base alloy of 12.9%. Consequently, the effect of SEED processing parameters on the microstructure of 0.03%Ti grain refiner modified AA7075 alloy is much slighter than that on base alloy.

Fig. 4.5 (b) gives the aspect ratio of 0.03%Ti modified AA7075 alloy. Similar tendency is found compared to aspect ratio for AA7075 base alloy. For a given temperature, the aspect ratio decrease with the increasing frequency from 120 rpm to 180 rpm, due to the swirling movement, but with further increase in frequency, the aspect ratio keeps constant or increases slightly. At meantime, the aspect ratio decreases with the increasing demolding temperature.

4.3 Effect of Grain Refiners on SEED Processed Microstructures of AA7075 Alloys

In order to optimize the microstructure of SEED processed AA7075 alloy, two kinds of typical grain refiner were added to the base alloy. Firstly, two percentages of TiB_2 (0.03%Ti and 0.06%Ti) were designed for the base alloy. Secondly, 0.1%Zr was added to the base alloy. After that, the AA7075 alloy with the combination of 0.1%Zr and 0.06%Ti was designed. The additions of grain refiner are summarized in **Table 4.1**. All of the alloys were SEED processed into the semisolid state following the same processing conditions as described before.

Table 4.1 Designed additions of grain refiners for AA7075 alloy (wt%)

Alloy#	1	2	3	4	5
TiB_2	**0**	**0.03**	**0.06**	**0**	**0.06**
Zr	**0**	**0**	**0**	**0.06**	**0.06**

4.3.1 Effect of grain refiner on primary α-Al grains

Figure 4.6 shows the morphologies of SEED processed AA7075 alloy under the optimum swirling frequency obtained from section 4.2, which is 180 rpm, and the same demolding temperature 616 ℃.

With the increasing amount of TiB_2, the grains transfer from dendrite to rosette-like to globular particles (**Fig. 4.6 (1)**, **(2)** and **(3)**). Meanwhile, there is an evident decrease in grain size with the increasing percentage of TiB_2. The AA7075 base alloy with addition of 0.06wt%Zr is mainly composed of the dendrite grains, shown in **Fig. 4.6 (4)**, which is similar to the AA 7075 base alloy. When the same amount of Zr was added to the AA7075 alloy with 0.06wt%Ti, the gains transform into fine globular particles, which is slightly larger than that of AA7075 alloy with only 0.06wt%Ti (**Fig. 4.6 (5)**).

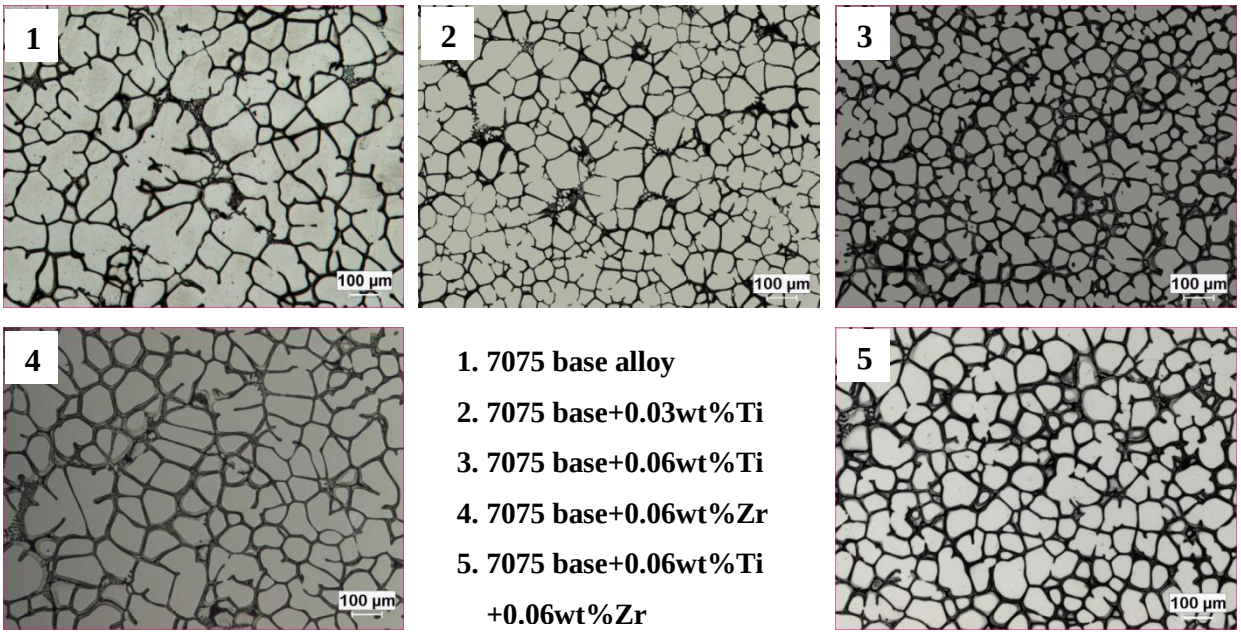

Fig. 4.6 Optical micrographs of SEED processed AA7075 semisolid billets with various grain refiners at 616℃ and 180 rpm

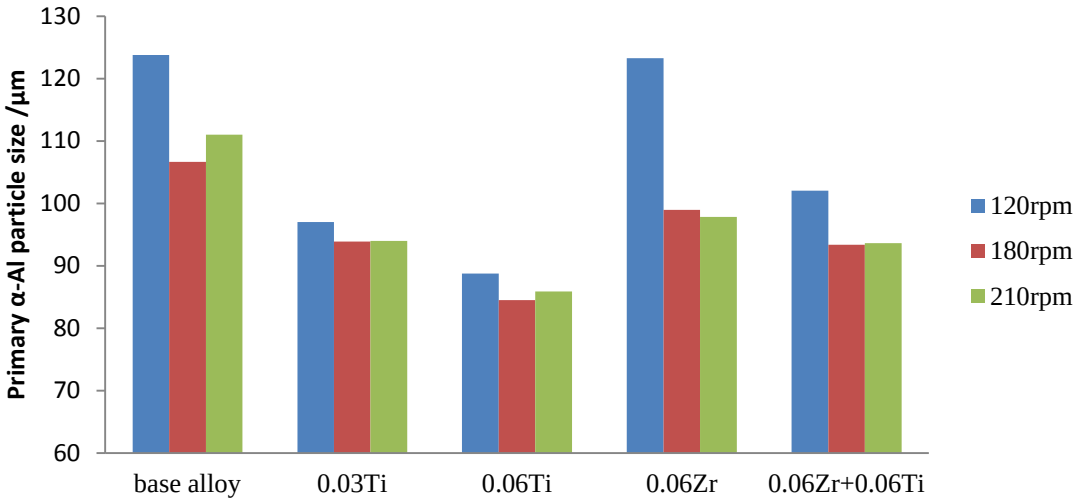

Fig. 4.7 Mean size of primary α-Al particles in AA7075 alloys (Processing temperature: 616℃)

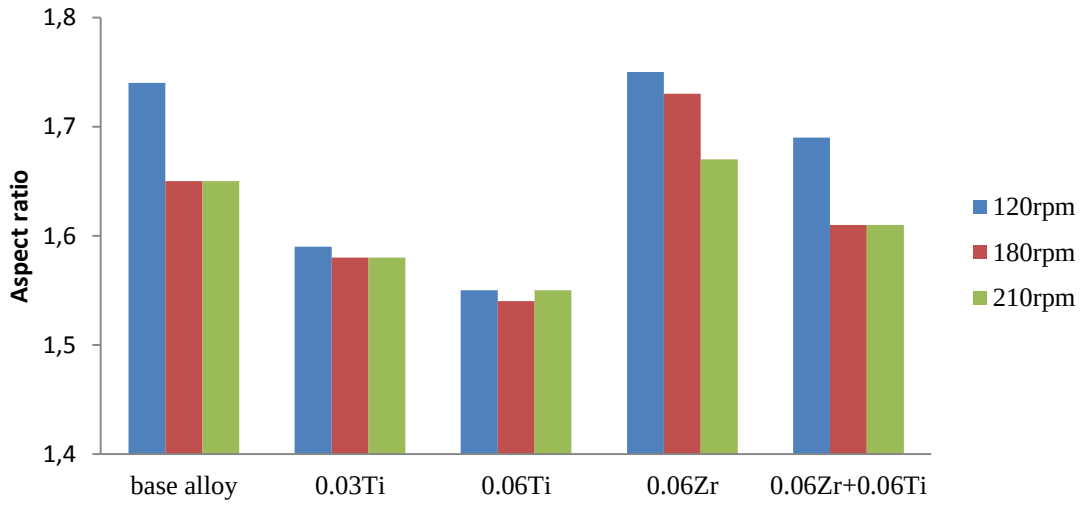

Fig. 4.8 Aspect ratio of primary α-Al particles in AA7075 alloys (Processing temperature: 616℃)

The mean grain size and the aspect ratio of primary α-Al particles of five categories of AA7075 alloys were measured with image analysis (Clemex) and presented in the histograms of **Fig. 4.7** and **Fig. 4.8**. It can be seen from **Fig.4.7** that as the percentage of TiB_2 increases, the grain size of primary α-Al shows a significantly decrease. And meanwhile the aspect ratio also decreases significantly, showing excellent grain refinement and morphology improvement, as

shown in **Fig.4.8**. Comparing base alloy with 0.06Zr, it can be seen that the Zr doesn't spur obvious refinement for the grain size, and the morphology of the primary α-Al deteriorates significantly.

AA7075 alloy with 0.06wt% TiB_2

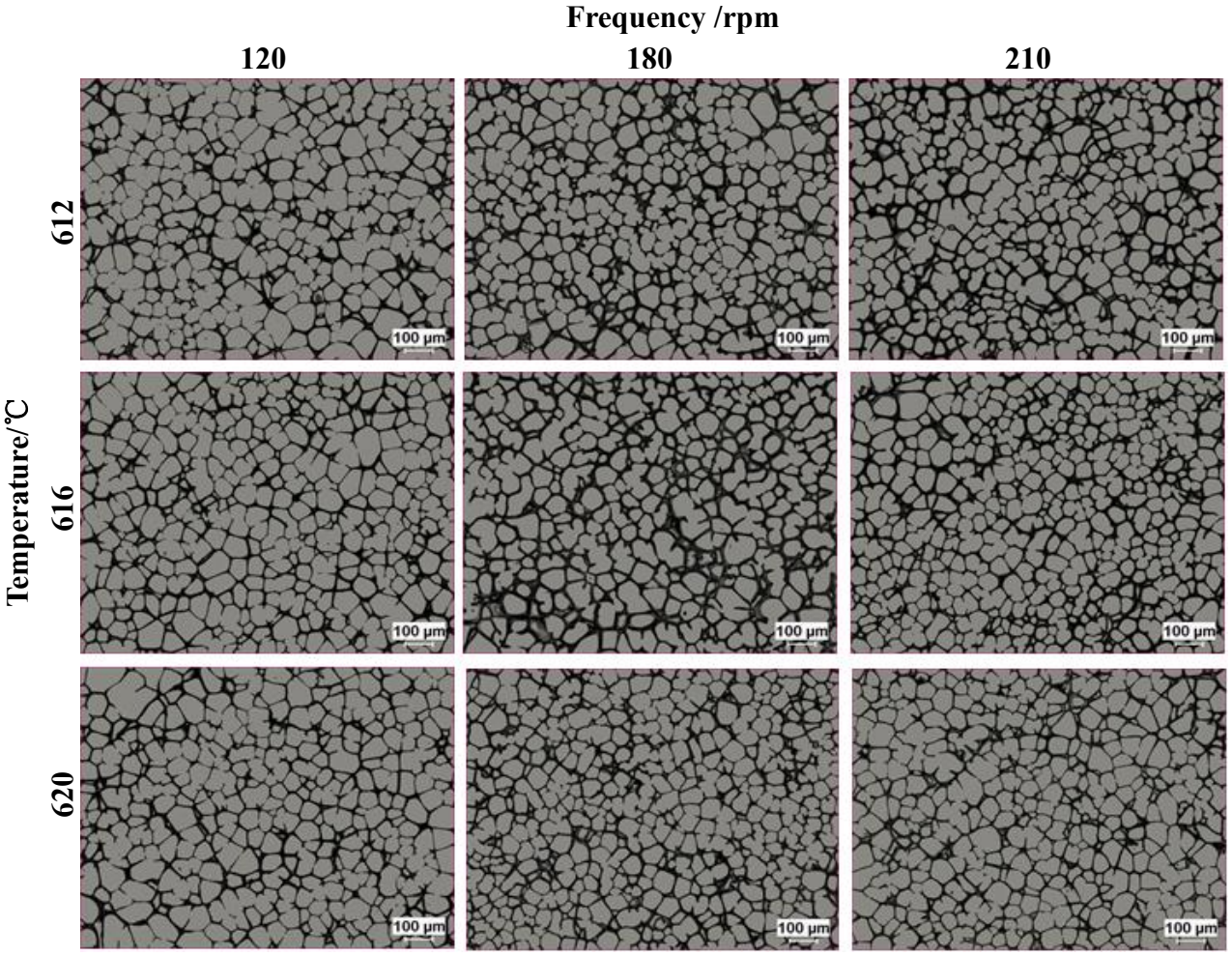

Fig. 4.9 Optical micrographs of SEED processed semisolid billets of AA7075 alloy modified with 0.06%TiB_2 under different processing conditions

Furthermore, when the Zr is combined with Ti, the grain size of primary α-Al increases from 85μm in only 0.06Ti alloy to more than 100μm. And relatively the aspect ratio also

increases almost 10%. The results indicated that the TiB_2 has positive refinement on primary α-Al grains of AA7075 alloy and higher amount of TiB_2 promote the transformation from large dendrite or rosette to finer spherical one. However, the Zr presents negative effect on microstructure of AA7075 alloy, especially combined with TiB_2.

All these grain-refined AA7075 alloys were SEED processed under various swirling frequencies and demolding temperatures, as described as section 4.2. And all the microstructures were optically observed and quantitively characterized

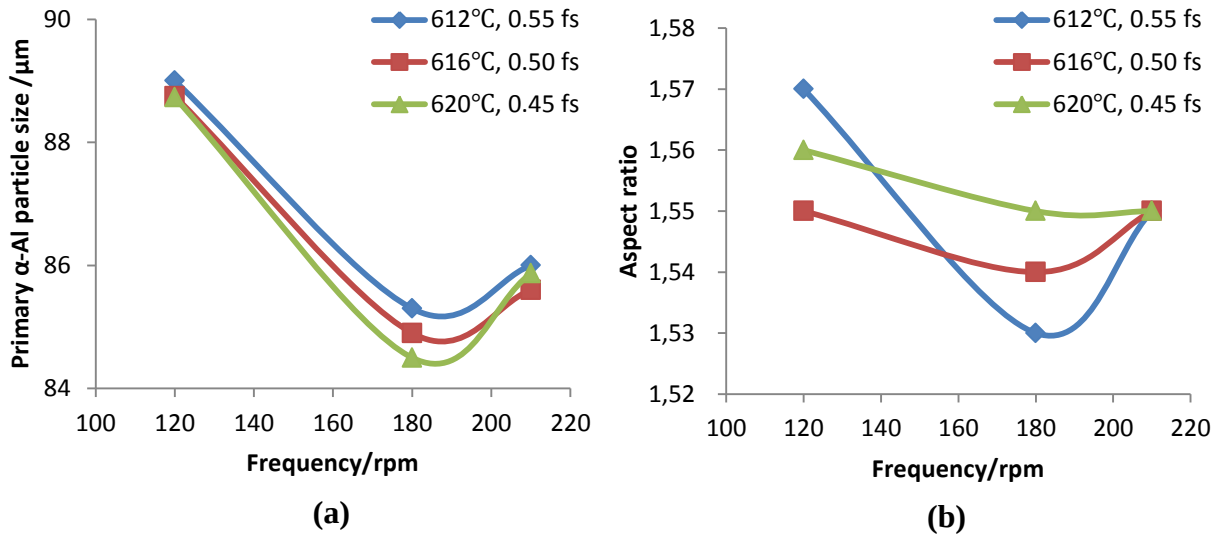

Note: an error of ±10% must be considered for graphs.

Fig. 4.10 Effect of SEED processing parameters on (a) Mean grain size and (b) Grain aspect ratio of 0.06wt%TiB_2 modified AA7075 alloy

Fig. 4.9 shows the optical micrographs of SEED processed semisolid billets of AA7075 alloy modified with 0.06%TiB_2 under different processing conditions. It is clear to notice that this SEED processed alloy mainly consists of fine globular primary α-Al grains surrounded by eutectic liquid phase. With the refinement of 0.06%TiB_2, it is hard to find large rosette-like morphology. The grains are further finer and more globular compared to 0.03%TiB_2 AA7075

alloy. Likewise, there is no considerable difference on the morphology of the Sudoku micrographs. Therefore, it is confirmed again that SEED processing parameters no longer have strong effect on the microstructures of TiB_2 refined AA7075 alloy.

AA7075 alloy with 0.06wt% Zr

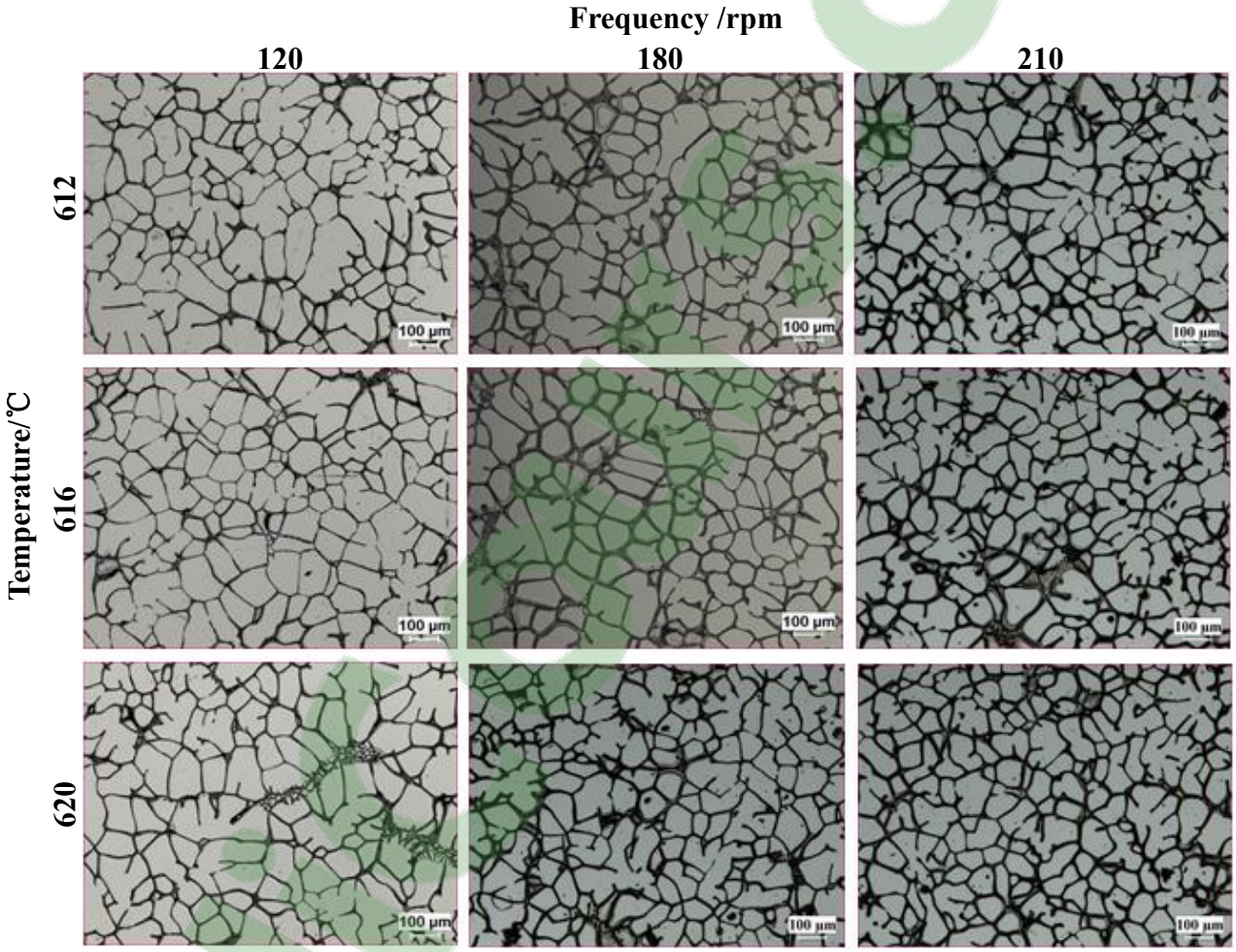

Fig. 4.11 Optical micrographs of SEED processed semisolid billets of AA7075 alloy modified with 0.06wt% Zr under different processing conditions

From the quantitative characterization shown in **Fig. 4.10**, it can be seen that the mean grain size changes from 89μm at 120 rpm frequency to 85μm at 180 rpm then up to 86μm at 210

rpm. **Fig. 4.10 (b)** shows the aspect ratio of 0.06TiB_2 refined AA7075 alloy. Except the similar tendency as found before, the aspect ratio exhibit smaller value, performing excellent shape factor.

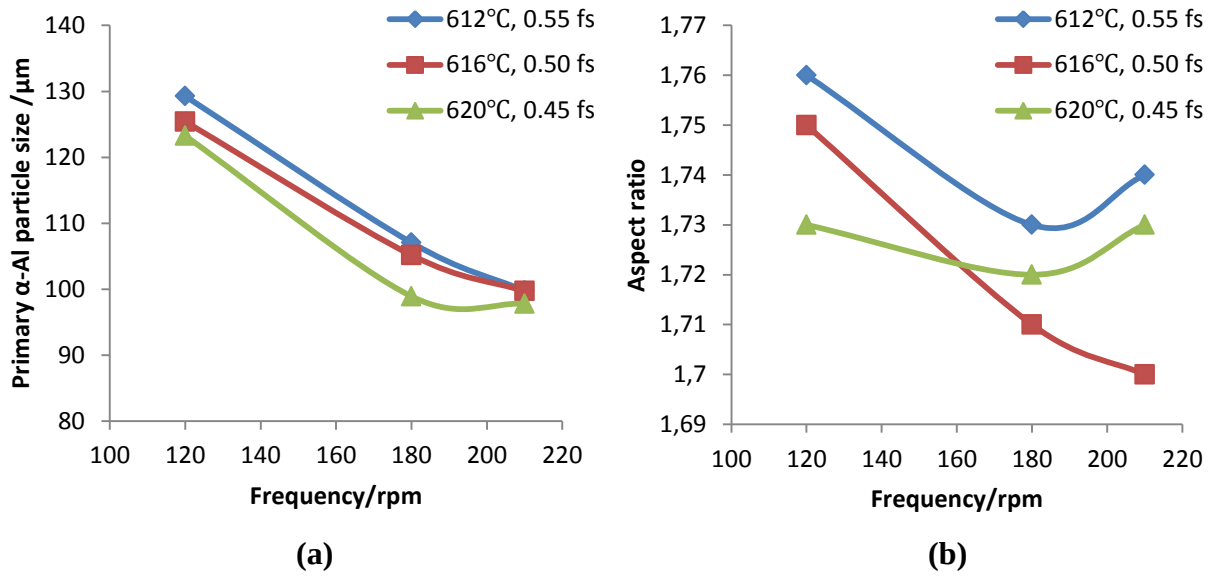

Note: an error of ±10% must be considered for graphs.

Fig. 4.12 Effect of SEED processing parameters on (a) Mean grain size and (b) Grain aspect ratio of 0.06wt%Zr refined AA7075 alloy

Fig. 4.11 shows the optical micrographs of SEED processed semisolid billets of AA7075 alloy refined by 0.06wt% Zr under various processing conditions. It is clearly shown that the observed microstructure is quite similar to that of base alloy. The refinement of 0.06wt% Zr is not that much significant compared to TiB_2. And the measured mean grain size and aspect ratio of the primary α-Al particles confirmed the similarity with base alloy, as shown in **Fig. 4.12 (a)** and **(b)**.

AA7075 alloy with 0.06wt%TiB_2 + 0.06wt% Zr

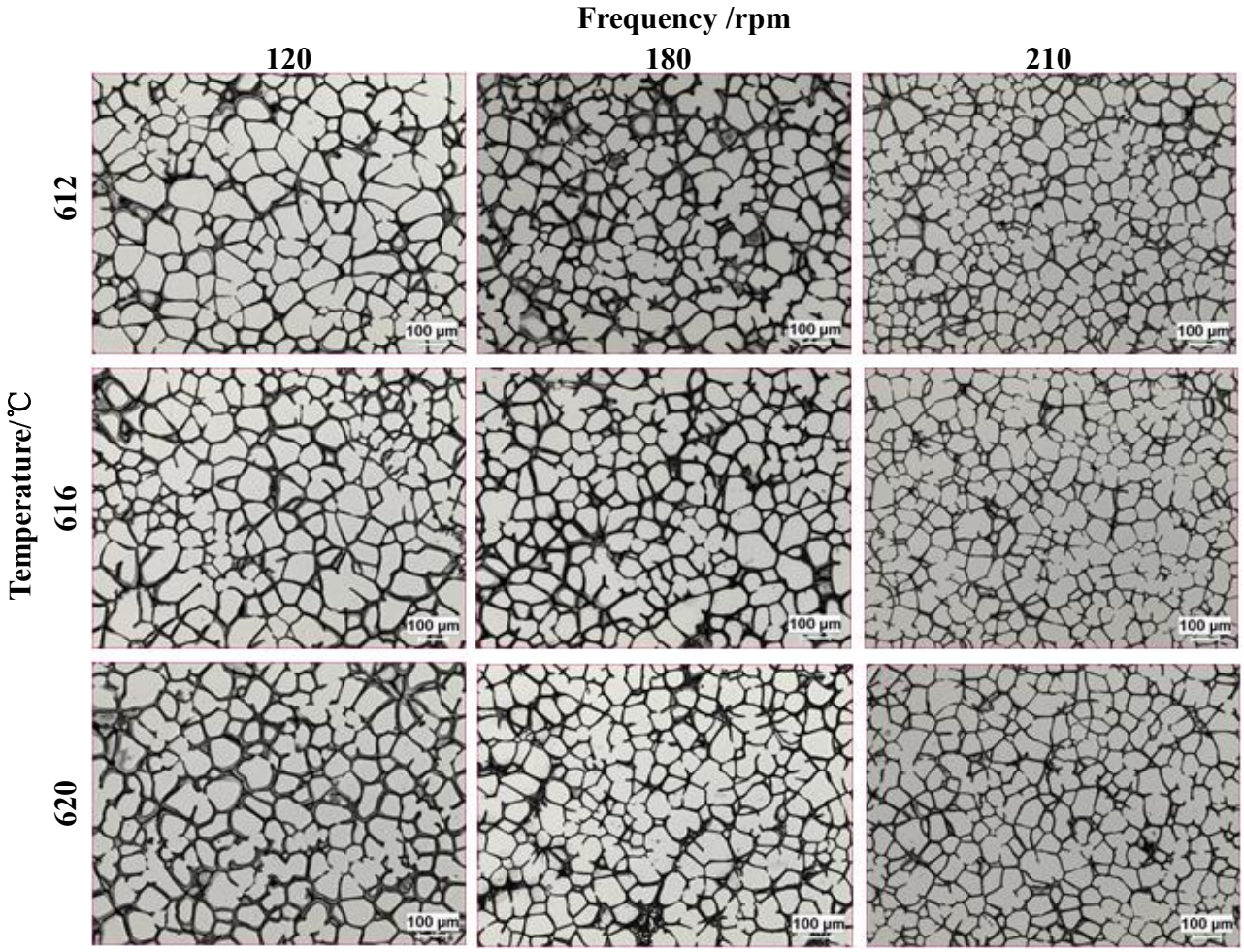

Fig. 4.13 Optical micrographs of SEED processed semisolid billets of AA7075 alloy modified with 0.06wt% Zr +0.06wt% TiB_2 under different processing conditions

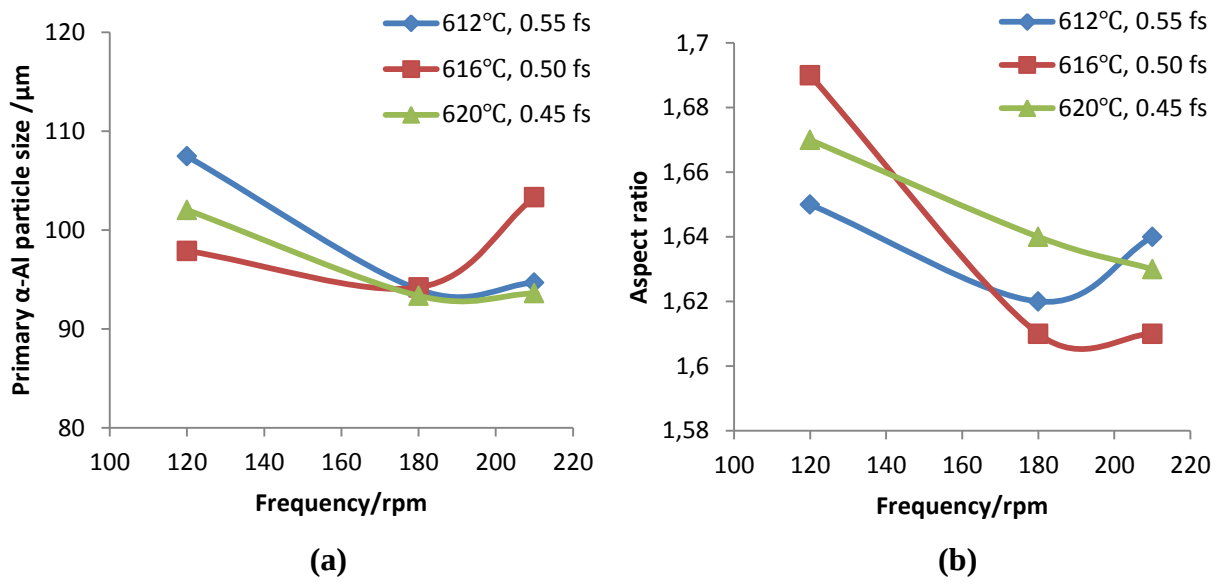

Note: an error of ±10% must be considered for

Fig. 4.14 Effect of SEED processing parameters on (a) Mean grain size and (b) Grain aspect ratio of 0.06wt%TiB_2 + 0.06wt%Zr refined AA7075 alloy

Fig. 4.13 and **Fig. 4.14** give the observed microstructure and image analysis results of the 0.06wt%TiB_2 + 0.06wt%Zr refined AA7075 alloy under various SEED processing conditions. Results show that the addition of 0.06wt% Zr didn't cause obvious change on the microstructure from the 0.06wt%TiB_2 refined alloy. Comparing the mean grain size and aspect ratio from 0.06wt%TiB_2 refined alloy and 0.06wt%TiB_2 + 0.06wt%Zr combined refined alloy (**Fig. 4.14** and **Fig. 4.10**), it is interesting to find that the addition of 0.06wt%Zr increased the grain size and aspect ratio slightly, showing a negative refinement.

4.3.2 Effect of grain refiner on intermetallic phases

It is found that the typical microstructure of as-cast AA7075 alloy are mainly composed of primary α-Al grains and three kinds of intermetallic phases along the grain boundary (shown in **Fig. 4.15 (a)**). According to the SEM-EDX analysis (**Table 4.2**) and literatures[4-7], these three kinds of intermetallic phase are identified as bright quaternary $Mg(Zn,Cu,Al)_2$ phase, grey iron rich phase Al(Fe,Mn)Si and black Mg_2Si phase (**Fig. 4.15**).

It is noted that Zn, Mg and Cu are the main alloying elements in AA7075 alloy. Therefore, among three intermetallic particles, the quaternary $Mg(Zn,Cu,Al)_2$ phase has the highest volume fraction of 4% approximately. It is generally believed that this kind of quaternary phase is mainly derived from the binary Zn_2Mg phase, in which the Zn was substituted by Cu and Al simultaneously[4]. Under high magnification observation (**Fig. 4.15 (b)**), it can be seen that the $Mg(Zn,Cu,Al)_2$ is network-like, eutectic structure with primary α-Al. When it is observed under relative low magnification, the whole eutectic structure attached along the grain boundary looks like string. Mg_2Si phase exhibits two morphologies at the grain boundary. When Mg_2Si is generated at the triple boundary area among three grains, it presents triangle network morphology (**Fig. 4. 15 (b)**); when at the boundary of two adjacent grains, Mg_2Si is found to be string-like blocky particle or linear shape network structure. The iron rich phase Al(Fe,Mn)Si almost has the equal volume fraction with Mg_2Si, which is mostly found to be Chinese script blocky morphology along the grain boundary. It is noted that the Al(Fe,Mn)Si phase is derived from the typical δ-AlFeSi phase which is quite common in Al-Si alloy. During the formation of δ phase in the solidification process, part of the Fe atoms were substituted by Mn atoms, leading to coexistence of Fe and Mn in δ phase[7].

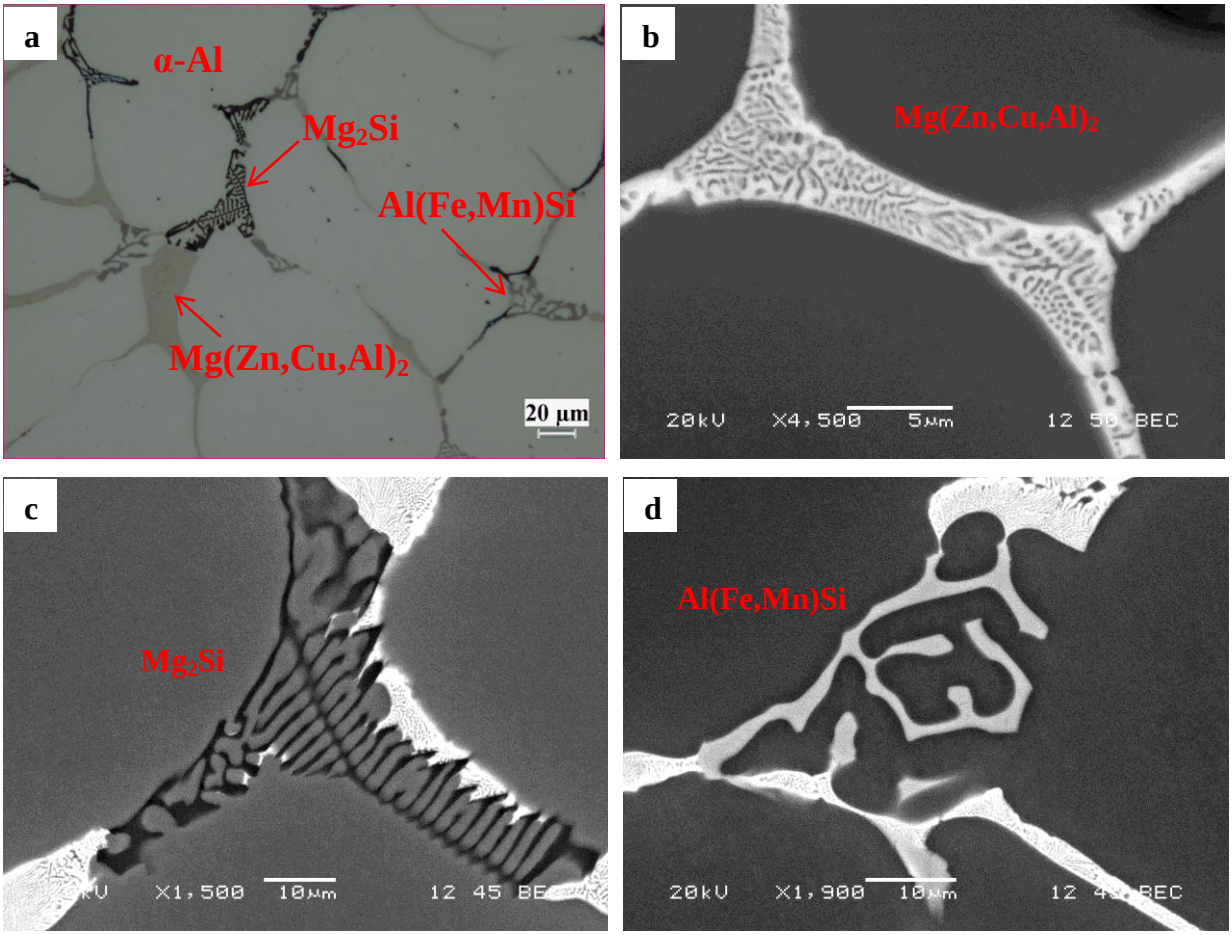

Fig. 4.15 (a) Optical micrograph and SEM micrographs:
(b) $Mg(Zn,Cu,Al)_2$, (c) Mg_2Si, (d) Al(Fe,Mn)Si of AA7075 alloy

Table 4.2 SEM-EDX analysis results of AA7075 semisolid sample processed by SEED (at.%)

Element	Al	Zn	Mg	Cu	Fe	Si	Mn
$Mg(Zn,Cu,Al)_2$	55.11	18.77	16.59	9.52	0.00	0.00	0.00
Al(Fe,Mn)Si	77.88	0.00	0.00	0.00	14.45	4.11	3.56
Mg_2Si	25.26	0.00	41.95	0.00	0.00	32.79	0.00
α-Al	93.47	3.76	2.77	0.00	0.00	0.00	0.00

To some extent, size and shape of the grains can be controlled by the grain refiner through heterogeneous grain nucleation, as results proved in present project. Simultaneously, the grain refiner can also modify the size, shape and distribution of the intermetallic phases at the grain boundary.

Figure 4.16 shows the optical micrographs of semisolid alloys corresponding to the (a, b) 7075 base alloy, (c, d) 0.03wt%Ti addition and (e, f) 0.06wt%Ti addition. The microstructure of the SEED processed semisolid AA7075 alloys shown in **Fig. 4.16** consist of dendrite primary α-Al particles, surrounded by three types of intermetallic structures. The black particles circled in green line are Mg_2S; the gray particles fenced in blue line are iron rich Al(Fe,Mn)Si; the bright string-like phase enclosed in red line is $Mg(Zn,Cu,Al)_2$.

As shown in **Figure 4.16 (a)** and **(b)**, the $Mg(Zn,Cu,Al)_2$ phase in the base alloy exhibits a coarse string-like morphology. However, after adding 0.03wt% Ti, the $Mg(Zn,Cu,Al)_2$ string phase becomes shorter and narrower as shown in **Fig. 4.16 (c)** and **(d)**. But the refinement and the modification with the addition of 0.06wt% Ti is not much more obvious than that with 0.03wt% Ti addition as shown in **Fig. 4.16 (e)** and **(f)**. After comparing all images in **Fig. 4.16**, it is interesting to find out that, with addition of 0.06wt% Ti to the AA7075 alloy, the $Mg(Zn,Cu,Al)_2$ string phase become very fine, indicating that addition of 0.06wt% Ti has effective refinement on this intermetallic phase.

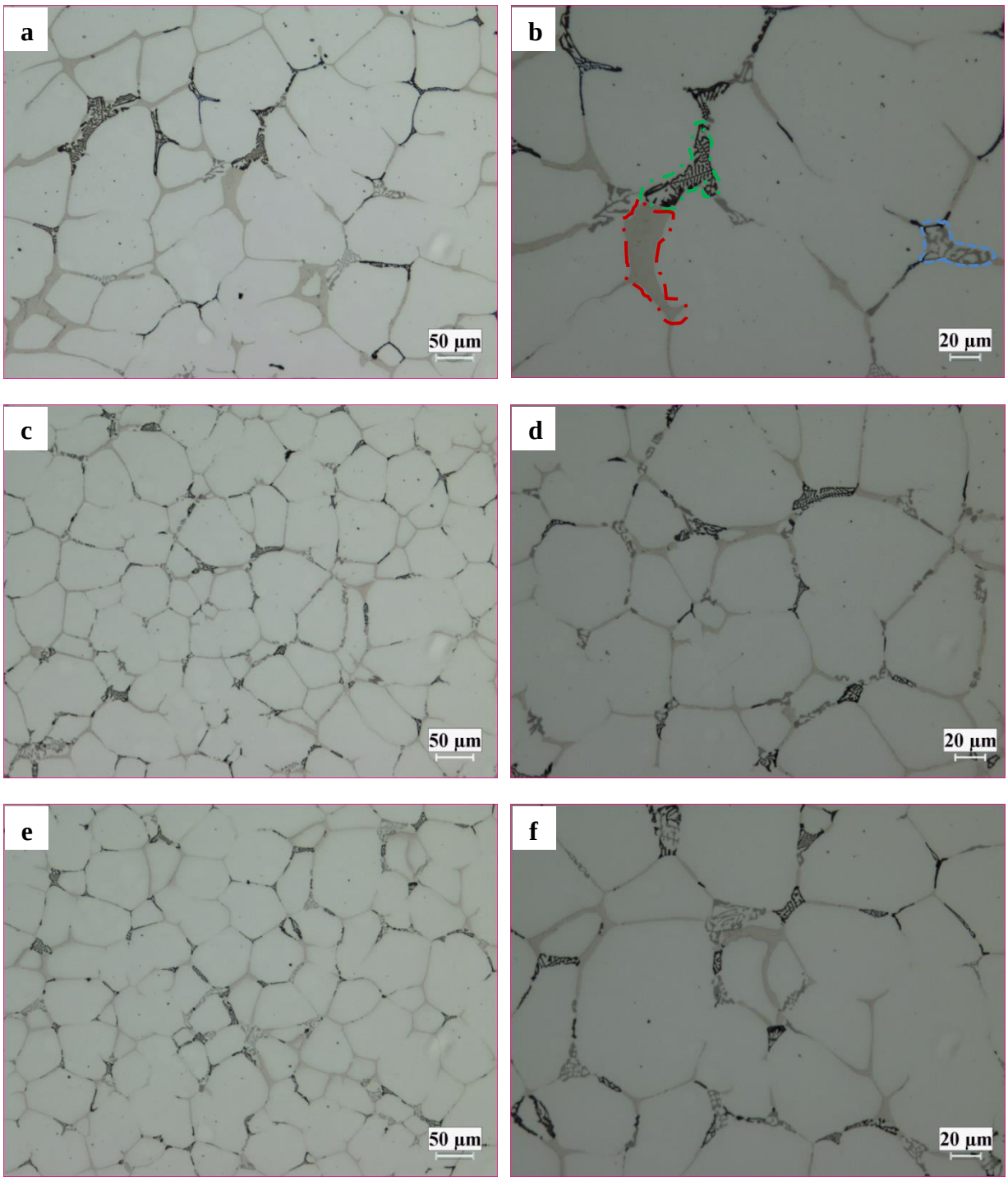

Fig. 4.16 Optical micrographs showing effect of Ti on the intermetallic phases of (a), (b) AA7075 base alloy; (c), (d) 0.03wt%Ti; (e), (f) 0.06wt%Ti

Figure 4.16 also shows the effect of TiB_2 on the formation of Mg_2S and Al(Fe,Mn)Si intermetallic phases in AA7075 semisolid alloy. These two eutectic phases have the similar volume fraction of around 1.00%. As shown in the picture, the Mg_2S phase in the unmodified AA7075 alloy displays an aggregate grille-like morphology. Meanwhile, the iron rich phase has a complicated Chinese script-like structure as indicated in **Fig. 4.16**. However, with the Ti addition these two phases are both well refined, resulting in smaller size "grilles" and "Chinese scripts". At the same time, their distributions become more uniform, surrounding the primary α-Al grains.

From the optical micrographs, it is shown that accompanied with the refined primary α-Al grains, the addition of TiB_2 leads to substantial difference in the size, morphology and distribution of three types of intermetallic phases. To quantitatively characterize to effect of Ti on these intermetallic phases, the string length, string width, area percentage and particle density of three types of intermetallic were quantitively characterized by Clemex analyzer **(Fig. 4.17** and **Fig. 4.18**).

Figure 4.17 illustrates the string size of $Mg(Zn,Cu,Al)_2$ phase as a function of addition of Ti. The string length decreases from 47.1 (base alloy) to 22.3 (0.03Ti) and 14.0μm (0.06Ti), as shown of the red bar in **Fig. 4.17 (a)**. The string width decreases from 0.96 (base alloy) to 0.80 (0.03Ti) and 0.69μm (0.06Ti). The sharp decrease of the string length and width of $Mg(Zn,Cu,Al)_2$ phase obvious reveal the refinement of this intermetallic phase through Ti addition. Results in **Fig. 4.17** also indicates that the string length and width of Mg_2Si and Al(Fe,Mn)Si intermetallic compounds both decrease with the increasing addition of Ti.

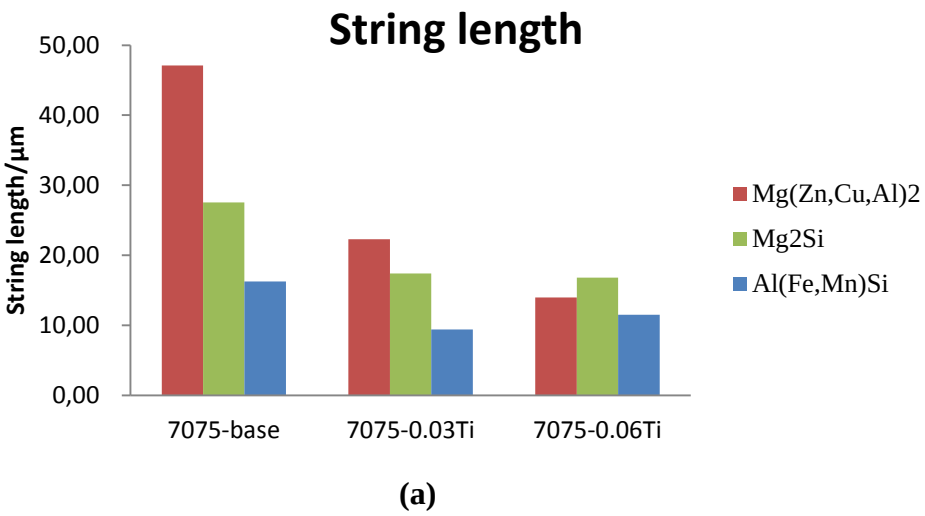

(a)

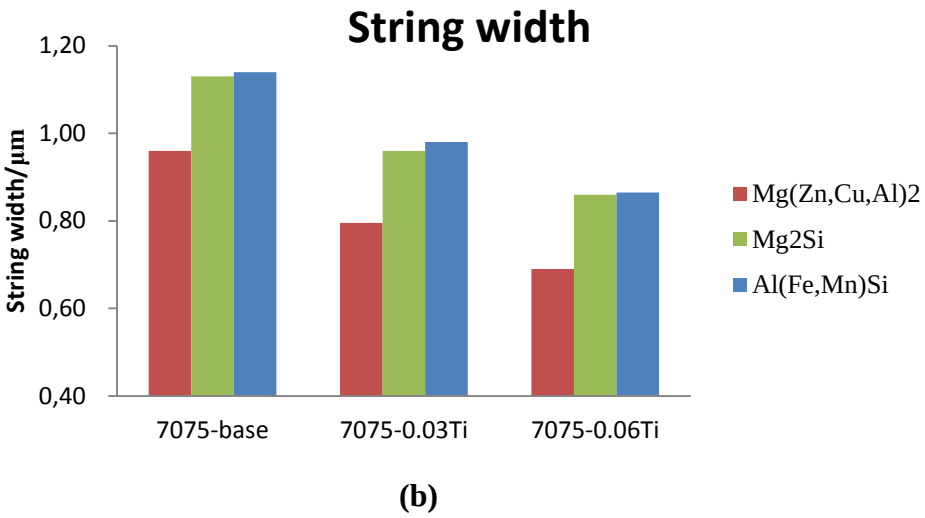

(b)

Fig. 4.17 (a) The string length and (b) width of three types of intermetallic in AA7075 base alloy and alloys modified with TiB_2.

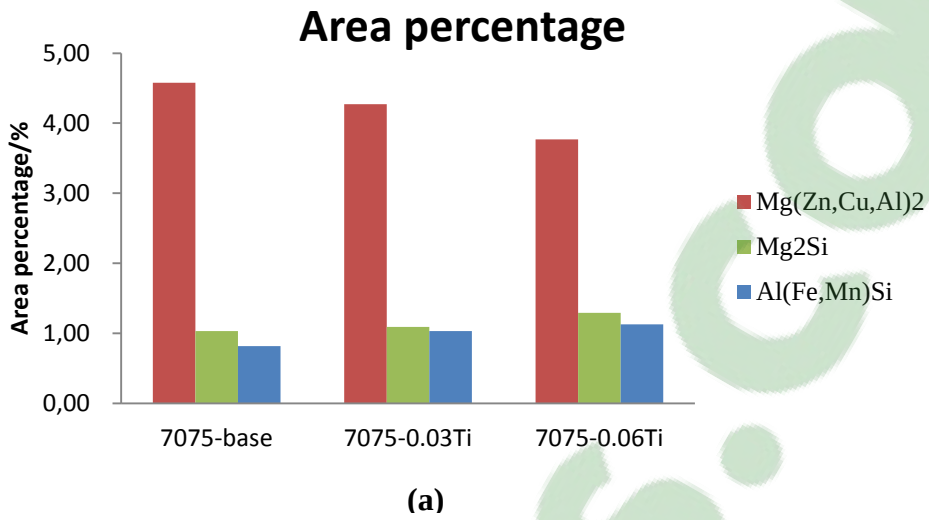

(a)

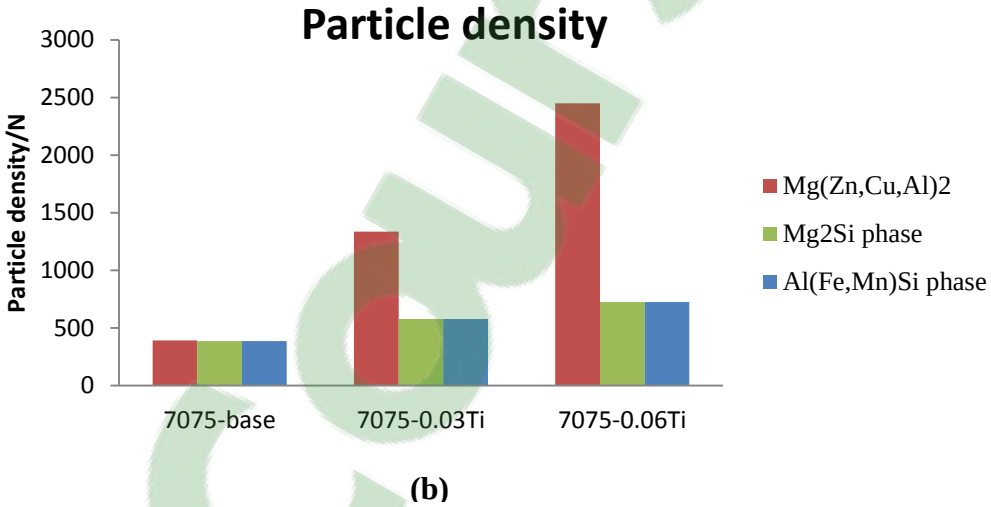

(b)

Fig. 4.18 (a) The area percentage and (b) particle density of three types of intermetallic of AA7075 base alloy and alloys modified with TiB_2.

Fig. 4.18 shows the area percentage and the particle density of this string-like phase in the base alloy and in the Ti-containing alloys. The area percentage of the $Mg(Zn,Cu,Al)_2$ phase shows a slight decrease with the increasing amount of Ti, while the area percent of Mg_2Si and Al(Fe,Mn)Si particles almost keep constant (**Fig. 4.18(a)**). The particle density results indicates

that the density of $Mg(Zn,Cu,Al)_2$ phase particles increases significantly with the addition of Ti because of their size reduction in the refinement processing.; meanwhile, the densities of Mg_2Si and Al(Fe,Mn)Si particles also increase by the increasing addition of Ti (**Fig. 4.18(b)**).

4.4 Rheoformability and Microstructure of Semisolid AA7075 Alloys

4.4.1 Rheoformability and microstructure of semisolid AA7075 base alloy

4.4.1.1 Microstructure of deformed semisolid AA7075 base alloy

Figure 4.19 shows the microstructures of the deformed billets of the base AA7075 alloy at different compression temperatures, as well as various solid fractions. Micrographs of the zones at the center, middle and edge of the deformed billets are exhibited. It can be seen that the microstructure of the deformed billet of base alloy is mainly made up of two phases, the dark phase and the bright phase. The bright phase consists of the primary α-Al particles preferentially solidified in dendrite-like or rosette-like grains, evenly distributed in the liquid matrix. The dark phase is regarded as the liquid phase, constituted by several eutectic phases discussed in chapter 4.3.2. As shown in **Fig. 4.19**, with the implementation of compression test, it was found that the liquid phase is forced to the exterior portion of the deformed billet, leaving the solid α-Al particles segregated to the center part. It was also found that the liquid segregation phenomenon looks much more obvious with lower solid fraction. This can be explained by the lower resistance for the liquid to flow long distance at lower solid fraction. Identically, this liquid segregation phenomenon was also observed by other researchers in semisolid field [8-10].

Edge **Middle** **Center**

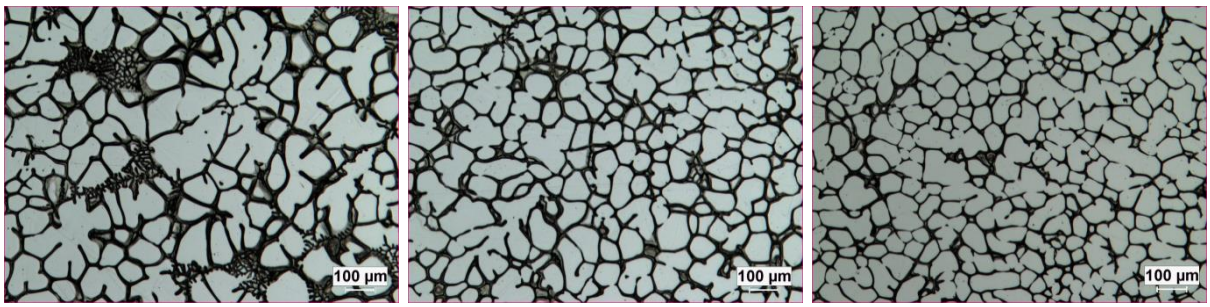

(a) 622℃ (0.42 fs)

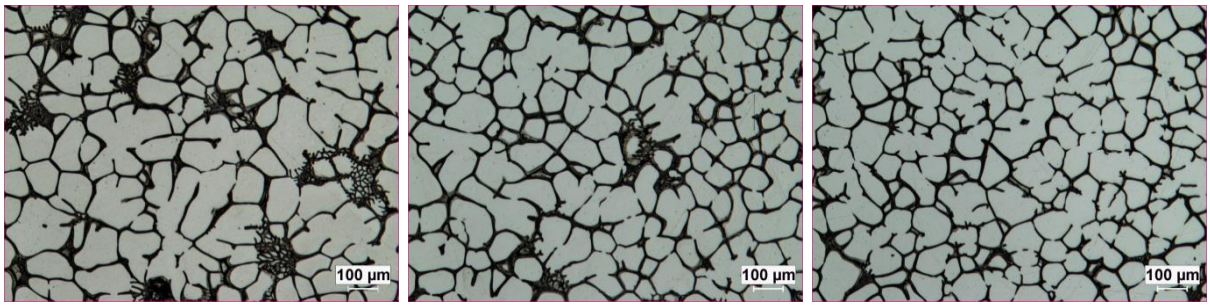

(b) 620℃ (0.45 fs)

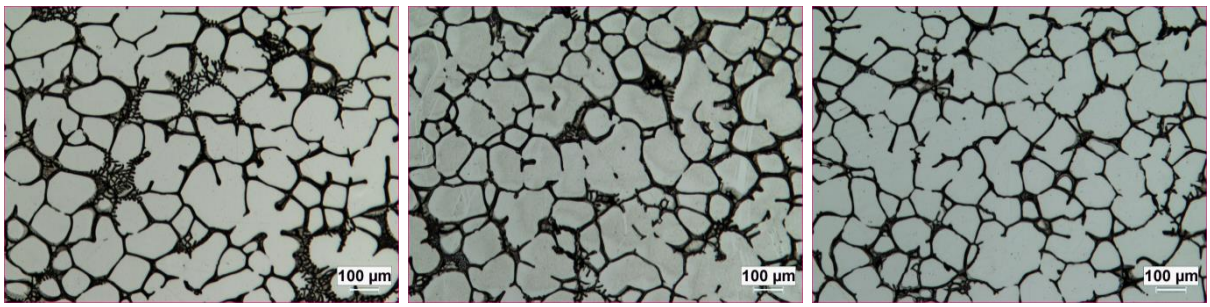

(c) 618℃ (0.48 fs)

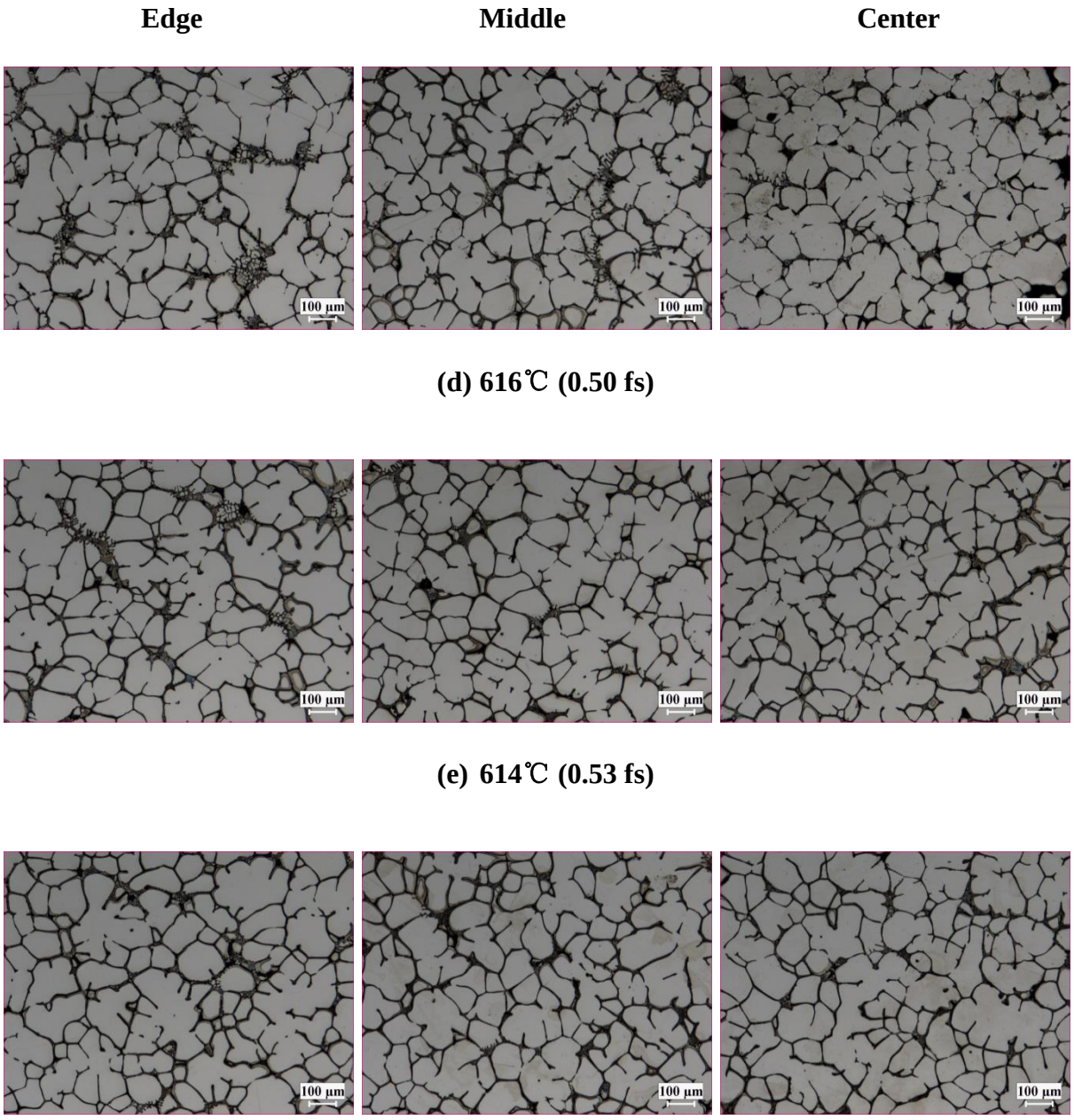

Fig. 4.19 Microstructure of deformed semisolid billets of AA7075 base alloy from the edge to the center, compressed at different temperatures (solid fractions): (a) 622℃ 0.42 fs, (b) 620℃ 0.45 fs, (c) 618℃ 0.48 fs, (d) 616℃ 0.50 fs, (e) 614℃ 0.53 fs, (f) 612℃ 0.55 fs.

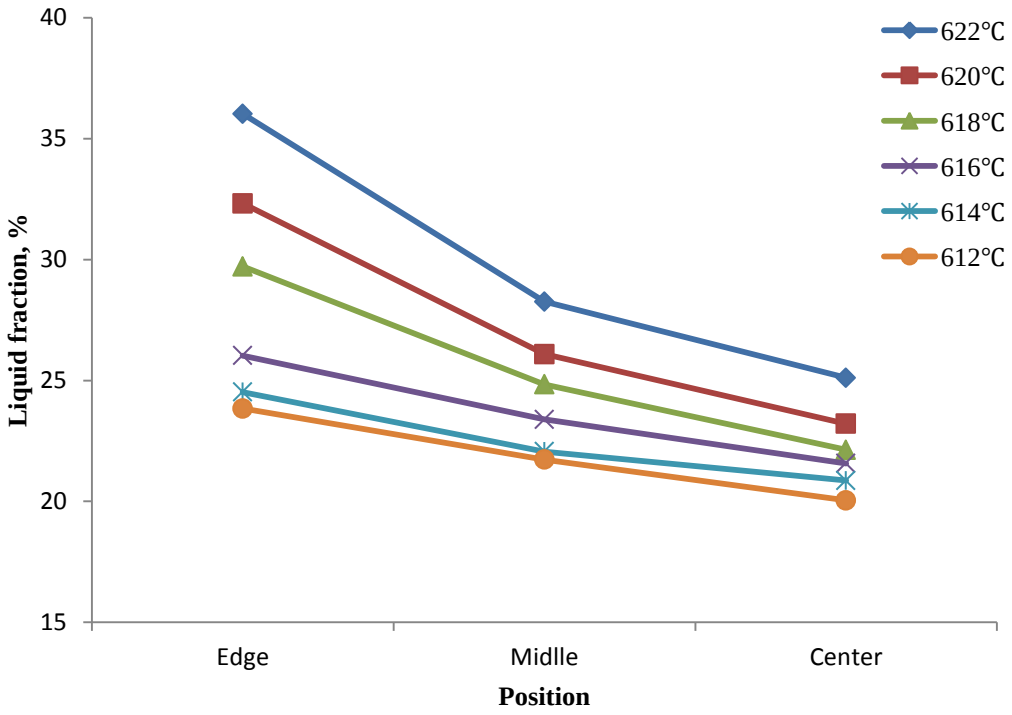

Fig. 4.20 Measured liquid fractions of deformed samples from edge to center at various compression temperatures.

Figure 4.20 illustrates the measured liquid fraction of the quick water quenched deformed billets right after compression test. Results show that the volume fraction of the liquid phase at the edge part of the specimens improved due to the liquid segregation from the center to the edge of the deformed billets. At higher compression temperature, the liquid segregation phenomenon becomes more significant than that at lower temperature.

4.4.1.2 Height reduction curves

During the parallel plate compression test on the AA7075 base alloy, the displacement to time curve will be obtained. This curve records the instantaneous height of semisolid sample according to time, which has been converted into height reduction, h/h_0, for analysis, where h_0 and h are the initial and instantaneous heights of the billet during compression test, respectively.

Fig. 4.21 shows the influence of different semisolid temperature, as well as various solid fractions, on the height reduction-time curves of the unrefined AA7075 base alloy. Results show that the height reduction rate decreases with the increasing semisolid temperature, which means the resistance to deformation increases with the increasing solid fraction. For AA7075 base alloy, the billets with solid fraction lower than 0.45 have the similar deformation behaviors, which the solid particles can roll and move easily under a given constant pressure. However, the billets with an increasing solid fraction higher than 0.45 can't be compressed quickly and completely. This is mostly because there are more opportunities for collisions between solid particles at a higher solid fraction.

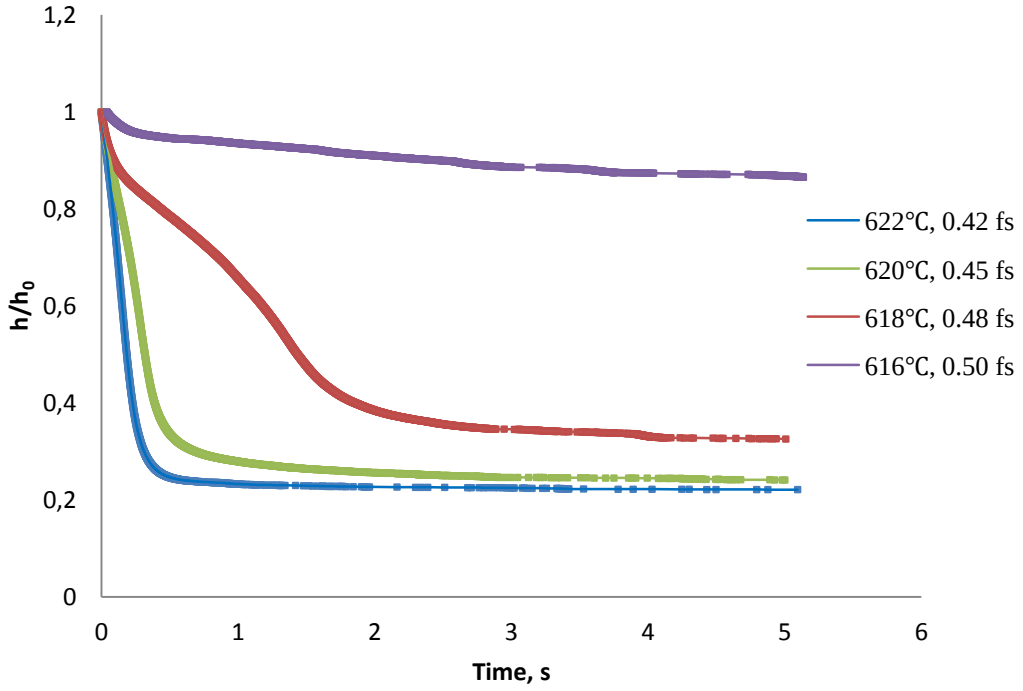

Fig. 4.21 Height reduction-time curves at different temperatures (℃) of AA7075 base alloy

Fig. 4.22 gives the real images of the deformed semisolid billets of AA7075 base alloy. It can be clearly seen that at 620℃ and 622℃, the deformation of the semisolid billets is quite sufficient and complete. At 618℃, the resistance to deformation starts to increase slightly, but the grains still can move great distances, resulting in insufficient and incomplete deformation. When the demolding temperature is lower than 616℃ (solid fraction is higher than 0.50), the billets preform great resistance to the deformation, mainly because there is not enough "liquid space" for the solid particles to move and roll, they are contacting each other and cannot move large distance in the melt. When the solid fraction reaches 0.55 (612℃), the semisolid billet ceases the compression because a solid network of particles in the center of the billet has formed and this network can support the weight of the dead weight applied in parallel-plate viscometer. Obviously, semisolid billets of base alloy under 618℃ show poor rheoformability and die filling capability. Meanwhile, the final heights of these deformed billets are equivalent or even larger than their radius, making them unsuitable for the rheological analysis model introduced above.

Fig. 4.22 Physical images of compressed billets by parallel plate viscometer at different temperatures of AA7075 base alloy

4.4.1.3 Shear rate to time curves

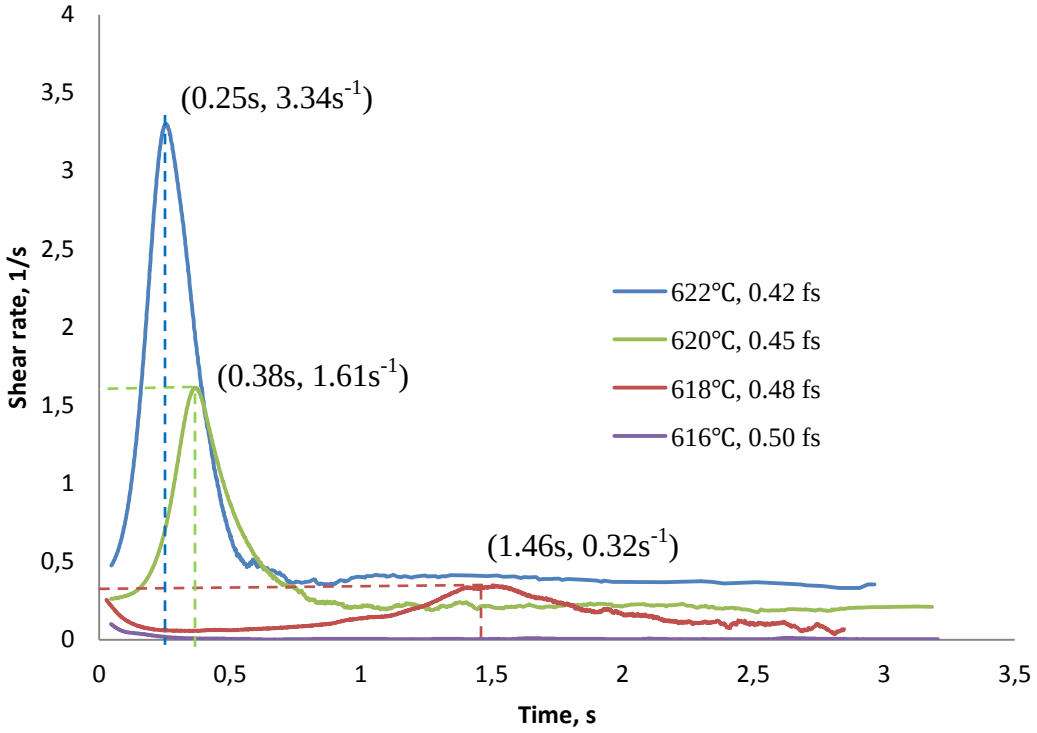

Fig. 4.23 Shear rate-time curves at different temperatures (℃) of AA7075 base alloy

It is commonly admitted that shear rate has an influence on the flow behavior of the semisolid alloys. Once the semisolid billets is under shear, the agglomeration and the de-agglomeration phenomena of the suspended particles and the flow of the liquid matrix occur on the micro level, while deformation happens on the macro level. The apparent viscosity of the slurry strongly depends on the agglomeration and de-agglomeration phenomena under shear. Therefore, to predict the viscosity of the semisolid billet, the evolution of the shear rate of slurry under a fixed dead weight is analyzed.

Fig. 4.23 shows the corresponding evolution of shear rate to time at four different solid fractions of 0.50, 0.48, 0.45, 0.42. Results show that at a particular solid fraction, the shear rate firstly increases with time and then it decrease to steady state condition. When the semisolid billet is at static condition, a network among solid particles tends to be formed to make billet self-support. Under shear, the bridge network can easily break down, and solid particles start moving and rolling, resulting in increasing shear rate. As the deformation continuing, agglomeration of the solid particles leads to a decreasing shear rate.

Comparing the shear rate curves of different solid fractions, it can be seen that the shear rate jump occurs at various time and the peak value of the shear rate differs significantly. **Fig. 4.23** shows that the lower the solid fraction, the sooner the shear rate jump occurs, the higher the peak value of the shear rate. This can be explained by the particle interactions. At lower solid fraction, solid particles are easier to move large distance in the melt. However, as the solid fraction increases, there is great possibility to form a thick skeleton wall at the edge of the semisolid billet. Once the upper plate drops down, the outer skeleton first reduces the movement of plate, resulting in first decreasing of shear rate. After the crack of this skeleton, the shear rate starts to increases first and then decrease (shear rate-time curve at fraction solid of 0.48 in **Fig. 4.23**). It is interesting to note that with further increasing of solid fraction to 0.50 (616℃), the "shear rate jump" phenomenon disappears. It is slightly decreasing in a very low range (10^{-1} to 0) and this processing usually last a long time. This is mainly because of the formation of solid network at the center of the billets besides the skeleton, both causing resistance to deformation.

4.4.1.4 Rheology comparison

The rheology test was conducted under a certain dead weight on the rheocast semisolid billets fabricated in previous section. Two alloys were tested under different temperatures (solid fractions of the alloy). In this section, the AA7075 base alloy was compressed. The initial upper plate height was set at 25.0cm constantly and the dead weight was 20.0kg. The solid fraction varied between 0.50 and 0.42.

After the calculation of viscosity and shear rate from the recorded displacement-time data, a typical curve of viscosity and shear rate as a function of time at the solid fraction of 0.45 is plotted in **Fig. 4.24 (a)**. The rapid compression of the billet is conducted in less than 1 second. **Fig. 4.24 (a)** shows that the shear rate rapidly increases then decreases, with the maximum shear rate of 1.64 s^{-1} obtained at 0.34 second. Accordingly, the viscosity first drops rapidly and then increases during decreasing shear rate section. This inverse revelation between viscosity and shear rate characterizes the shear thinning behavior, which is found by many researchers [11-14]. Plotting the viscosity data as a function of shear rate from **Fig. 4.24 (a)**, the relationship of viscosity and shear rate is characterized in **Fig. 4.24 (b)**. It is found out that due to the various shear rate changings, the curve of viscosity-shear rate presents two sections: increasing shear rate section and decreasing shear rate section. It is found that the rate of change of viscosity is greater during the increasing shear rate section, which indicates the kinetic of disagglomeration is more rapid than that of agglomeration in the semisolid slurry[8].

Fig. 4.25 gives the rheological curves at the relative high solid fraction (0.48) of AA7075 base alloy. At solid fraction of 0.48, the shear rate first decreased before 0.3 second (marked Part O in **Fig. 4.25**) and then followed the increasing and decreasing period as described in **Fig. 4.24**.

Accordingly, the viscosity during Part O increased rapidly. This can be explained from the crash of the outer solidified skeleton. During the rheocasting process, the outer side of the billet solidified quickly because of large temperature gradient at the edge of the billet, forming a thin solid skeleton. With the falling down of the upper plate, the skeleton ceased the quick movement of the plate and crashed suddenly, resulting in shear rate decreasing. The plotted viscosity as a function of shear rate is shown in **Fig. 4.25 (b)**. It is found that the viscosity-shear rate curve presents three parts as predicted.

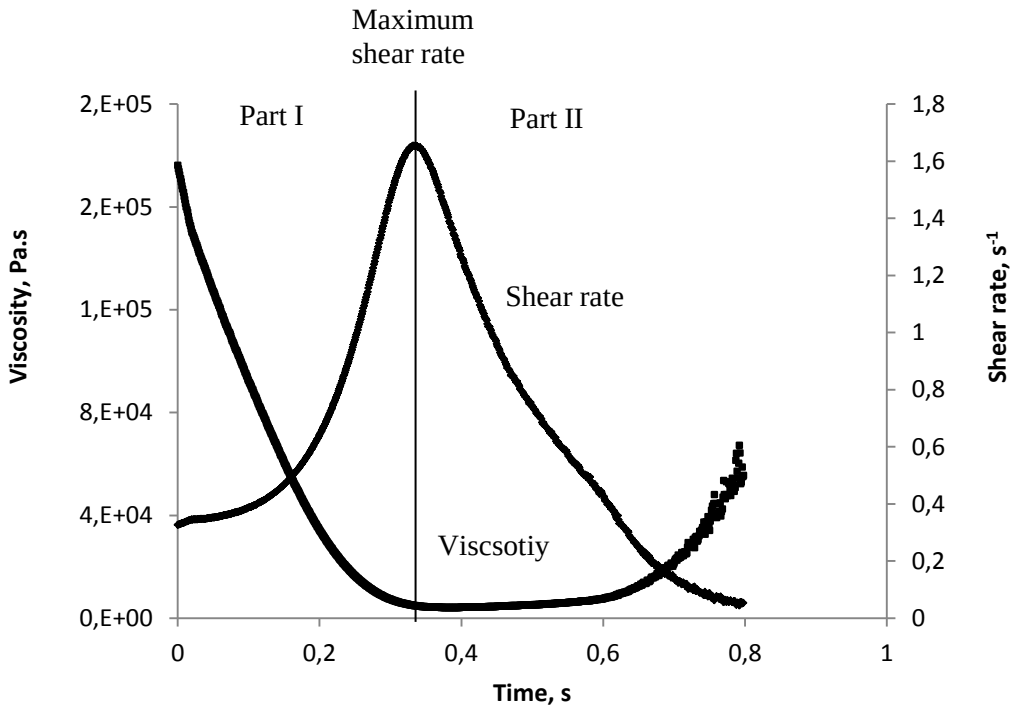

(a)

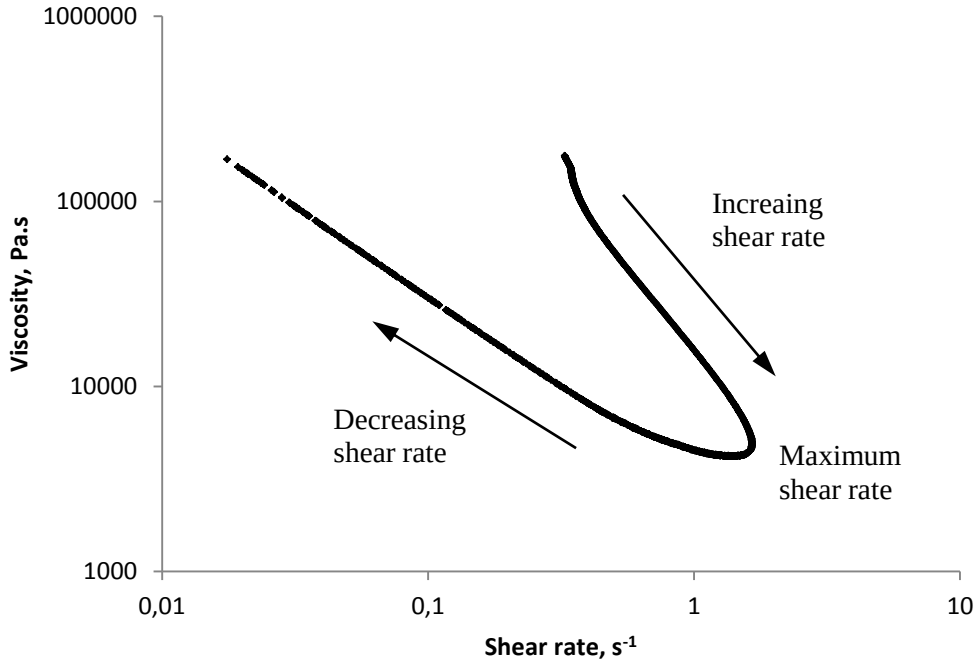

(b)

Fig. 4.24 Typical rheology curves used to analysis: (a) Instantaneous viscosity and shear rate as a function of time; (b) Viscosity as a function of shear rate.

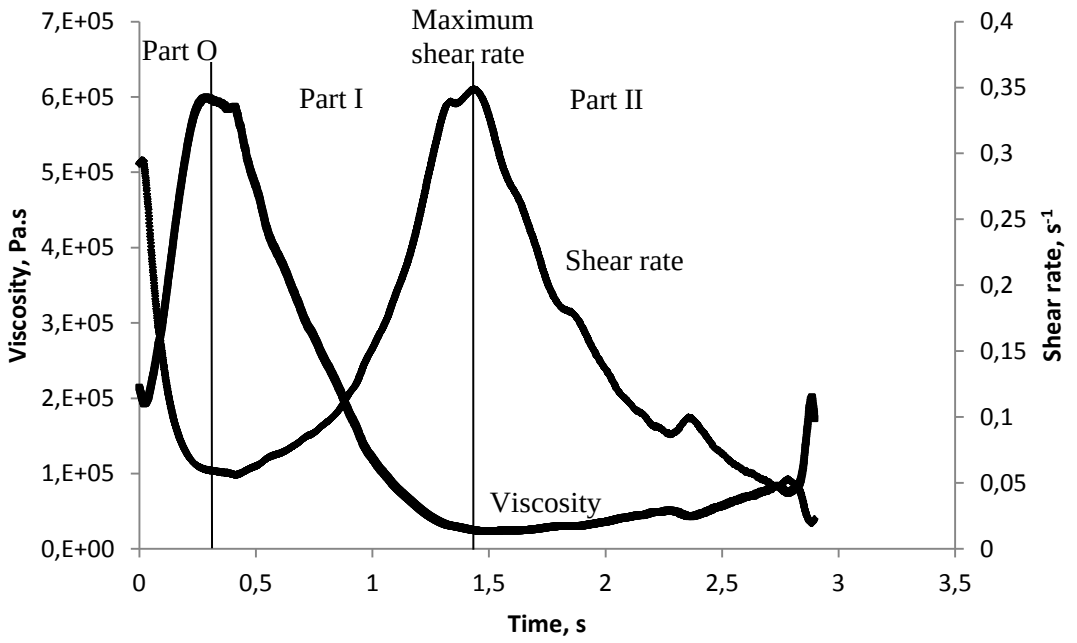

(a)

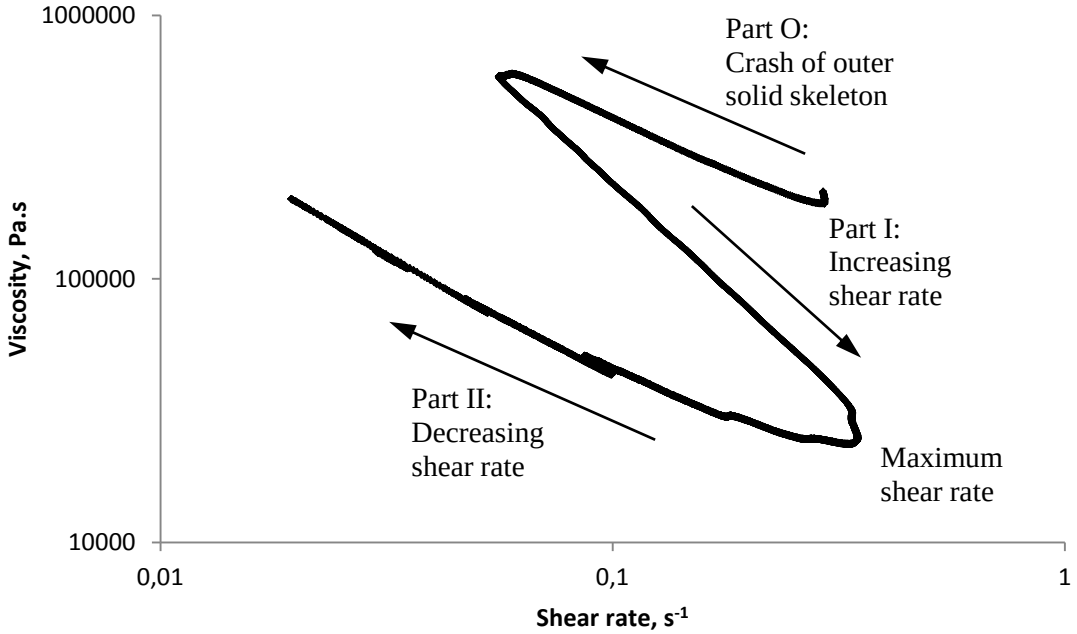

(b)

Fig. 4.25 Typical rheology curves used to analysis: (a) Instantaneous viscosity and shear rate as a function of time; (b) Viscosity as a function of shear rate. Condition: AA7075 base alloy at 618℃ (0.48 fs)

For a semisolid billet at an ideal solid fraction, the solid grains distribute uniformly in the liquid phase, with thin "bridges" between particles and particles, forming a solid network make the billet self-support. Once the compression happens, the bridges break up easily, grains can move large distance freely through the liquid space in a short time, resulting in the increasing shear rate part. As the compression continues, liquid phase segregates from the center to the edge of the billets, which narrows the liquid zone between grains in the central part of the billet. At this point the solid particles cannot move a large distance anymore because they are contacting each other, making deformation harder and slower. But grains still can rearrange over a short distance by rolling or sliding, resulting in the decreasing shear rate part.

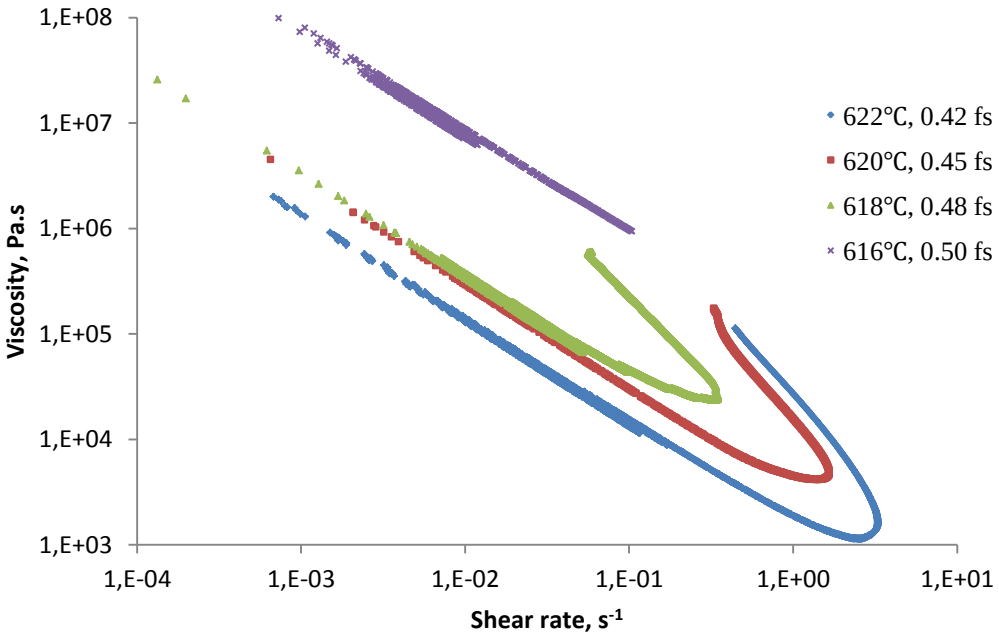

Fig. 4.26 Calculated viscosities as function of shear rate of AA7075 base alloy at various fractions solid.

Fig. 4.26 shows the calculated viscosity vs shear rate at various solid fractions from 0.50 to 0.42 during the parallel-plate compression viscometer experiment. Comparing the increasing shear rate section of solid fraction of 0.48, 0.45 and 0.42, it is found that the maximum shear rate increases significantly with the increasing of solid fraction due to the reduction of liquid space for free movement of solid particles. Accordingly, the viscosity at the maximum shear rate point drops dramatically, over one order of magnitude from 0.48 fs to 0.42 fs. It is interesting to note that with the solid fraction of 0.50, the increasing shear rate section is missing. This indicates that for AA7075 base alloy tested under current viscometer, when the solid fraction is higher than 0.50 there is no shear rate jump behavior happening during compression. The deformation directly turns into quasi steady state. That means billet with 0.48 solid fraction is the maximum solid fraction that can be rapidly compressed for base alloy under current experiments, which can be proved from the actual view of the compressed billets in **Fig. 4.22**. Comparing all the decreasing shear rate parts, it is found that at any given shear rate, the corresponding viscosity increases with the increasing solid fraction. It can be explained that billets at higher solid fraction has larger and more irregular grains. Besides, the liquid phase as the lubricant for grains sliding and rolling reduces with increasing solid fraction. Both explanations above will lift the resistance of deformation, resulting in increasing viscosity.

4.4.2 Rheoformability and microstructure of TiB_2 modified semisolid AA7075 alloy

4.4.2.1 Microstructure of deformed semisolid AA7075 alloy modified by TiB_2

Edge **Middle** **Center**

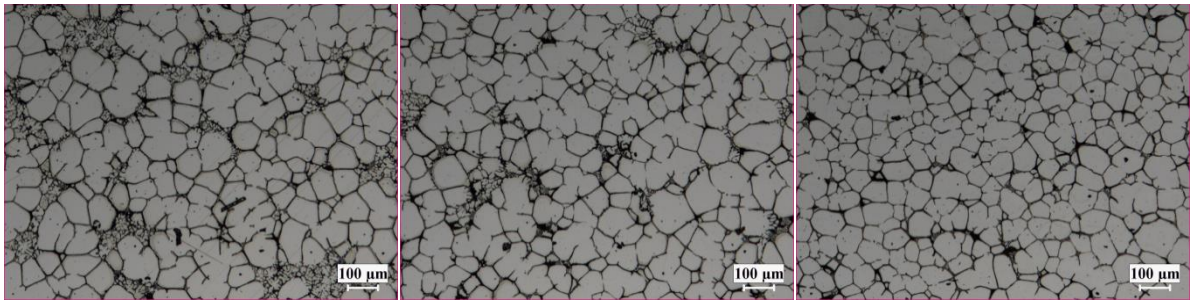

(a) 622℃ (0.42 fs)

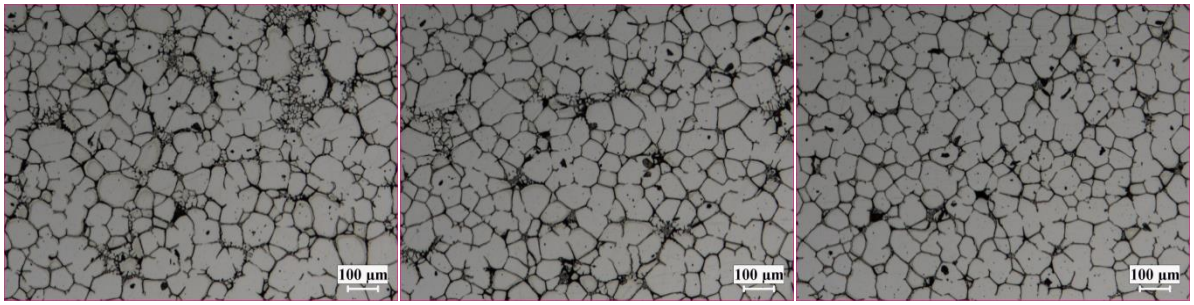

(b) 620℃ (0.45 fs)

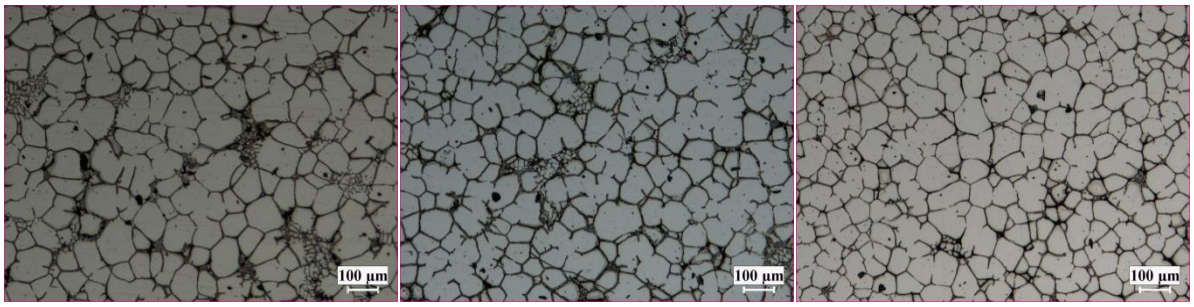

(c) 618℃ (0.48 fs)

Edge **Middle** **Center**

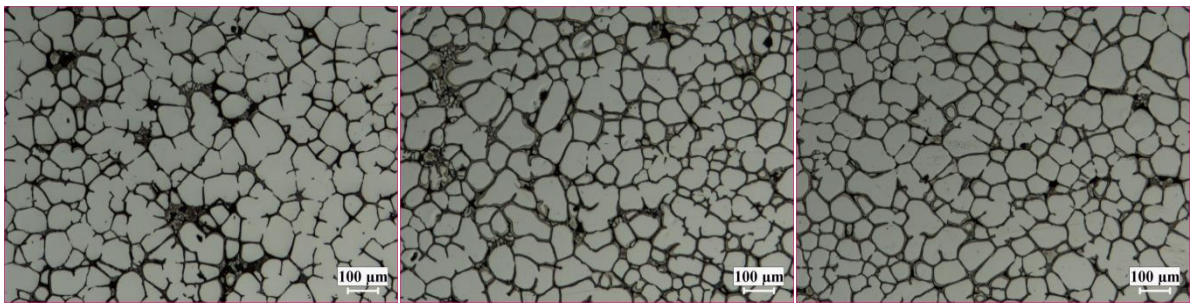

(d) 616℃ (0.50 fs)

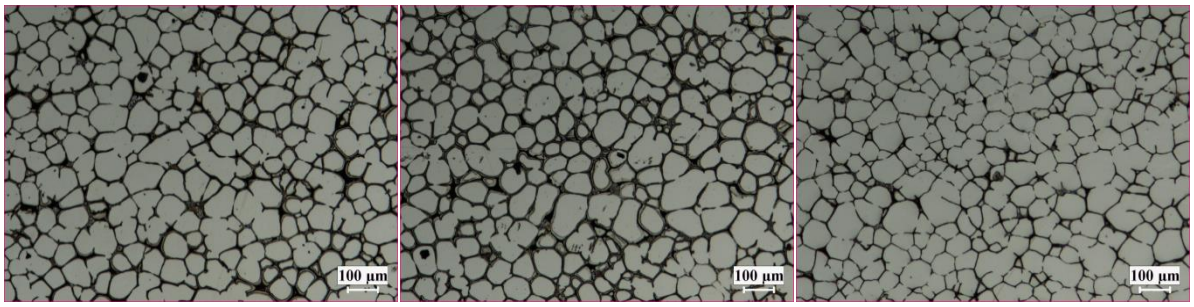

(e) 614℃ (0.53 fs)

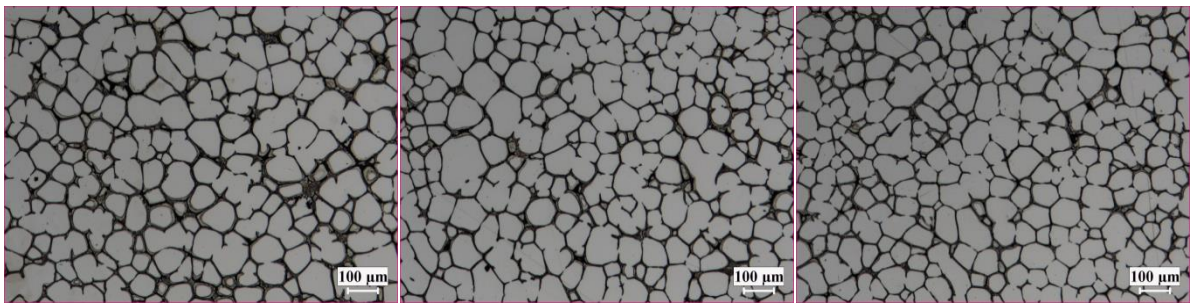

(f) 612℃ (0.55 fs)

Fig. 4.27 Microstructure of deformed semisolid billets of TiB_2 modified AA7075 alloy from the edge to the center, compressed at different temperatures (solid fractions): (a) 622℃ 0.42 fs, (b) 620℃ 0.45 fs, (c) 618℃ 0.48 fs, (d) 616℃ 0.50 fs, (e) 614℃ 0.53 fs, (f) 612℃ 0.55

Figure 4.27 presents the microstructure of the compressed billets from TiB_2 refined AA7075 alloy. In these optical micrographs, the bright particles are preferentially solidified primary α-Al grains, surrounded by the dark eutectic liquid phase. It can be seen that most of the α-Al grains developed into much finer globular particles next to each other due to the effective grain refinement of TiB_2. Micrographs obtained from three different positions of the deformed billets show that the liquid segregation phenomenon also occurred during compression test. As the compression was carried out on the semisolid billets, the solid particles (primary α-Al) aggregate at the center of the billet, while the unsolidified eutectic liquid was forced toward the edge of the billet due to the applied shear force. A close observation of the microstructure of the edge part of the billet, it is found that some of the segregated liquid phase latterly solidified to granule particles attached on adjacent primary particles. This secondary solidification may happen during the compression or quench process due to temperature drop.

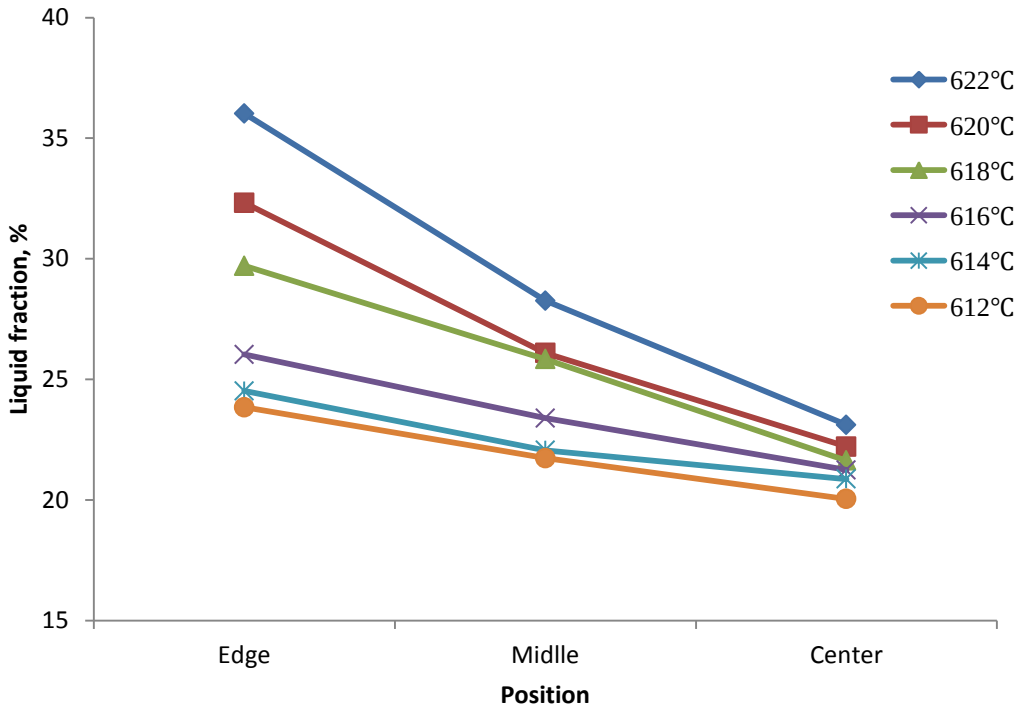

Fig. 4.28 Measured liquid fractions of deformed samples from edge to center at various compression temperatures.

Figure 4.28 quantitatively characterizes the liquid segregation phenomenon occurred during compression. Volume fraction of the liquid phase at edge, middle and center of the water quenched deformed billets was measured by image analysis system. Results illustrates that the liquid fraction at the edge part is higher than that at the middle, and then higher than center. And billets at higher compression temperature indicate more distinct segregation.

4.4.2.2 Height reduction curves

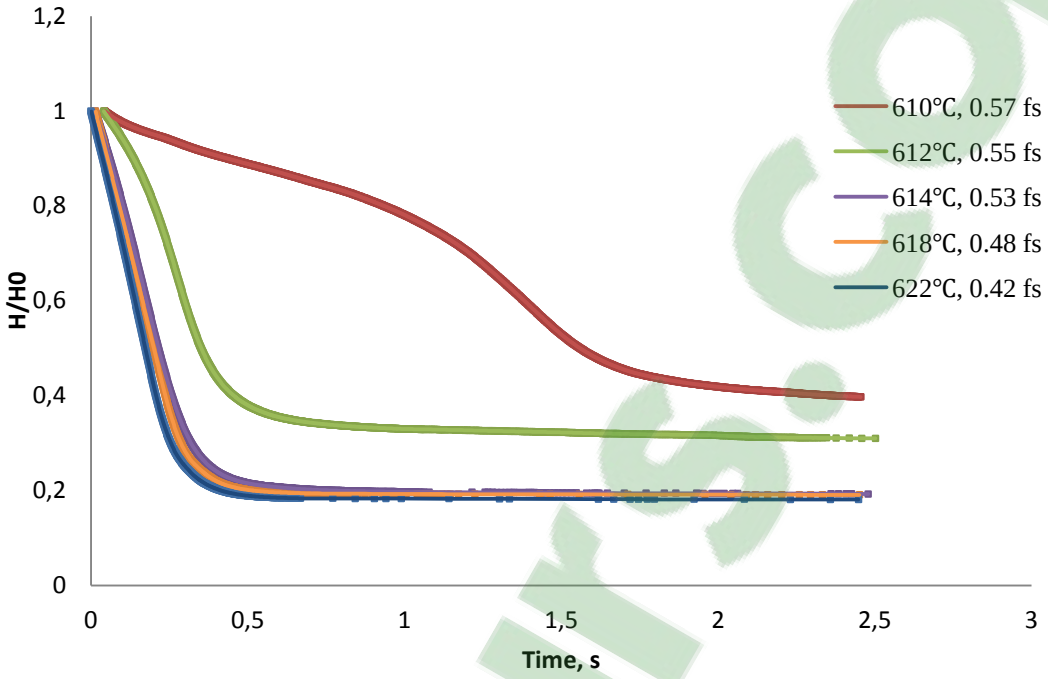

Fig. 4.29 Height reduction-time curves at different temperatures (℃) of TiB_2 modified semisolid AA7075 alloy

Fig. 4.29 shows the effect of demolding temperatures (solid fractions) on the height reduction to time curves of TiB_2 modified AA7075 alloy in semisolid state. In general, the height reduction rate increases with the decreasing solid fraction, because there are more collisions between the solid particles at high solid fraction, enhancing the resistance to deformation. To be specific, these height reduction-time curves can be generally divided into three categories, 610 ℃, 612 ℃ and 614 to 622 ℃, similar to 618, 620 and 622℃ for base alloy respectively. At 610 ℃ (0.57 fs), the height of the semisolid billet reduces slowly, and the final h/h_0 is up to 0.4, showing great resistance to deformation because of high solid fraction. When the billet is compressed at 612 ℃ temperature (0.55 fs), the deformation becomes easier and faster, and the final height reduction value reaches to 0.3. The billets compressed between the

temperature of 614 and 622 ℃ (solid fraction between 0.53 and 0.42) show complete deformation behavior, contributing much wider semisolid processing window compared to AA7075 base alloy, because of much smaller grain size.

Fig. 4.30 Actual view of compressed billets by parallel plate viscometer at different temperatures of TiB_2 modified AA7075 alloy

Fig. 4.30 shows the pictures of deformed billets of TiB_2 modified AA7075 alloy. It can be seen that this grain refined alloy presents extreme better rheoformability than that of AA7075 base alloy. It is generally believed that the solid fraction, the grain size and morphology are three main factors that affect the rheoformability of a semisolid alloy. Lower solid fraction, smaller grain size and more globular morphology lead to excellent rheoformability. At 610℃(0.57 fs), the billet of grain refined AA7075 alloy could be compressed to a certain extent, presenting huge potential of deformation. With comparison, the billet of base alloy at 610 ℃ cannot be compressed at all. Starting from 612℃ (0.55 fs), all the semisolid billets of the grain refined alloy can be compressed completely, which starts from 620℃ (0.45 fs) for base alloy. This can be explained in terms of effective grain refinement of TiB_2. With addition of 0.03wt% TiB_2, the grains become smaller and globular, which can easily move large distance in the melt even

though at high solid fraction. However, large and dendrite-like or rosette-like particles are unable to move long distance even though at low solid fraction because particles are tend to contact with each other.

4.4.2.3 Shear rate to time curves

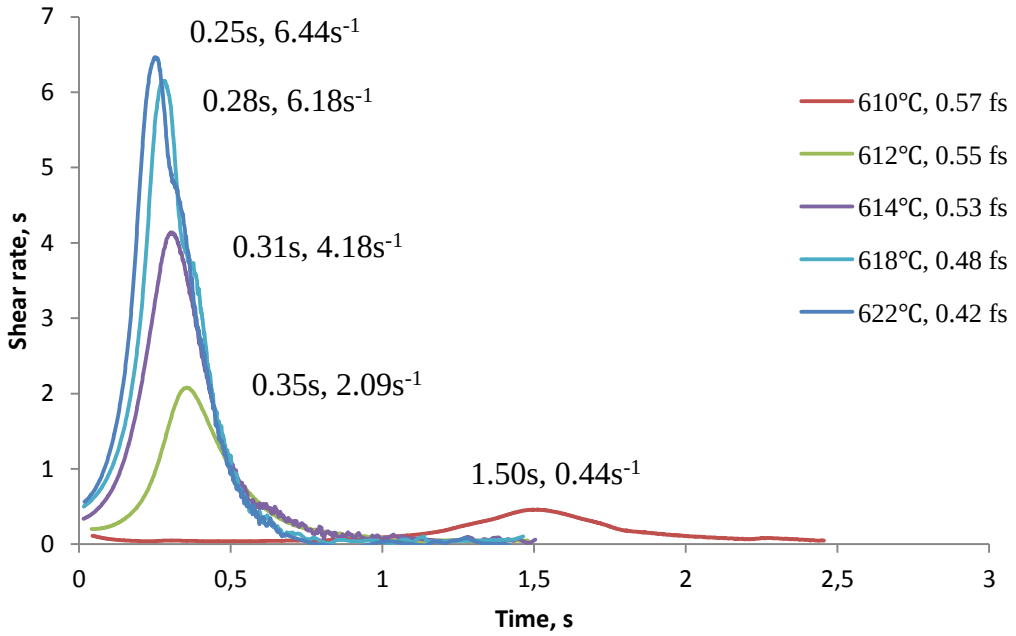

Fig. 4.31 Shear rate-time curves at different temperatures (℃) of TiB_2 modified AA7075 alloy

The shear rate evolution during compression test of TiB_2 modified semisolid AA7075 alloy was calculated and plotted into **Fig. 4.31**. Similar to base alloy, a positive peak appeared on the shear rate to time curve at each particular semisolid temperature, as well as solid fraction. The shear rate first increases to a maximum value then decreases to near zero in a short time period, featuring classic transient state behavior in rheology analysis. The shear rate jump up and down processing can be explained by the de-agglomeration and agglomeration happened in micro view.

Comparing five shear rate-time curves in **Fig. 4.31**, it can be found out that the solid fraction has significant influence on the evolution of shear rate. Results show that shear rate of the compressed semisolid billet with lower solid fraction has higher maximum value and spends less time reaching its peek value. This is because of the particle mobility in the liquid melt. At lower solid fraction, the solid particles possess more "liquid space" moving a large distance. However, as the solid fraction increases, the solid particles are more likely to collide with each other, making them difficult to move and slide easily and quickly, leading to poor rheoformability. One point need to be mentioned is that, most of the shear rate jump processing (from rest to near rest) finish in one second except that at 610 and 612℃ temperature.

4.4.2.4 Rheology comparison

Besides rheological analysis of base alloy, the alloy refined with 0.03wt% TiB_2 was also chosen to conduct the compression test. As usual, the typical curves of viscosity and shear rate as a function of time and the viscosity vs shear rate curve at the solid fraction of 0.45 was plotted. It is found that curves from TiB_2 refined 7075 alloy were quite similar with that from base alloy, shown in **Fig. 4.24** in last section. The shear rate experienced rapid increasing and decreasing process within 0.6 second. The correspond viscosity first dropped rapidly and then recovers during the decreasing shear rate section. This inverse change between viscosity and shear rate is evident that the fluid also behaves in shear thinning manner. The maximum shear rate obtained in the experiment reaches 5.16 s^{-1} compared with 1.64 s^{-1} obtained for base alloy in the same test conditions.

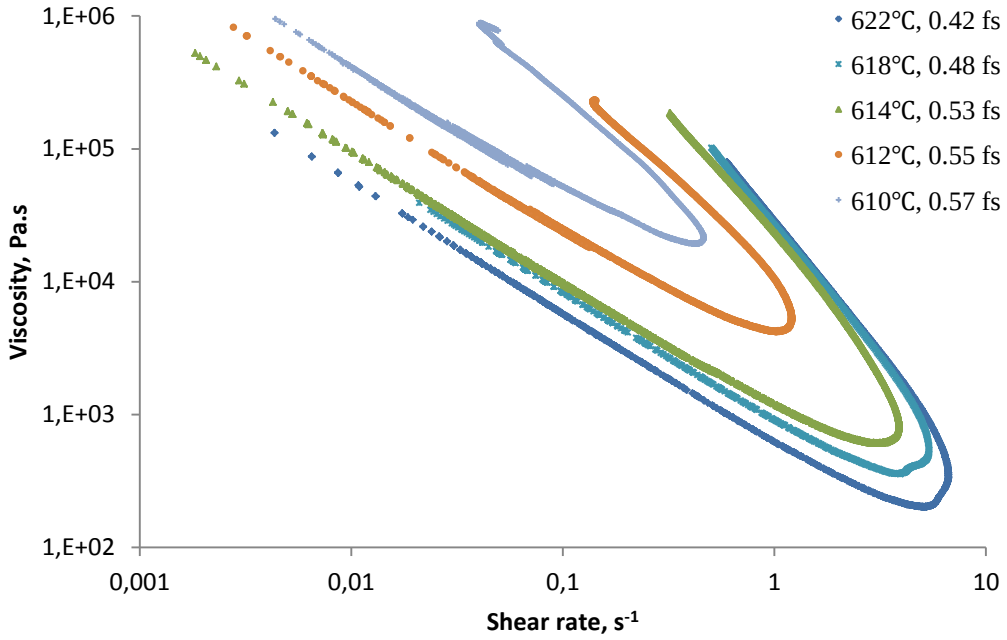

Fig. 4.32 Calculated viscosities as function of shear rate of TiB_2 modified AA7075 alloy at various fractions solid from 0.57 to 0.42.

Due to the smaller and more regular α-Al grains in refined alloy, its packing solid fraction (f_s^{pk}) is much higher than that of base alloy, resulting in a much wider solid fraction range that suitable for semisolid casting. The packing solid fraction proposed by A.K. Dahle *et al*[15] is a maximum solid fraction that grains are unable to move large distance by any deformation mechanisms. This index is dependent on the temperature, grain size and shape and the alloy composition. Therefore, in present experiments the refined alloy shows effective deformation among the solid fraction range of 0.57 to 0.42. And their calculated viscosities as function of shear rate were plotted in **Fig. 4.32**. Results show that all the viscosity-shear rate curves present increasing-shear rate and decreasing-shear rate portions. As expected, the viscosity increases with the increasing of solid fraction in each portion. During the increasing shear rate portion, the obtained maximum shear rate increases with the decreasing of the solid fraction. In the shear rate decreasing section, at a given shear rate the calculated average

viscosity increases with the increasing solid fraction. In detail, at the higher solid fraction range (more than 0.53), from solid fraction 0.53 to 0.55 and 0.55 to 0.57 the increasing of the viscosity is much more significant. While for the low solid fraction billets (from 0.53 to 0.42), the viscosity to shear rate curves tend to overlap together with the decreasing of fraction solid. It is found that those curves at low solid fraction can be well fitted into a power law equation $\mu = k \cdot \gamma^{-m}$ at two periods (increasing-shear rate and decreasing-shear rate), as shown in **Fig. 4.33**, where k is the constant associated with solid fraction, m is the power index dependent on the alloy type.

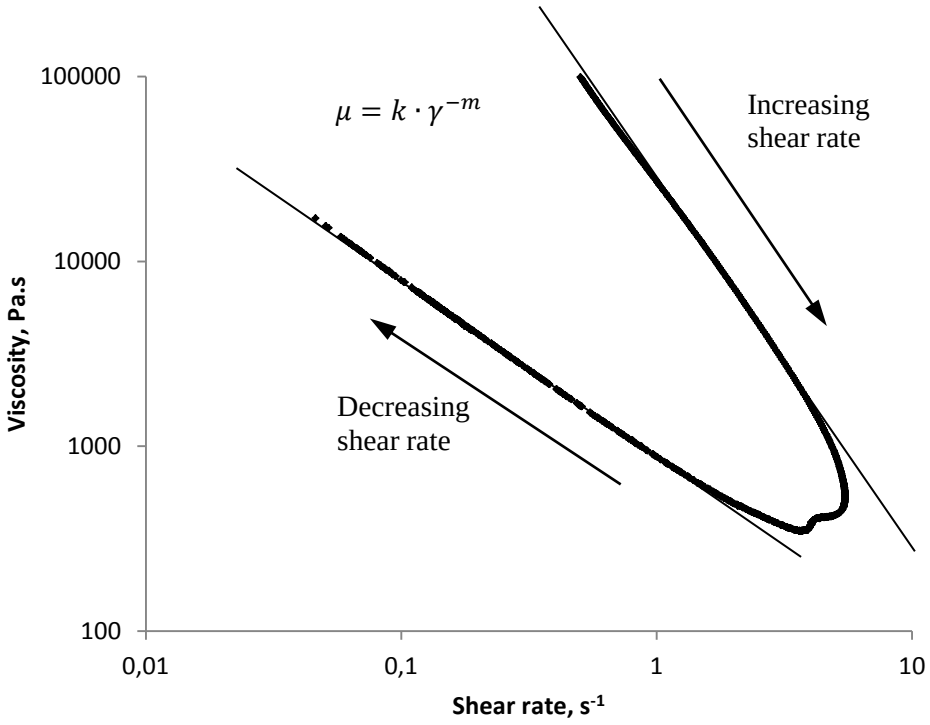

Fig. 4.33 Typical rheology curves of viscosity as a function of shear rate of refined alloy at the fraction solid of 0.45.

There are two types of parameters in the simulated power law equation of refined semisolid AA7075 alloys, which have been summarized into **Table 4-3**. In the table, k_1 and m_1 are extracted from the power law equation for the increasing-shear rate section; while, k_2 and m_2 are for the decreasing-shear rate section. It is believed that constant k is related to the solid fraction of the semisolid alloy and the index m is related to the alloy type. To have a deep understanding of these two parameters, they are plotted into curves according to the liquid fraction, as shown in **Fig. 4.34**.

Table 4-3 Parameters obtained from fitted power law equations of relationship between viscosity and shear rate under various temperature conditions

Temperature/℃	Solid fraction	K1	M1	K2	M2
614	0.53	20888	2.056	1383.5	0.821
616	0.50	24573	2.095	1160.0	0.860
618	0.48	26526	2.080	1119.1	0.868
620	0.45	26742	2.057	1074.0	0.819
622	0.42	29695	2.128	723.5	0.831

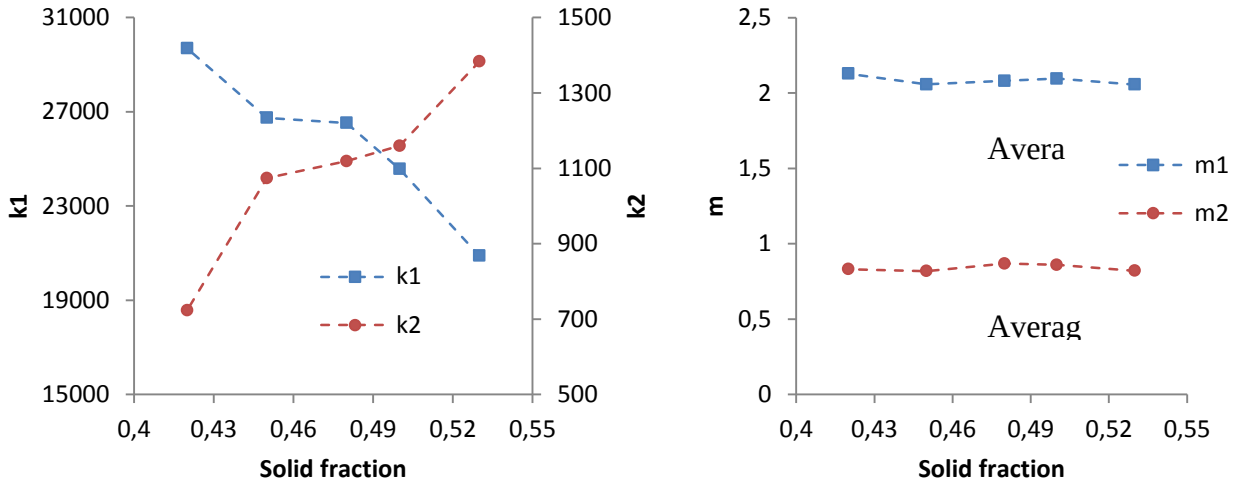

(a) (b)

Fig. 4.34 Parameters k and m in power law equation to various solid fractions

From **Fig. 4.34 (a)**, it can be seen that both k_1 and k_2 vary significant with the solid fraction, that k_1 increases continuously from 20888 to 29695 with the decreasing solid fraction from 0.53 to 0.42; while k_2 keeps decreasing from 1384 to 724 with the same reducing range of solid fraction.

Fig. 4.34 (b) presents the power index m to variation solid fraction. It is found that both m_1 and m_2 keep near constant to various solid fraction, evidencing its independence to solid fraction. For a certain semisolid alloy, it is generally believed that the power index m is a constant value independent of solid fraction. Results show that, in the increasing-shear rate section, the average m_1 value is 2.08; and in the decreasing-shear rate section, the average m_2 value is near 0.84.

4.4.3 Discussion

4.4.3.1 Quantitative characterization and comparison of deformed microstructures of two alloys

It is widely admitted that the fraction solid and the microstructure are the two main critical factors that have an important influence on rheological behavior of a semisolid alloy. As described before, two alloys, base and TiB_2 refined alloys, show significant difference on their rheoformability during compression. Results showed that base alloy only indicated good rheoformability at 622 and 620℃ (0.42 and 0.45 fs), and deformation started to become incomplete from 618℃ (0.48 fs), and temperatures below 616℃ (0.50 fs), the deformation turned out to be impossible in present experimental conditions. However, with TiB_2 refiner, the alloy exhibited excellent rheoformability among the temperature range of 622 to 614℃ (0.42 to 0.53 fs), and compressions of the billets at 612 and 610℃ (0.55 and 0.57 fs) started to be incomplete but still possible. It is believed that the grain refiner TiB_2 has no effect on the thermodynamic behavior of AA7075 alloy, which means base AA7075 and refined AA7075 have the same solid fraction under same compression temperature. Therefore, the considerable difference on their rheoformability was somehow because of the difference on their deformed microstructure.

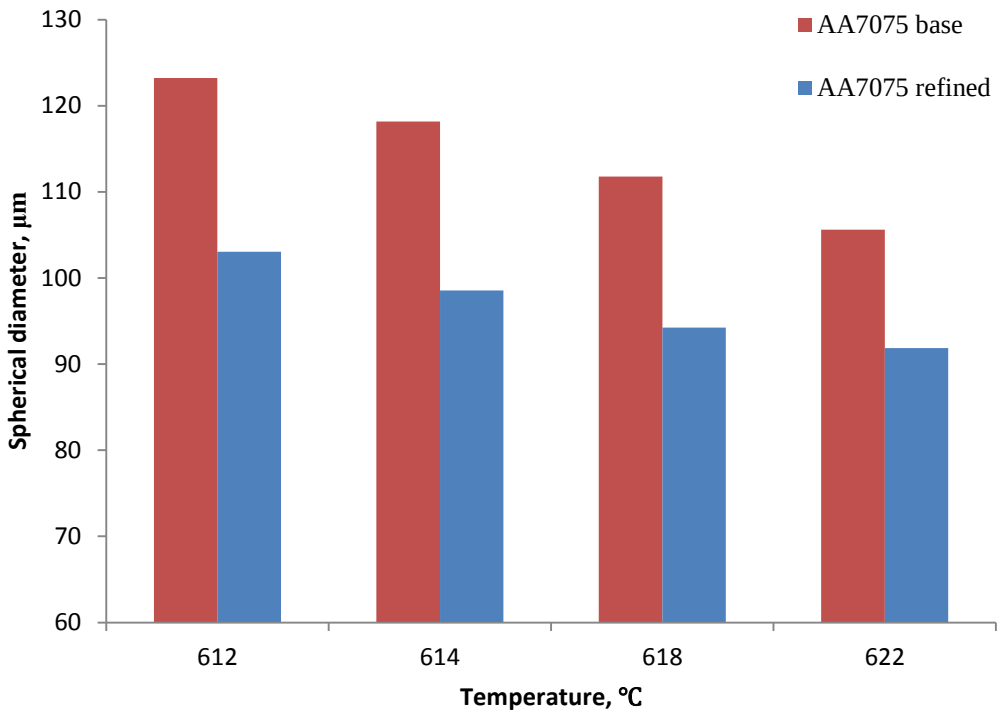

Fig. 4.35 Spherical diameter of the deformed billets of two alloys under various temperatures

Figure 4.35 presents the measured spherical diameter of the deformed microstructures of the two alloys. The size of the solid primary α-Al particles has a great effect on rheological behavior of the alloy in semisolid state. It is clearly shown in **Fig. 4.35** that the spherical diameter increased slightly with the decreasing compression temperature for both alloys, which is harmful to the rheoformability. This can be explained that during solidification more time needed to reach a lower temperature, giving grains more opportunity to grow larger. Furthermore, with the addition of 0.03wt% TiB_2, the spherical diameter of deformed grains decreases notably, resulting in excellent rheoformability of this grain refined AA7075 alloy. Additionally, at low temperatures (614 and 612℃), the grain refinement is much obvious, which gives reason that

rheoformability difference of two alloys becomes larger at low temperature. Compared with the previous work about the as cast microstructure of these two alloys in chapter 4.2, it is found that the grain size after deformation is slightly larger than that of as cast billets. This is mainly because the solid particles tend to attach each other and stick together during deformation under the applied shear force.

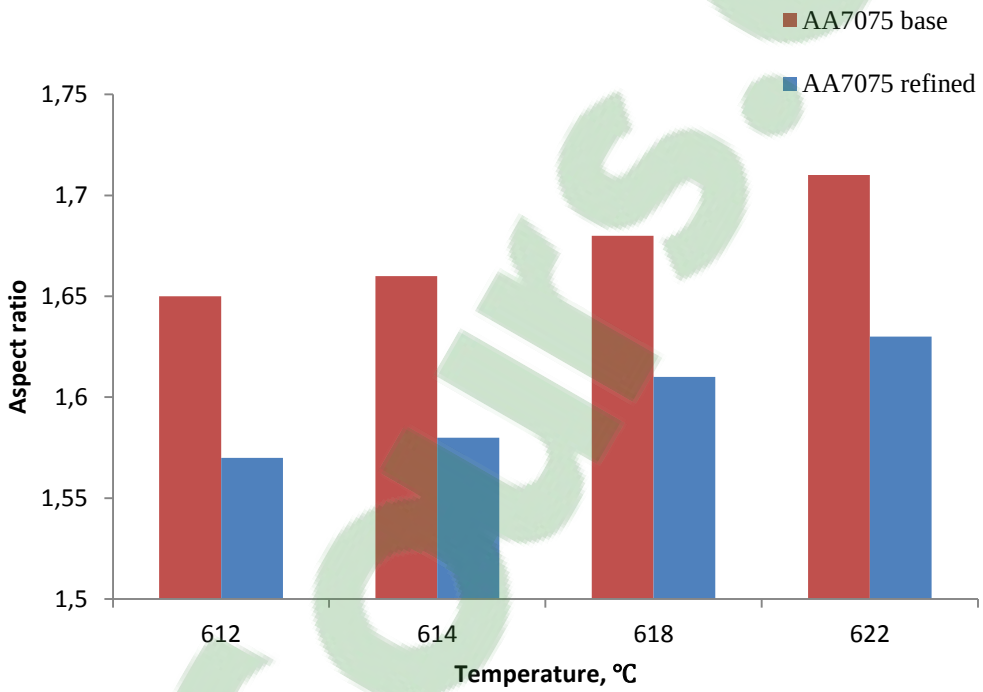

Fig. 4.36 Aspect ratio of the deformed microstructures of two alloys under various temperatures

Apart from the grain size, the morphology of deformed microstructure of two alloys is also characterized by aspect ratio, shown in **Fig. 4.36**. The shape of the grains also has a remarkable impact on the rheological behavior of a semisolid alloy. Under same circumstance, the globular grains are definitely easier to travel a long distance by sliding or rolling than the grains in dendrite or rosette form. It is evidently shown in **Fig. 4.36** that the aspect ratio of

deformed grains in TiB_2 modified alloy is smaller than that in base alloy, proving good globularity after grain refinement. Consequently, this good globularity leads to the reduction of apparent viscosity, resulting in excellent rheoformability through a wide temperature range. Besides, the aspect ratio of the deformed grains decreases with the decreasing compression temperature due to the long-term string during stock preparation by SEED processing, which agrees with the previous results in section 4.2.

4.4.3.2 Comparison of apparent viscosity of two alloys

The addition of grain refiner TiB_2 has modified the microstructure of the alloy, leading to an important influence on the rheological behavior of the semisolid AA7075 alloys. Through the rheology test experiments, the most critical difference between two alloys is the compressible solid fraction range. For the base alloy, the billet only can be successfully compressed at a narrow solid fraction range of 0.48 to 0.42; while for the refined alloy, the range expends to 0.55 to 0.42. And all the test experiments are summarized in **Table 4-4**.

Table 4-4 Rheology test experiments discussed in present work

Test	Alloy	Temperature/℃	Predicted solid fraction	Maximum shear rate/s^{-1}	Final billet height/(h/h_0)	Duration of compression
1	AA7075 Base	616	0.50	0.10	0.62	67s
2	AA7075 Base	618	0.48	0.33	0.34	4.5s
3	AA7075 Base 5	620	0.45	1.64	0.30	0.98s
4	AA7075 Base	622	0.42	3.29	0.23	0.82s
5	AA7075 Refined	610	0.57	0.45	0.37	5.0s
6	AA7075 Refined	612	0.55	1.19	0.31	2.0s
7	AA7075 Refined	614	0.53	3.78	0.20	1.6s
8	AA7075 Refined	616	0.50	5.13	0.19	1.2s
9	AA7075 Refined	618	0.48	5.39	0.19	0.88s
10	AA7075 Refined	620	0.45	5.48	0.20	0.80s
11	AA7075 Refined	622	0.42	6.64	0.19	0.70s

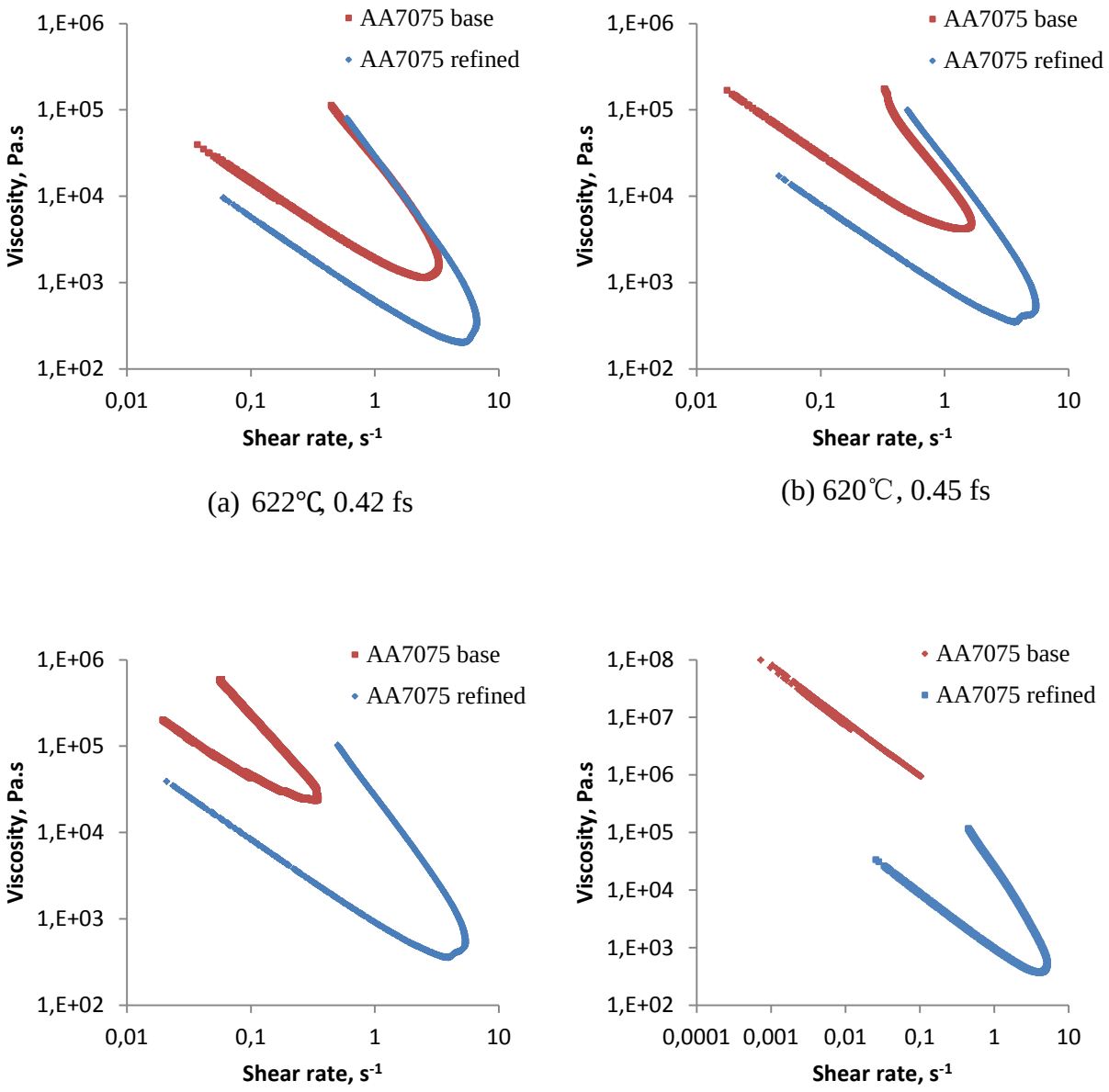

Fig. 4.37 Plotted viscosity to shear rate curves of base AA7075 and TiB_2 refined AA7075 alloys with various solid fractions of (a) 0.42, (b) 0.45, (c) 0.48 and (d) 0.50, corresponding to compression temperatures of 622, 620, 618℃and 616℃ respectively.

Figure 4.37 compares the viscosity evolution of these two alloys, unrefined and refined AA7075 at different compression temperatures corresponding to different solid fractions. Curves

in **Fig. 4.37** show a reclining greater than symbol (>) shape curve. It is interesting to note that most part of the reclining "> shape" curve from base alloy is "encircled" by the curve from refined alloy. That indicates that at the same solid fraction condition, the obtained maximum shear rate of refined alloy is always larger than that of base alloy due to the effective refinement to the size of solid grains. And the higher of the solid fraction, the larger of the difference of maximum shear rate between two alloys. In the increasing shear rate part, the viscosities of two alloys are quite similar at the same given shear rate at solid fraction of 0.42 and 0.45, as shown in **Fig. 4.37 (a)** and **(b)**. This similarity tells that the viscosity is not only solid fraction and grain size and morphology dependent. At a certain solid fraction range (relatively low), the viscosity tends to keep similar for various solid fraction, and independent to the microstructures, only showing the nature of the alloy. In the decreasing shear rate part, at a given shear rate, the viscosity of refined alloy is significantly smaller than that of refined alloy at any solid fraction. This indicated that smaller and more globular grains are easier to roll and slide over each other, resulting in lower viscosity. This is mainly because that with the grain refinement, the interfacial area between solid particles and liquid phase increases significantly. As a result, there is more liquid appearing between solid particles, which acts as the lubricant, reducing the friction between solid particles. Furthermore, it is found from **Fig. 4.37 (d)** that at the solid fraction of 0.50, the missing of the increasing shear rate part on the viscosity-shear rate curve of the base alloy indicates that it cannot be rapidly compressed any more. However, at the same solid fraction of 0.50, the refined alloy still shows similar viscosity and shear rate relationship as in low solid fraction. Consequently, the grain refinement significantly extends the solid fraction range of rapid compression for AA7075 alloy.

4.4.3.3 Comparison with literatures

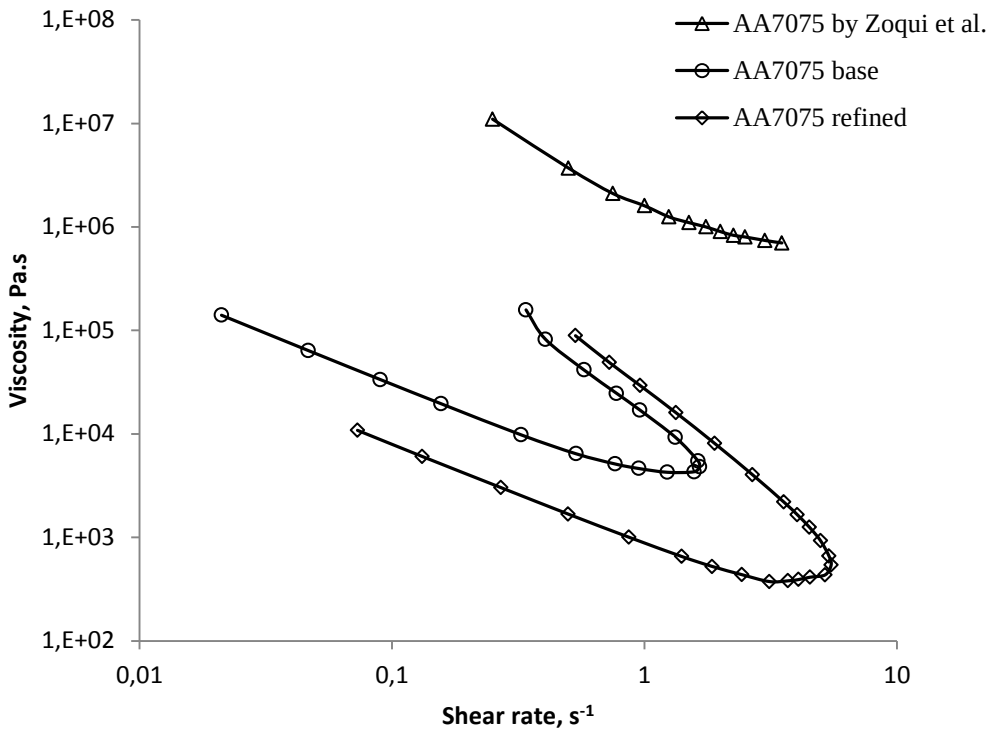

Fig. 4.38 Comparison of the relationship between viscosity and shear rate for AA7075 alloy at solid fraction of 0.45 from this work and Zoqui *et al*.

Fig. 4.38 compared the apparent viscosities as a function of shear rate of both unrefined and TiB_2 refined AA7075 alloys in present work with that studied by Zoqui *et al*[16] using Inconel 718 parallel plates viscometer which is quite similar to the viscometer used in present work. In Zoqui's test, the samples are 15mm in height and 20mm in diameter. And the compression velocity is controlled constant at 10mm/s, while the compression force is controlled constant in present work. From **Fig. 4.38** is can be seen that there is only one shear rate period on the curve of viscosity-shear rate by Zoqui, which is similar to the decreasing-shear rate period in present work. It is found that the viscosity found by Zoqui is quite larger than the viscosity

during decreasing-shear rate period of both alloys in this work. The large difference in viscosity observed between this work and Zoqui is mainly due to the low shear rate applied in Zoqui's test. Due to the low constant compression velocity in Zoqui's work, 10mm/s, the maximum shear rate is $3.5s^{-1}$. Another reason may be the larger size and more irregular morphology of grains in the alloy used by Zoqui. This difference of viscosities makes good agreement that the viscosity is not only dependent on the temperature (solid fraction), but also dependent on the applied shear rate as well as the size and morphology of the grain of semisolid alloys. On the other hand, it can be seen from **Fig. 4.38** that the viscosity-shear rate curve found by Zoqui can also be well fitted into the power law equation described before.

1. Birol, Y., *Solid fraction analysis with DSC in semi-solid metal processing.* Journal of Alloys and Compounds, 2009. **486**(1–2): p. 173-177.
2. Patel, J.B., et al., *Rheo-processing of an alloy specifically designed for semi-solid metal processing based on the Al–Mg–Si system.* Materials Science and Engineering: A, 2008. **476**(1–2): p. 341-349.
3. D. Doutre, G.H., and P. Wales, *Semi-solid Concentration Processing of Metallic Alloys.* U.S. Patent August 2002. **6**(428): p. 636 B2.
4. Xie, F., et al., *A study of microstructure and microsegregation of aluminum 7050 alloy.* Materials Science and Engineering: A, 2003. **355**(1–2): p. 144-153.
5. Birol, Y., *Heat treatment of twin-belt cast EN AW 7075 alloy.* Materials Characterization, 2012. **63**: p. 1-8.
6. Lemieux, A., et al., *Effect of Si, Cu and Fe on mechanical properties of cast semi-solid 206 alloys.* Transactions of Nonferrous Metals Society of China, 2010. **20**(9): p. 1555-1560.
7. Zhong, G., et al., *Effects of ultrasonic vibration on the iron-containing intermetallic compounds of high silicon aluminum alloy with 2% Fe.* Journal of Alloys and Compounds, 2010. **492**(1–2): p. 482-487.
8. Yurko, J.A. and M.C. Flemings, *Rheology and microstructure of semi-solid aluminum alloys compressed in the drop-forge viscometer.* Metallurgical and Materials Transactions A. **33**(8): p. 2737-2746.
9. Birol, Y., *Thermomechanical processing of an aluminium casting alloy for thixoforming.* Journal of Alloys and Compounds, 2009. **479**(1–2): p. 113-120.
10. Khosravani, A., et al., *Liquid segregation behavior of semi-solid AZ91 alloy during back extrusion test.* Journal of Alloys and Compounds, 2009. **477**(1–2): p. 822-827.
11. Fukui, Y., D. Nara, and N. Kumazawa, *Evaluation of the Deformation Behavior of a Semi-solid Hypereutectic Al-Si Alloy Compressed in a Drop-Forge Viscometer.* Metallurgical and Materials Transactions A, 2015. **46**(5): p. 1908-1916.
12. Brabazon, D., D.J. Browne, and A.J. Carr, *Experimental investigation of the transient and steady state rheological behaviour of Al–Si alloys in the mushy state.* Materials Science and Engineering: A, 2003. **356**(1–2): p. 69-80.
13. Zoqui, E.J. and M.A. Naldi, *Evaluation of the thixoformability of the A332 Alloy (Al–9.5 wt%Si–2.5 wt%Cu).* Journal of Materials Science, 2011. **46**(23): p. 7558-7566.
14. Blanco, A., et al., *Rheological characterization of A201 aluminum alloy.* Transactions of Nonferrous Metals Society of China, 2010. **20**(9): p. 1638-1642.
15. Dahle, A.K. and D.H. StJohn, *Rheological behaviour of the mushy zone and its effect on the formation of casting defects during solidification.* Acta Materialia, 1998. **47**(1): p. 31-41.
16. Zoqui, E.J. and L.V. Torres, *EValuation of the thixoformability of AA7004 and AA7075 alloys.* Materials Research, 2010. **13**: p. 305-318.

CHAPTER 5

CONCLUSIONS AND RECOMMENDATIONS

5.1 Conclusions

Results and discussions of present work are made up of four parts. The first part (4.1) deals with the DSC analysis and the evolution of liquid fraction to temperature. Therefore, the semisolid temperature window of AA7075 alloy was determined. The second part (4.2) investigates the effect of SEED processing parameters on the microstructure of semisolid AA7075 alloy. Both base alloy and 0.03wt% TiB_2 refined alloy were studied in this part. The third part (4.3) involves the TiB_2 and Zr refinement and modification effect on the SEED processed microstructures of AA7075 alloys. In the fourth part (4.4) the rheoformability and microstructure of base alloy and 0.03wt% TiB_2 refined alloy were investigated. The main conclusions are drawn as below.

Part 1 DSC Analysis and Liquid Fraction

1. The liquidus and solidus temperature of AA7075 alloy are 631℃ and 490℃ respectively. The solidification temperature range is 141℃.

2. The semisolid temperature for AA7075 alloy is between 610 ℃ and 625℃. Under 610 ℃, the billets will be over solidified, resulting in poor deformation behavior;

while over 625℃, the billet consists of a great amount of liquid, losing self-support ability.

Part 2 Effect of SEED Processing Parameters on the Microstructure of Semisolid 7075 Alloys

3. The SEED processing parameters have strong influence on the morphology of 7075 wrought aluminum alloy. And the optimum swirling frequency of SEED processing is proved to be 180 rpm.

4. For base alloy, with the variation of the swirling speed, the average reduction of the grain size and aspect ratio reach 12.9% and 6.2% respectively, the obtained minimum grain size and aspect ratio are 106.65μm and 1.64 respectively.

5. For 0.03wt% TiB_2 refined alloy, the average reduction of the grain size and aspect ratio under various SEED processing frequencies are 6.0% and 1.0%, and the obtained minimum grain size and aspect ratio are 93.86μm and 1.56 respectively.

6. SEED processing parameters have a strong influence on the microstructure of AA7075 base alloy, but a slight influence on that of 0.03wt% TiB_2 refined alloy.

Part 3 Effect of Grain Refiners on SEED Processed Microstructures of AA7075 Alloys

7. TiB_2 shows great refinement and modification effect on the microstructure of semisolid AA7075 alloy, both the primary α-Al particles and the intermetallic phases. However, Zr didn't show effective refinement on the microstructure.

8. TiB_2 promotes the transformation of α-Al particles from large dendrite or rosette to finer spherical ones. The addition of 0.06wt% TiB_2 triggers 23.7% and 6.7% reduction in grain size and aspect ratio of α-Al particles respectively at the optimum SEED processing conditions compared to base alloy. The obtained minimum grain size and aspect ratio are 84.5μm and 1.54 respectively.

9. With the addition of Zr to base alloy, the grain size decreases from about 110μm to 104μm, but the aspect ratio increases from 1.68 to 1.72. With the combination of TiB_2 and Zr, both the grain size and aspect ratio of α-Al particles increase.

10. The morphology and size of three intermetallic phases were effectively modified by the addition of TiB_2. The 4.0% volume fraction of string like $Mg(Zn,Cu,Al)_2$ becomes much shorter and narrower, the 1.0% volume fraction of grille-like Mg_2S phase and the Chinese script-like Al(Fe,Mn)Si both turn into smaller size of grills and Chinese-scripts.

Part 4 Rheoformability and Microstructure of Semisolid AA7075 Alloys

11. Characterization of microstructure of deformed billets indicates that the liquid segregation from the center to the edge of the billet of both alloys happened during the compression, and the higher of the compression temperature (higher liquid fraction), the more significant of the liquid segregation phenomenon.

12. In the typical compression test using parallel-plate viscometer, the shear rate has a maximum peak value, resulting in two parts of the viscosity-shear rate curve: increasing shear rate part and decreasing shear rate part. In each part, the viscosity decreases with increasing shear rate, indicating a shear thinning behavior.

Furthermore, the viscosity of both alloys increases with increasing solid fraction in both increasing-shear rate part and decreasing-shear rate part.

13. The relationship between viscosity and shear rate in each part of the refined alloy can be well fitted into a power law equation $\mu = k \cdot \gamma^{-m}$, showing a guidance for simulation. In the increasing-shear rate part, the constant k_1 increase with decreasing solid fraction, and the power index m is about 2.08. In the decreasing-shear rate part, the constant k_2 decreases with decreasing solid fraction, and the power index is about 0.84.

14. The viscosity and shear rate relationship between base and refined AA7075 alloys were compared. It indicates that the refined alloy can obtain a higher maximum shear rate at the same solid fraction compared with base alloy. During the decreasing-shear rate part, the viscosity of refined alloy is smaller than that of base alloy at any given shear rate.

15. Grain refiner TiB_2 reduces the grain size and modified the morphology of the grains more globular, making grains either move larger distance easily or roll and slide over each other easily. The refinement significantly expands the solid fraction range of good rheoformability from 42%-48% for the base alloy to 42%-55% for the refined alloy.

5.2 Recommendations for Future Work

1. The effect of the SEED processing parameters on microstructure is mainly focus on these two parameters: swirling frequency and demolding temperature. The effect of

other parameters like the pouring temperature and holding time could be further investigated to produce the semisolid AA7075 alloy with superior quality structure and excellent rheoformability.

2. Study the effect of SEED processing and grain refinement on the mechanical properties of the semisolid AA7075 alloy after high pressure die casting.

3. The minimum grain size for AA7075 alloy is 84.5μm obtained by the addition of 0.06wt% TiB_2, and it is interesting to find out other grain refiners adding to the AA7075 alloy to obtain much finer and globular α-Al particles to further lift the rheoformability.

4. Investigation of the deformation behavior of the semisolid AA7075 alloy under various ram speed and dead weight of the plate using parallel-plate viscometer.